

Dissertation zur Erlangung des Doktorgrades
der Fakultät für Chemie und Pharmazie
der Ludwig-Maximilians-Universität München

Analytic Gradient Techniques for Investigating the
Complex-Valued Potential Energy Surfaces of
Electronic Resonances

Zsuzsanna Koczor-Benda

(geb. Benda)

aus

Budapest, Ungarn

2019

Erklärung

Diese Dissertation wurde im Sinne von §7 der Promotionsordnung vom 28. November 2011 von Herrn Dr. Thomas-Christian Jagau betreut.

Eidesstattliche Versicherung

Diese Dissertation wurde eigenständig und ohne unerlaubte Hilfe erarbeitet.

München, 12.03.2019

.....
Zsuzsanna Koczor-Benda

Dissertation eingereicht am:	01.02.2019
1. Gutachter:	Dr. Thomas-Christian Jagau
2. Gutachter:	Prof. Dr. Christian Ochsenfeld
Mündliche Prüfung am:	04.03.2019

Summary

Electronic resonances are metastable atomic or molecular systems that can decay by electron detachment. They play an important role in biological processes such as DNA fragmentation induced by slow electrons or in interstellar reactions as in the formation of neutral molecules and molecular anions. As opposed to bound states, resonances do not correspond to discrete eigenstates of a Hermitian Hamiltonian, and therefore their theoretical description requires special methods. The complex absorbing potential (CAP) method can be used to calculate both the energy and the lifetime of a resonance as a discrete eigenstate in a non-Hermitian time-independent framework. The CAP method allows for applying well-known bound-state electronic structure methods to resonances as well.

In this work, the applicability of CAP-augmented equation-of-motion coupled-cluster (CAP-EOM-CC) methods is extended for locating equilibrium structures and crossings on complex-valued potential energy surfaces of electronic resonances by introducing analytic energy gradients. The structure and energy of these points are needed for, e.g., estimating the importance of a specific dissociation route or deactivation process. The accuracy of structural parameters, vertical and adiabatic electron affinities, and resonance widths obtained with approximate methods and various diffuse basis sets is investigated. Applications of optimization methods are also presented for systems that are relevant in interstellar or biological processes. Properties of the complex-valued potential energy surfaces of anionic resonances of acrylonitrile and methacrylonitrile are connected to experimental observations. Dissociative electron attachment to chloro-substituted ethylenes is also investigated. This can help in understanding detoxification processes of these compounds and might facilitate the exploration of DEA pathways for other halogenated molecules as well.

Anyának és Apának

Acknowledgments

First of all, I would like to thank my supervisor, Thomas Jagau for providing me support during my PhD, and for giving me freedom to shape my research goals. I am grateful for the many opportunities to participate in workshops and conferences, and for his encouragement in preparing presentations of my results.

I thank the fellow members of the research group, Victoria and Mario for valuable discussions, and Kerstin for her careful work in our joint publication.

Christian Ochsenfeld and his research group provided an ideal environment for pursuing my research, and I appreciate their hospitality and technical assistance very much. I am also thankful for the scientific feedback that I received at the theoretical chemistry seminars.

I would like to express my gratitude to Anna Krylov for providing her advice and opinion on all my research articles and conference talks. Her enthusiasm has encouraged me to pursue these projects further.

This work would not have been possible without my family and friends, and I would like to take this opportunity to thank them all for their support. I am very grateful to Kata, Gábor, Petra and Vanda for creating a lively, homelike environment for us in Munich.

Last but in no way least, I thank my husband, Bálint, for all the scientific discussions and technical advice that helped me move forward with my work, and of course for all the love and support he gave during these years.

Contents

1	Introduction	1
2	Theoretical Background	3
2.1	Theory of bound states and resonances	3
2.2	Separation of nuclear and electronic motion	5
2.3	Electronic structure methods for bound states	7
2.3.1	The Hartree-Fock method	7
2.3.2	The coupled-cluster method	8
2.3.3	The equation-of-motion coupled-cluster method	9
2.4	Non-Hermitian description of resonances	11
2.4.1	The complex absorbing potential method	13
2.4.2	Complex absorbing potential coupled-cluster methods	14
2.4.3	Characterization of resonances	15
2.5	Special points on potential energy surfaces	15
2.5.1	Crossing conditions	16
2.5.2	Locating equilibrium structures and surface crossings	18
2.6	Analytic energy gradients	20
2.6.1	Coupled-cluster analytic gradient	21
2.6.2	Equation-of-motion coupled-cluster analytic gradient	22
3	Results	23
3.1	Analytic gradients for complex absorbing potential methods	24
3.1.1	Publication 1	25
3.2	Structure optimization of temporary anions	30
3.2.1	Publication 2	31
3.3	Crossing points between anionic and neutral surfaces	42
3.3.1	Publication 3	43
3.4	Locating exceptional points	51
3.4.1	Publication 4	52
3.5	Future plans and further possible applications	59
4	Conclusion	61
	Bibliography	63
5	Supporting Information	71
5.1	SI for Publication 1	72
5.2	SI for Publication 2	77
5.3	SI for Publication 3	98
5.4	SI for Publication 4	110
	List of Publications	119

1 Introduction

Resonances are metastable states of a system that have the energy to break up into subsystems but remain intact long enough to be detected experimentally. They are, perhaps, most well-known in connection with α -decay [1], in which a metastable nuclid decays by emitting an α -particle. However, resonances are important in many other processes: for atomic and molecular systems, resonances are a key for understanding inelastic scattering, photo-, and autoionization [2], Auger-decay [3], predissociation [4], predesorption [5, 6] and high harmonic generation [7]. In the present work, autoionizing electronic resonances are investigated.

Metastable molecular systems can be formed by collision or by half collision experiments, for example electron impact to a stable molecule or excitation of a bound state. In biological environments, slow electrons can create autoionizing resonances by attaching temporarily to biomolecules, and such resonances can lead to the formation of harmful radicals, and can cause strand breaks in DNA [8–11]. In plasmas, the role of autoionizing states in the recombination of ionized molecules with electrons is important for understanding chemical evolution in interstellar molecular clouds, combustion engines and fusion reactors [12]. To characterize resonances experimentally, electron impact [13] and photodetachment spectroscopy [14] can be used, for example. The decay of a resonance is a stochastic process, which is characterized by a decay rate. The decay rate of the metastable system can sometimes be determined from the width of the resonance peak, and is consequently often called resonance width.

Resonances can usually be divided into shape and Feshbach resonances based on their decay mechanisms. Shape resonances are formed, e.g., when particles can tunnel through a potential barrier to escape the system (see References [15] and [16]). In the case of autoionizing states, shape resonances are above their own ionization threshold and decay by a one-electron process. Shape resonances have higher energies than their parent states, and thus are embedded in the continuum (see Figure 1.1). Autoionizing shape resonances are not stable with respect to electron detachment, and their lifetime is usually in the femtosecond-picosecond range. In contrast, autoionizing Feshbach resonances lie below their ionization

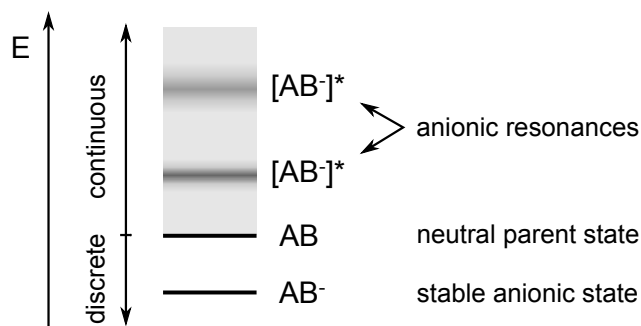


Figure 1.1: Bound states and autoionizing shape resonances in the eigenvalue spectrum of an anionic system. The energy of the neutral parent state corresponding to these anionic states is also shown.

CHAPTER 1. INTRODUCTION

threshold and decay by a two-electron process through a different decay channel, thus they usually have a longer lifetime than shape resonances. In this work only shape-type autoionizing resonances are considered.

The theoretical description of resonances is more involved than that of bound states. Resonances are not stationary states, thus cannot be studied within the time-independent formalism, at least not by applying a Hermitian Hamiltonian operator as in the standard formulation of quantum mechanics. As will be discussed in this work, a resonance can be investigated in the time-independent framework, e.g., by modifying the Hamiltonian with a complex absorbing potential (CAP). In this case, the resonance is calculated as a discrete square-integrable state having a complex energy whose real part gives the position and its imaginary part yields the width of the resonance. This is in contrast to bound states, which have purely real energies. The addition of the CAP allows for applying standard methods and tools developed for bound states. A complex-valued potential energy surface (CPES) can be constructed for each resonance by applying the Born-Oppenheimer approximation, in analogy with the real-valued PES of bound states.

CPESs facilitate the modeling of processes that involve multiple interacting resonances, such as the dissociative electron attachment (DEA) process. DEA is important, for example, in the already mentioned slow electron-induced damage to DNA, in which shape resonances initially localized on the nucleobases convert to dissociative states that lead to strand breaks [8, 9, 11]. The interplay of resonances with different lifetimes and different asymptotic behavior is a key for understanding these processes and it is relevant for many other molecules exposed to low-energy electrons both in the gas phase and in the bulk phase [10]. For the investigation of such processes, special points on the CPESs, such as equilibrium structures or intersections of different states need to be located. These points affect the nuclear dynamics strongly. The autoionization lifetimes of resonances and their changes along the reaction pathway also need to be considered in order to assess the relative importance of autoionization and dissociation, which can be competing mechanisms for the deactivation of resonances.

In this work, it is shown that the CAP augmented equation-of-motion coupled-cluster (CAP-EOM-CC) method can be applied to such problems. Using analytic energy gradients and modified versions of regular optimization techniques, it is possible to locate special points on multidimensional CPESs efficiently. For many bound-state methods, analytic energy gradients are well-known and are available in quantum chemistry programs. However, gradients for metastable-state methods were not available prior to this work. Here, it is demonstrated how the CPES of a resonance can be studied, and how its characteristics can be connected to experimental observations.

Before discussing these topics, a short overview of the relevant quantum chemical methods is given in Chapter 2. The original publications that contain the main results of this PhD work are presented in Chapter 3, where a short outlook discussing further project plans is also given. Finally, the thesis is summarized in Chapter 4.

2 Theoretical Background

In this chapter, the theoretical foundations for describing resonances are given with a focus on the time-independent non-Hermitian description in CAP-EOM-CC methods. Properties of bound state methods are discussed as well, and it is reviewed how electronic states can be investigated within the Born-Oppenheimer approximation by studying their potential energy surfaces. Throughout the chapter, differences and similarities between the treatment of resonances and bound states are pointed out. Analytic gradient theory is discussed in connection with CC and EOM-CC methods.

2.1 Theory of bound states and resonances

The postulates of the standard formulation of quantum mechanics state [17] that vectors $|\Phi\rangle$, that correspond to states of the quantum system at a given time, are elements of a complex Hilbert space \mathcal{H} . Observables, that are associated with physical properties of the system, are Hermitian operators acting on the elements of \mathcal{H} . For a system in state $|\Phi\rangle$, the expectation value A of an observable \hat{A} is given by

$$A = \frac{\langle \Phi | \hat{A} | \Phi \rangle}{\langle \Phi | \Phi \rangle}. \quad (2.1)$$

If the system is in an eigenstate of \hat{A} , the expectation value is the corresponding eigenvalue. The eigenvalues of Hermitian operators are always real numbers which is consistent with the fact that measurable quantities are real-valued.

The time evolution of the system is given by the time-dependent Schrödinger equation (TDSE)

$$\hat{H}|\Psi_n(\mathbf{x}, t)\rangle = i\frac{\partial|\Psi_n(\mathbf{x}, t)\rangle}{\partial t} \quad (2.2)$$

in atomic units. \hat{H} is the Hamiltonian, which is associated with the total energy of the system E_n , and $|\Psi_n\rangle$ is the wave function of state n which is dependent on position \mathbf{x} and time t .

For a time-independent Hamiltonian, integrating (2.2) yields

$$|\Psi_n(\mathbf{x}, t)\rangle = e^{-i\hat{H}t}|\Psi_n(\mathbf{x}, 0)\rangle. \quad (2.3)$$

Bound states $|\Psi_n^b\rangle$ are discrete eigenstates of \hat{H} and can be calculated from the time-independent Schrödinger equation (TISE)

$$\hat{H}|\Psi_n^b(\mathbf{x}, 0)\rangle = E_n^b|\Psi_n^b(\mathbf{x}, 0)\rangle. \quad (2.4)$$

They are elements of the L^2 Hilbert space of square-integrable functions, where the inner product is defined as

$$\langle \Phi_i | \Phi_j \rangle = \int \Phi_i^*(\tau)\Phi_j(\tau)d\tau, \quad (2.5)$$

where the star denotes complex conjugation. These states necessarily satisfy the boundary conditions

$$\Psi_n^b(\mathbf{x} \rightarrow \pm\infty) = 0. \quad (2.6)$$

For bound states, (2.3) can be simplified into

$$|\Psi_n^b(\mathbf{x}, t)\rangle = e^{-iE_n^b t} |\Psi_n^b(\mathbf{x}, 0)\rangle, \quad (2.7)$$

which describes a stationary state, whose probability density ρ_n^b does not change in time

$$\rho_n^b(\mathbf{x}, t) \equiv |\Psi_n^b(\mathbf{x}, t)|^2 = |\Psi_n^b(\mathbf{x}, 0)|^2 = \rho_n^b(\mathbf{x}, 0), \quad (2.8)$$

thus a bound state has an infinite lifetime.

In contrast, resonances are not solutions of the TISE in the usual Hermitian formalism and thus cannot be represented by single discrete states. They can be calculated in the Hermitian formalism by solving the TDSE for the time evolution of wave packets, which are superpositions of a continuous range of eigenstates.

The possibility of a time-independent description for resonances can be understood by, e.g., considering the model problem of Klaiman and Gilary [15]. According to that, a one-dimensional potential well that supports a bound state is perturbed in a way that a potential barrier is formed, which creates a shape resonance. The wave packet that corresponds to the resonance remains localized for some time in the region where the previously bound state was confined (interaction region), although the system now has the energy to break up into subsystems. The long-time behavior of the resonance $|\Psi_n^r\rangle$ in the interaction region L can be approximated by an exponentially decaying time-dependent probability density [15]

$$|\Psi_n^r(x, t)\rangle = e^{-i(E_{R,n} - i\Gamma_n/2)t} |\Psi_n^r(x, t_0)\rangle \quad \text{for } |x| < L, \text{ and } t > t_0, \quad (2.9)$$

$$\rho_n^r(x, t) = |\Psi_n^r(x, t)|^2 = e^{-\Gamma_n t} |\Psi_n^r(x, t_0)|^2 = e^{-\Gamma_n t} \rho_n^r(x, t_0) \quad \text{for } |x| < L, \text{ and } t > t_0, \quad (2.10)$$

where t_0 and L are problem-dependent.

The decay of the resonance is a stochastic process, its rate is given by the resonance width Γ_n , which is the inverse of the average lifetime. From (2.9), one can see that the resonance behaves like a stationary state with complex energy $E_n^r = E_{R,n} - i\Gamma_n/2$. This property can be used to obtain the resonance as a discrete solution of the TISE by imposing outgoing boundary conditions (also called Siegert boundary conditions)

$$\Psi_n(x \rightarrow \pm\infty, t_0) = c e^{ik_n x}, \quad (2.11)$$

where c is a constant and k_n is the wavenumber ($k_n = \sqrt{2E_n}$). For decaying states, conditions $\text{Re}(k_n^r) > 0$ and $\text{Im}(k_n^r) < 0$ need to be fulfilled. Bound states are also solutions to the TISE with boundary conditions (2.11), but in that case conditions $\text{Re}(k_n^b) = 0$ and $\text{Im}(k_n^b) > 0$ need to be applied, in line with (2.6).

A very important difference from bound states is that the Siegert resonance wave function is not square-integrable. A solution to this problem is to calculate resonances by analytic continuation of the Hamiltonian into the complex plane or to apply a CAP. These transformations yield square-integrable resonance wave functions, that enables the description of resonances with techniques similar to bound state methods.

In the following sections, bound state methods are reviewed, then in Section 2.4 modifications needed for treating resonances with similar methods in the time-independent non-Hermitian framework are discussed.

2.2 Separation of nuclear and electronic motion

The molecular Hamiltonian can be written as the sum of the nuclear kinetic energy operator \hat{T}^n and the electronic Hamiltonian \hat{H}^e

$$\hat{H} = \hat{T}^n + \hat{H}^e \quad (2.12)$$

$$\hat{H}^e = \hat{T}^e + \hat{V}^{en} + \hat{V}^{ee} + \hat{V}^{nn} \quad (2.13)$$

where \hat{T}^e is the kinetic energy operator of the electrons, and potentials \hat{V} are the electron-nucleus (en), electron-electron (ee) and nucleus-nucleus (nn) Coulomb potentials

$$\hat{T}^n = - \sum_n^{N_n} \sum_\alpha \frac{1}{2M_n} \frac{\partial^2}{\partial R_{n\alpha}^2} \quad (2.14)$$

$$\hat{T}^e = - \sum_i^{N_e} \sum_\alpha \frac{1}{2} \frac{\partial^2}{\partial r_{i\alpha}^2} \quad (2.15)$$

$$\hat{V}^{en} = - \sum_i^{N_e} \sum_n^{N_n} \frac{Z_n}{|\mathbf{R}_n - \mathbf{r}_i|} \quad (2.16)$$

$$\hat{V}^{ee} = \sum_i^{N_e} \sum_{j<i}^{N_e} \frac{1}{|\mathbf{r}_i - \mathbf{r}_j|} \quad (2.17)$$

$$\hat{V}^{nn} = \sum_n^{N_n} \sum_{m<n}^{N_n} \frac{Z_n Z_m}{|\mathbf{R}_n - \mathbf{R}_m|} \quad (2.18)$$

\mathbf{R} , M , and Z denote nuclear coordinates, masses, and charges, while \mathbf{r} is used for electronic coordinates. N_n is the number of nuclei, N_e is the number of electrons, and α denotes dimensions x, y, z .

\hat{T}^e and \hat{V}^{en} can be written as a sum of one-electron operators \hat{h}_i

$$\hat{T}^e + \hat{V}^{en} = \sum_i^{N_e} \hat{h}_i, \quad (2.19)$$

$$\hat{h}_i = - \sum_\alpha \frac{1}{2} \frac{\partial^2}{\partial r_{i\alpha}^2} - \sum_n^{N_n} \frac{Z_n}{|\mathbf{R}_n - \mathbf{r}_i|}. \quad (2.20)$$

Within the Born-Oppenheimer (BO) approximation [18] the motion of the electrons and the nuclei can be separated, and the problem is divided into two lower-dimensional problems. In the first part of the calculation, the electronic SE is solved with nuclei fixed at certain positions \mathbf{R}

$$\hat{H}^e |\Psi_k^e(\mathbf{r}, \mathbf{R})\rangle = E_k^e(\mathbf{R}) |\Psi_k^e(\mathbf{r}, \mathbf{R})\rangle, \quad (2.21)$$

this is called the clamped-nuclei approximation. The electronic SE yields the electronic wave function $|\Psi_k^e\rangle$, and the electronic energy E_k^e of state k at a specific nuclear configuration. The surface formed by E_k^e as a function of \mathbf{R} is called the potential energy surface (PES), as it appears as the potential term that governs the motion of nuclei in the nuclear SE

$$(\hat{T}^n + E_k^e(\mathbf{R})) |\Psi_l^n(\mathbf{R})\rangle = E_{kl}(\mathbf{R}) |\Psi_l^n(\mathbf{R})\rangle, \quad (2.22)$$

where $|\Psi_l^n\rangle$ is the nuclear wave function. Thus in the BO approximation, the total energy can be determined by solving the nuclear SE (2.22), while the total wave function is given as the direct product of electronic and nuclear components

$$\Psi(\mathbf{r}, \mathbf{R}) = \Psi^e(\mathbf{r}, \mathbf{R}) \otimes \Psi^n(\mathbf{R}). \quad (2.23)$$

When the electronic states are well separated, they vary slowly with nuclear coordinates, and the coupling between nuclear and electronic motion can be completely neglected. However, the BO approximation breaks down when electronic states get close in energy. In that case, nuclear motion, usually molecular vibrations, can mix electronic states, so nuclear and electronic motion become coupled. In the so-called adiabatic basis of the electronic wave functions $|\Psi_k^e\rangle$, \hat{H}^e is diagonal, and the coupling is due to \hat{T}^n only.

$$\begin{aligned} \langle \Psi_k^e(\mathbf{r}, \mathbf{R}) \Psi_l^n(\mathbf{R}) | \hat{T}^n | \Psi_{k'}^e(\mathbf{r}, \mathbf{R}) \Psi_{l'}^n(\mathbf{R}) \rangle &= - \sum_{n\alpha} \frac{1}{2M_n} \langle \Psi_k^e(\mathbf{r}, \mathbf{R}) \Psi_l^n(\mathbf{R}) | \Psi_{k'}^e(\mathbf{r}, \mathbf{R}) \frac{\partial^2 \Psi_{l'}^n(\mathbf{R})}{\partial R_{n\alpha}^2} \rangle \\ &\quad - \sum_{n\alpha} \frac{1}{M_n} \langle \Psi_k^e(\mathbf{r}, \mathbf{R}) \Psi_l^n(\mathbf{R}) | \frac{\partial \Psi_{k'}^e(\mathbf{r}, \mathbf{R})}{\partial R_{n\alpha}} \frac{\partial \Psi_{l'}^n(\mathbf{R})}{\partial R_{n\alpha}} \rangle \\ &\quad - \sum_{n\alpha} \frac{1}{2M_n} \langle \Psi_k^e(\mathbf{r}, \mathbf{R}) \Psi_l^n(\mathbf{R}) | \frac{\partial^2 \Psi_{k'}^e(\mathbf{r}, \mathbf{R})}{\partial R_{n\alpha}^2} \Psi_{l'}^n(\mathbf{R}) \rangle. \end{aligned} \quad (2.24)$$

By integrating over electronic coordinates, (2.24) can be rewritten as

$$\begin{aligned} \langle \Psi_k^e(\mathbf{r}, \mathbf{R}) \Psi_l^n(\mathbf{R}) | \hat{T}^n | \Psi_{k'}^e(\mathbf{r}, \mathbf{R}) \Psi_{l'}^n(\mathbf{R}) \rangle &= - \sum_{n\alpha} \frac{1}{2M_n} \langle \Psi_l^n(\mathbf{R}) | \frac{\partial^2 \Psi_{l'}^n(\mathbf{R})}{\partial R_{n\alpha}^2} \rangle \delta_{kk'} \\ &\quad - \sum_{n\alpha} \frac{1}{M_n} \langle \Psi_l^n(\mathbf{R}) | g_{kk'}^{n\alpha} \frac{\partial \Psi_{l'}^n(\mathbf{R})}{\partial R_{n\alpha}} \rangle \\ &\quad - \sum_{n\alpha} \frac{1}{2M_n} \langle \Psi_l^n(\mathbf{R}) | h_{kk'}^{n\alpha} \Psi_{l'}^n(\mathbf{R}) \rangle. \end{aligned} \quad (2.25)$$

The first term in (2.25) contributes only to the diagonal elements with respect to electronic states. The interaction of different electronic states comes from the derivative (also called nonadiabatic) coupling matrix elements

$$g_{kk'}^{n\alpha} = \langle \Psi_k^e(\mathbf{r}, \mathbf{R}) | \frac{\partial \Psi_{k'}^e(\mathbf{r}, \mathbf{R})}{\partial R_{n\alpha}} \rangle, \quad (2.26)$$

$$h_{kk'}^{n\alpha} = \langle \Psi_k^e(\mathbf{r}, \mathbf{R}) | \frac{\partial^2 \Psi_{k'}^e(\mathbf{r}, \mathbf{R})}{\partial R_{n\alpha}^2} \rangle, \quad (2.27)$$

which are neglected in the BO approximation. h can be expressed using g (see, e.g., Reference [19]), and g , often referred to as the derivative coupling, can be written as

$$g_{kk'}^{n\alpha} = \frac{1}{E_{k'}^e(\mathbf{R}) - E_k^e(\mathbf{R})} \langle \Psi_k^e(\mathbf{r}, \mathbf{R}) | \frac{\partial \hat{H}^e}{\partial R_{n\alpha}} | \Psi_{k'}^e(\mathbf{r}, \mathbf{R}) \rangle, \quad (2.28)$$

which follows from differentiating (2.21) with respect to $R_{n\alpha}$. According to (2.28), the coupling and thus the probability of a nonadiabatic transition is higher for close lying PESs. At the crossing of two PESs, the derivative coupling diverges, which shows the breakdown of the BO approximation. Diverging couplings can be avoided by using a quasideiabatic basis which transfers the coupling from the kinetic term to the potential term [20]. This is the basis of linear vibronic coupling models, that have been developed

2.3. ELECTRONIC STRUCTURE METHODS FOR BOUND STATES

both for stable states [21] and resonances [22], and have been very successful in simulating vibronic transitions. Possible applications of this model using CAP-EOM-CC methods are discussed in Section 3.5. The quasidiabatic representation is also used in Section 2.5.1 to derive the crossing conditions of two stable and of two metastable states.

The BO approximation facilitates the description of molecular systems significantly, still, the electronic SE can be solved for the simplest systems only. For most applications, further approximations have to be made. In the following sections, approximate methods for solving the electronic SE for bound states and for resonances are discussed. For the sake of simplicity, the superscript 'e' will be omitted. The characteristics of the PES and its implications on nuclear motion are discussed in Section 2.5.

2.3 Electronic structure methods for bound states

2.3.1 The Hartree-Fock method

An approximate method for solving the electronic TISE, and the basis for other more accurate methods, is the Hartree-Fock (HF) method [23]. The wave function is approximated by a single Slater determinant in this case, which is a normalized and antisymmetrized linear combination of products of spin-orbitals $|p\rangle$ (called molecular orbitals, MOs, in the case of molecules). In the HF method every electron interacts with the average field of the other electrons, thus the correlation (instantaneous interaction) of electrons is not considered.

According to the variational principle, the expectation value of \hat{H} calculated with an approximate wave function Φ is higher or equal to the exact ground state energy E_0^{exact}

$$E_0^{\text{exact}} \leq \frac{\langle \Phi | \hat{H} | \Phi \rangle}{\langle \Phi | \Phi \rangle}, \quad (2.29)$$

where equality holds only when $\Phi = \Psi_0^{\text{exact}}$. The HF method is variational: the MOs are optimized in order to get the best approximation of E_0^{exact} with Φ as a single Slater determinant.

The MOs are expanded in terms of basis functions $|\mu\rangle$, which are usually atom-centered Gaussians

$$|p\rangle = \sum_{\mu} C_{\mu p} |\mu\rangle, \quad (2.30)$$

where $C_{\mu p}$ are elements of the MO coefficient matrix \mathbf{C} . Here and in the following, MO indices i, j, \dots are used for occupied orbitals, a, b, \dots for virtual orbitals, while p, q, \dots denote general orbitals. In the basis of the atomic orbitals (AOs), denoted by greek letters, the HF energy can be expressed as:

$$E_{\text{HF}} = \frac{1}{2} \sum_{\mu\nu} D_{\mu\nu}^{\text{HF}} (h_{\mu\nu} + F_{\mu\nu}) + V_{\text{nn}}. \quad (2.31)$$

The density matrix D^{HF} is built from the expansion coefficients

$$D_{\mu\nu}^{\text{HF}} = \sum_i C_{\mu i}^* C_{\nu i}. \quad (2.32)$$

The one-electron integrals in the AO basis are given by $h_{\mu\nu} = \langle \mu | \hat{h}_1 | \nu \rangle$, and the Fock matrix \mathbf{F} has the form

$$F_{\mu\nu} = h_{\mu\nu} + \sum_{\sigma\rho} D_{\sigma\rho}^{\text{HF}} \langle \mu\sigma || \nu\rho \rangle, \quad (2.33)$$

where $\langle \mu\sigma || \nu\rho \rangle = \langle \mu\sigma | \frac{1}{|\mathbf{r}_1 - \mathbf{r}_2|} | \nu\rho \rangle - \langle \mu\sigma | \frac{1}{|\mathbf{r}_1 - \mathbf{r}_2|} | \rho\nu \rangle$ are antisymmetrized two-electron integrals of AOs.

The MO coefficients are determined from the Roothaan-Hall equations

$$\mathbf{FC} = \mathbf{SC}\epsilon, \quad (2.34)$$

where \mathbf{S} is the overlap matrix $S_{\mu\nu} = \langle \mu | \nu \rangle$ and ϵ is a diagonal matrix that contains the orbital energies. These equations have to be solved iteratively, because \mathbf{F} depends on \mathbf{C} through the density matrix. The computational cost of a HF calculation scales with the number of basis functions N_{bf} as N_{bf}^4 .

The HF method is a good approximation if a single determinant wave function can describe the system correctly. The determinants created by all possible occupations of MOs form a complete set, which means that the exact wave function can be given as the linear combination of all possible determinants. Thus, to improve upon the HF method, one needs to include more determinants in the wave function. Dynamic correlation is associated with a wave function that has a single dominant determinant and a large number of additional determinants with small weights. Inclusion of such additional determinants can be done by the coupled-cluster (CC) method, for example. In the case of static correlation, the electronic state in question can be well described by a few determinants with similar weights. A method that includes static correlation is essential for, e.g., the description of radicals and bond-breaking situations. The distinction between the two types is not unambiguous, and in many situations both are needed.

Approximate quantum chemistry methods are ideally size-consistent and size-extensive. Size-consistency means that a system consisting of non-interacting subsystems is computed to have the same energy as the sum of the energies of the individual subsystems [24]. Size-extensivity means that the energy scales properly with the size of the system [25]. By using an appropriate parametrization of the wave function, like in the case of the CC method, one can ensure that even approximate methods are size-consistent and size-extensive.

2.3.2 The coupled-cluster method

In the CC method [26] the wave function is generated by an exponential excitation operator acting on a reference wave function, which is usually chosen as the HF wave function $|\Phi_{\text{HF}}\rangle$

$$|\Psi_{\text{CC}}\rangle = e^{\hat{T}} |\Phi_{\text{HF}}\rangle. \quad (2.35)$$

The excitation operator \hat{T} is called the cluster operator and it creates all possible singly, doubly, etc. excited determinants from the reference determinant

$$\hat{T} = \sum_{m=1}^M \hat{T}_m = \sum_a \sum_i t_i^a \hat{a}_a^\dagger \hat{a}_i + \frac{1}{4} \sum_{a,b} \sum_{i,j} t_{ij}^{ab} \hat{a}_a^\dagger \hat{a}_i \hat{a}_b^\dagger \hat{a}_j + \dots = \sum_n t_n \hat{\tau}_n, \quad (2.36)$$

where \hat{a}^\dagger are second-quantized creation operators [27], \hat{a} are annihilation operators, and t are the CC amplitudes. $\{t_n\}$ and $\{\tau_n\}$ are introduced to simplify the notation of amplitudes $\{t_i^a, t_{ij}^{ab}, \dots\}$ and excitation operators $\{\hat{a}_a^\dagger \hat{a}_i, \hat{a}_a^\dagger \hat{a}_i \hat{a}_b^\dagger \hat{a}_j, \dots\}$, respectively.

If \hat{T} includes all possible orders of excitation, i.e. M is chosen as the number of electrons in the system, the CC wave function is the exact wave function. When truncating \hat{T} at a given order of excitation, e.g. as $\hat{T} = \hat{T}_1 + \hat{T}_2$, called singles and doubles approximation (CCSD) [28], the wave function still includes higher excited determinants due to the exponential operator in (2.35). Truncated CC wave functions can be systematically improved towards the exact solution by including higher excitations in

2.3. ELECTRONIC STRUCTURE METHODS FOR BOUND STATES

\hat{T} . This, however, entails a considerable increase in computational cost. CCSD has an N_{bf}^6 scaling [28], which allows it to be used for intermediate-sized systems. However, the next level method, CCSDT ($\hat{T} = \hat{T}_1 + \hat{T}_2 + \hat{T}_3$) [29, 30], scales as N_{bf}^8 , thus it is applicable only to small systems.

The unknown quantities, the amplitudes are determined by solving the CC equations

$$\langle \Phi_n | \bar{H} | \Phi_{\text{HF}} \rangle = 0, \quad (2.37)$$

for all determinants $|\Phi_n\rangle = \tau_n |\Phi_{\text{HF}}\rangle$ that are excited up to order M . Thus, in the case of CCSD, projection is performed only on singly and doubly excited determinants. \bar{H} is the similarity transformed Hamiltonian which can be expanded in terms of commutators as

$$\bar{H} = e^{-\hat{T}} \hat{H} e^{\hat{T}} = \hat{H} + [\hat{H}, \hat{T}] + \frac{1}{2!} [[\hat{H}, \hat{T}], \hat{T}] + \dots \quad (2.38)$$

$$= \hat{H} + (\hat{H}\hat{T})_c + \frac{1}{2!} ((\hat{H}\hat{T}_c)\hat{T})_c + \dots = (\hat{H} e^{\hat{T}})_c \quad (2.39)$$

where the subscript 'c' indicates that only connected terms survive. The expansion truncates after the fifth term [31], because \hat{H} contains only one-, and two-electron operators, thus can be connected to maximally four \hat{T} operators. The presence of only connected terms ensures size extensivity.

The CC equations (2.37) have to be solved iteratively to obtain amplitudes up to order M . After that, the CC energy can be calculated as

$$E_{\text{CC}} = \langle \Phi_{\text{HF}} | \bar{H} | \Phi_{\text{HF}} \rangle = E_{\text{HF}} + \sum_{i < j} \sum_{a < b} (t_{ij}^{ab} + t_i^a t_j^b - t_i^b t_j^a) \langle ij || ab \rangle, \quad (2.40)$$

where only singles and doubles amplitudes contribute. Higher order amplitudes contribute to the energy indirectly, through the CC equations (2.37).

2.3.3 The equation-of-motion coupled-cluster method

When calculating energy differences between electronic states, the most straightforward method seems to be calculating the two states separately and then taking their energy difference. However, excitation energies (ionization and attachment energies as well) can be very small compared to the total energy of the system, and are size-intensive. This means that they should be the same in a noninteracting supersystem AB as in the subsystem A (if B is not excited) [32], so calculating them accurately from total energies becomes even more difficult in larger systems. For the systems investigated in this work, attachment energies are under a few electronvolts, while total energies are between 10^4 - 10^6 eV. It is thus advantageous to calculate the energy difference directly: this yields a more balanced description of states.

The equation-of-motion coupled-cluster (EOM-CC) method [33–35] can be used to study multiple states simultaneously and calculate energy differences directly. According to this approach, target states $|\Psi_k\rangle$ are generated from the CC reference state by the excitation operator \hat{R}

$$|\Psi_k\rangle = \hat{R}_k |\Psi_{\text{CC}}\rangle, \quad (2.41)$$

where

$$\hat{R}_k = \sum_m^M \hat{R}_m^k = \sum_n r_n^k \hat{\rho}_n, \quad (2.42)$$

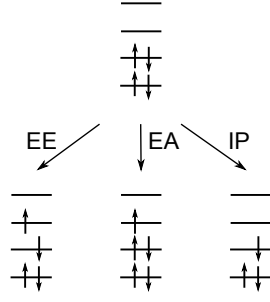


Figure 2.1: Variants of EOM-CC methods

and the choice of operators $\hat{\rho}_n$ determines what type of target states are created. Possible choices of $\hat{\rho}_n$ are, for example,

$$\{\hat{\rho}_n^{\text{EE}}\} = \{\hat{1}, \hat{a}_a^\dagger \hat{a}_i, \hat{a}_b^\dagger \hat{a}_j \hat{a}_a^\dagger \hat{a}_i, \dots\}, \quad (2.43)$$

$$\{\hat{\rho}_n^{\text{EA}}\} = \{\hat{a}_a^\dagger, \hat{a}_b^\dagger \hat{a}_j \hat{a}_a^\dagger, \dots\}, \quad (2.44)$$

$$\{\hat{\rho}_n^{\text{IP}}\} = \{\hat{a}_i, \hat{a}_b^\dagger \hat{a}_j \hat{a}_i, \dots\}. \quad (2.45)$$

If $\hat{\rho}_n$ operators conserve the number of electrons, thus consist of the same number of creation and annihilation operators (2.43), excited states are generated (see also Figure 2.1). This approach can be used for calculating excitation energies and is called EOM-EE [36]. In the electron attachment (EOM-EA) variant [37], $\hat{\rho}_n$ operators consist of one more creation operator than annihilation operator (2.44), and consequently the target states are electron attached states (Figure 2.1). In the ionization potential (EOM-IP) [38] variant, there is one extra annihilation operator in each $\hat{\rho}_n$ (see (2.45)), which creates singly ionized states in this case (Figure 2.1).

$|\Psi_k\rangle$ are the right eigenfunctions of \hat{H} corresponding to eigenvalue E_k^{EOM} , which is the energy of the excited/ionized/electron attached state

$$\hat{H}|\Psi_k\rangle = E_k^{\text{EOM}}|\Psi_k\rangle. \quad (2.46)$$

E_k^{EOM} are also eigenvalues of \bar{H} with eigenfunctions $|R_k\rangle = \hat{R}_k|\Phi_{\text{HF}}\rangle$

$$\bar{H}|R_k\rangle = E_k^{\text{EOM}}|R_k\rangle. \quad (2.47)$$

The excitation/ionization/attachment energy $\Delta E_k^{\text{EOM}} = E_k^{\text{EOM}} - E_{\text{CC}}$ is calculated by diagonalizing $\bar{H} - E_{\text{CC}}$ expressed in the basis of determinants

$$\sum_n \langle \Phi_m | (\bar{H} - E_{\text{CC}}) | \Phi_n \rangle r_n^k = \Delta E_k^{\text{EOM}} r_n^k. \quad (2.48)$$

Due to the non-Hermitian nature of \bar{H} , its right and left eigenfunctions differ. The right eigenvectors are given by (2.47), while the left eigenvectors are

$$\langle L_k | \bar{H} = \langle L_k | E_k^{\text{EOM}}, \quad (2.49)$$

with $\langle L_k | = \langle \Phi_{\text{HF}} | \hat{L}_k$, and the de-excitation operator \hat{L}_k defined as

$$\hat{L}_k = \sum_m^M \hat{L}_m^k = \sum_n l_n^k \hat{\rho}_n^\dagger. \quad (2.50)$$

2.4. NON-HERMITIAN DESCRIPTION OF RESONANCES

Right and left eigenfunctions are related by the biorthogonality condition

$$\langle L_k | R_{k'} \rangle = d \delta_{kk'}, \quad (2.51)$$

where d is usually chosen as 1. For the calculation of ΔE_k^{EOM} , only the right or left EOM amplitudes have to be determined. However, for the calculation of properties, like gradients, both are needed.

The dimension of the matrix to be diagonalized according to (2.48) is generally very large due to the large number of determinants even for truncated methods and moderate basis sets. Full diagonalization is therefore usually not possible, but generally only a small number of states are of interest anyway. The Davidson algorithm [39] modified for non-Hermitian matrices [40] can be used to calculate the lowest or some selected eigenstates iteratively.

An important advantage of EOM-CC methods is that the energy difference between the initial and the target state is calculated directly, this ensures a balanced description of the states that does not exist in methods where they are calculated independently. Also, the simultaneous calculation of several target states enables the calculation of coupling terms between interacting states. Furthermore, if the same level of truncation is used in \hat{R} as in \hat{T} , then ΔE_k^{EOM} is size-intensive [32].

The scaling of truncated EOM-CC methods is the same as of truncated CC methods, e.g. N_{bf}^6 for EOM-CCSD, in which the EOM part scales as N_{bf}^6 for EE, or N_{bf}^5 for EA and IP variants. The cost of the calculations can be reduced if second order Møller-Plesset perturbation theory (MP2) [41] is used instead of CCSD for the reference state. The EOM approach is then performed in a similar way as for EOM-CCSD. This approximate method is called EOM-CCSD(2) or also EOM-MP2, and scales as N_{bf}^5 for EOM-EA/IP-CCSD(2) and N_{bf}^6 for the EE variant [42]. EOM-CCSD performs well for states dominated by singly excited determinants, but higher level terms of \hat{R} are needed for describing multiply excited states.

2.4 Non-Hermitian description of resonances

In Section 2.1 it was shown, that by imposing outgoing boundary conditions on the solutions of the TISE, a decaying resonance arises as a discrete state with complex energy

$$E_n = E_{\text{R},n} - \frac{i}{2}\Gamma_n, \quad (2.52)$$

where E_{R} is the resonance position and Γ is the resonance width. This means that the TDSE does not need to be solved for a wave packet for describing resonances, it is enough to calculate only a single state in the non-Hermitian formalism. However, the exponential divergence of the wave function (2.11) poses a difficulty, and it is beneficial to transform the wave function into a square-integrable form and utilize the standard methods and tools of Section 2.3, developed for bound states, for handling resonances as well.

This transformation can be done by analytic continuation of the Hamiltonian into the complex plane. According to the complex scaling (CS) method [43–46], the coordinates of the Hamiltonian are scaled by a complex number $e^{i\theta}$. With the correct choice of the scaling parameter θ [16], the resulting Hamiltonian has the same bound state spectrum, but continuum states are rotated into the complex plane revealing discrete resonance states. It can easily be seen, that when scaling (2.11)

$$\Psi_n^\theta(x \rightarrow \pm\infty, t_0) = ce^{ik_n e^{i\theta} x} = ce^{i|k_n| e^{-i\phi} e^{i\theta} x} = ce^{i|k_n| \cos(\theta-\phi)x} e^{-|k_n| \sin(\theta-\phi)x}, \quad (2.53)$$

the transformed wave function is square-integrable if $0 < \theta - \phi < \pi$.

Scaling the Hamiltonian can be done either by using real basis functions and scaling the coordinates of the Hamiltonian operator (usually referred to as direct CS), or by using complex basis functions and leaving the Hamiltonian operator unchanged (CBF method) [47]. Adding a complex absorbing potential (CAP) [48, 49] to the Hamiltonian also yields square integrable resonance states [49], and it is known [50, 51] that specific forms of CAP are related to exterior complex scaling [52]. The CAP method is discussed in detail in Section 2.4.1.

Application of the direct CS method for molecular systems is more complicated than for atoms, because it is not straightforward to combine CS with the BO approximation [16]. In principle, both the electronic and the nuclear coordinates should be scaled, but that would lead to unphysical complex-valued structural parameters. On the other hand, the electronic coordinates cannot be scaled without scaling the nuclear coordinates as well, since the electron-nucleus potential is not analytic in the entire space. This problem can be solved by performing the complex scaling only in the external regions (exterior scaling and smooth exterior scaling) [52], or by using the complex scaled back-transformation approach [53]. In the latter approach both the electronic and nuclear coordinates are scaled, the electronic SE is solved for fixed nuclear coordinates, then the nuclear coordinates are rotated back to the real axis.

CBF and CAP methods do not have the problems of the direct CS method when applying the BO approximation, with these methods nuclear coordinates are always real. The electronic energy of resonances is complex-valued within the non-Hermitian formalism, which leads to complex-valued PESs (CPESs) for resonances. While CAP- and CBF-HF methods yield smooth CPESs, the width of the resonance does not go to zero at the crossing with its parent state (where it should become stable), and it was proposed that correlation methods are needed for a consistent CPES [54–56]. Combining the CAP or CBF method with the EOM-CCSD approach, a balanced description of resonance states and parent states is achieved, and consequently these methods yield smooth and consistent CPESs [57, 58].

Due to the non-Hermiticity of the CS or CAP Hamiltonian, the c-product [16, 59]

$$(\Phi_i | \Phi_j) = \int \Phi_i(\tau) \Phi_j(\tau) d\tau \quad (2.54)$$

is used instead of the scalar product (2.5), thus complex conjugation is not performed on the bra state. The c-product yields a complete set of orthogonal eigenfunctions for the CS or CAP Hamiltonian if there are no degeneracies. However, the c-norm can be zero for nonzero functions (self-orthogonality) at degeneracies. In that case, the Hamiltonian is defective and its spectrum is no longer complete. The self-orthogonality phenomenon and non-Hermitian degeneracies, called exceptional points are discussed in Section 2.5 and investigated in Publication 4 (Section 3.4).

For a c-normalizable trial wave function Φ , the complex variational principle is valid [59], thus

$$\bar{E} = \frac{(\Phi | \hat{H}_{\text{cx}} | \Phi)}{(\Phi | \Phi)}, \quad (2.55)$$

where \hat{H}_{cx} denotes a CS or CAP Hamiltonian, is a stationary approximation of the true complex-valued resonance energy, which justifies the use of standard methods and tools for resonances. However, in contrast to the standard variational principle (2.29), here \bar{E} is not an upper bound for the energy of the resonance.

2.4. NON-HERMITIAN DESCRIPTION OF RESONANCES

To understand how the CAP-EOM-CC method can be used for studying processes involving resonances, in the next sections the CAP approach and CAP-EOM-CC methods are discussed in more detail.

2.4.1 The complex absorbing potential method

In the CAP method, an artificial complex potential ($-i\eta W$) is added to the Hamiltonian

$$\hat{H}(\eta) = \hat{H} - i\eta W, \quad (2.56)$$

where η is called the CAP strength parameter. Originally, CAPs were introduced in time-dependent calculations to reduce reflections of the wavepacket from the edges of numerical grids [60]. The role of the CAP in calculating resonance energies is to change the boundary conditions, and thus turn resonances into discrete states [48, 49, 61]. In order to avoid large perturbations to the system, the CAP is introduced only in the outer region and is zero close to the molecule. Requirements for the form of the CAP to produce discrete resonance states were described by Riss and Meyer [49]. Usually W is chosen as a purely real, box-shaped quadratic potential

$$W = \sum_{\alpha} W_{\alpha}, \quad \alpha = x, y, z,$$

$$W_{\alpha} = \begin{cases} 0 & \text{if } |r_{\alpha} - o_{\alpha}| \leq r_{\alpha}^0, \\ (|r_{\alpha} - o_{\alpha}| - r_{\alpha}^0)^2 & \text{if } |r_{\alpha} - o_{\alpha}| > r_{\alpha}^0, \end{cases}$$

where r_{α}^0 are the CAP onset or box size parameters. o is the CAP origin, and in this work it is chosen as the center of nuclear charges

$$o_{\alpha} = \frac{\sum_n^{N_n} R_{n,\alpha} Z_n}{\sum_n^{N_n} Z_n}. \quad (2.57)$$

In a complete basis, a CAP of infinitesimal strength would turn the resonance into a discrete state without introducing perturbation to the system, thus the true resonance energy would be given in the limit $\eta \rightarrow 0$ [49, 51]. In a finite basis set this no longer applies, and the total error, which comes from the incomplete representation of the CAP by the finite basis set and the perturbation due to the CAP, has to be minimized. To get the best estimate for the resonance energy from a finite basis set calculation, the energy is calculated at a finite, so-called optimal η value (η_{opt}). A formula proposed by Riss and Meyer [49] for the calculation of η_{opt} is

$$|\eta \, dE/d\eta| = \min, \quad (2.58)$$

which requires the calculation of the energy at different η values. This involves usually a large number of calculations (typically of the order 10-100), as the magnitude of η_{opt} varies greatly with system, basis set, and box size, and thus cannot be estimated in advance. Also, the calculated η trajectories, $E(\eta)$, can have quite different shapes. It can happen that there are multiple parameter values that fulfill (2.58) or there are none at all. A careful investigation of the effects of the CAP parameters by Zuev et al. [62] showed that results for anionic resonances vary significantly with the applied box size. It was concluded that for these systems, if box size parameters are chosen as the spatial extent of the wave function of the neutral molecule $\sqrt{\langle \alpha^2 \rangle}$, the CAP is well-represented and bound states are perturbed minimally.

With the following correction scheme the perturbation due to the CAP can be removed in first order of η [49, 63]:

$$U = E - \eta \frac{dE}{d\eta}. \quad (2.59)$$

The corrected (also called de-perturbed) energy U was shown to be less sensitive to the choice of box size parameters [62, 63].

In the CAP method the resonance is a discrete state with a square-integrable wave function. This enables its combination with regular electronic-structure methods, that have been developed for bound states. The CAP method has been implemented for density-functional theory [64], algebraic diagrammatic construction [65, 66], multireference configuration-interaction [67, 68], multiconfigurational quasidenerate perturbation theory [69], symmetry-adapted-cluster configuration-interaction [70] (SAC-CI) (which is similar to EOM-CC), and EOM-CC [62, 71] methods. These introduce different levels of static and dynamic electron correlation, and have different computational cost, thus can be used accordingly.

2.4.2 Complex absorbing potential coupled-cluster methods

CAP-EOM-CC methods can be created by introducing the CAP either at the HF level or at the CC level [62, 71]. According to the implementation of Zuev et al. [62], which is used in this work, a CAP-HF calculation is performed first. The difference from regular HF is that now the c-product (2.54) is used instead of the scalar product (2.5), so that the variational principle is still valid in the CAP case [59]. Due to the use of the c-product, routines for real matrices have to be replaced by routines for general matrices. Solving the Roothaan-Hall equations (2.34) with a modified Fock matrix that contains the CAP results in complex MO coefficients and complex CAP-HF energy, that depend on the CAP parameters. AO integrals are real-valued, but transformation to the MO basis with complex coefficients results in complex MO integrals. The CC reference state is computed by solving the CC equations (2.37) which yield complex amplitudes. Usually a stable state is chosen as the CC reference state and resonance states are created by the EOM methods. In this case, the CAP-HF and CAP-CC energies have an imaginary part only because bound states are perturbed by the finite CAP. Resonances are then calculated from the eigenvalue equation of \bar{H} in a similar way as in (2.48), using the Davidson algorithm [39] modified for complex non-Hermitian matrices [62]. The resulting EOM amplitudes are also complex. The CAP-EOM-CC energy is calculated for a range of η values and η_{opt} is then determined by (2.58). The resonance position and width are given by the real and imaginary parts of the energy at the CAP strength value η_{opt} .

Biorthonormalization of left and right eigenstates according to the c-product (2.54) leads to the following conditions for the EOM amplitudes

$$\text{Re}(L_k | R_{k'}) = \sum_n (\text{Re}(l_n^k) \text{Re}(r_n^{k'}) - \text{Im}(l_n^k) \text{Im}(r_n^{k'})) = \delta_{kk'}, \quad (2.60)$$

$$\text{Im}(L_k | R_{k'}) = \sum_n (\text{Re}(l_n^k) \text{Im}(r_n^{k'}) + \text{Im}(l_n^k) \text{Re}(r_n^{k'})) = 0. \quad (2.61)$$

CAP-EOM-CC methods have the same scaling of the computational cost as regular EOM-CC methods, but the prefactor is larger due to the complex algebra applied, and multiple calculations are needed to determine η_{opt} . Also, storage requirements are two times larger due to the complex quantities. So far CAP-EOM-CCSD [62, 71], CAP-EOM-CCSD(2) and the non-iterative triples approximation CAP-EOM-CCSD(T)(a)* [72] have been implemented.

2.4.3 Characterization of resonances

For correlated wave functions ionization/electron attachment can involve multiple MOs. Dyson orbitals are one-electron quantities that can be used to characterize ionized or electron attached states [73, 74].

For (auto)ionizing states the Dyson orbital (Φ^d) can be interpreted as the wave function of the leaving electron. It is calculated as the overlap between N_e and $N_e - 1$ electron wave functions, so in the case of an anionic shape resonance, the overlap of the anionic resonance wave function and the wave function corresponding to its decay channel

$$\Phi^d(1) = \sqrt{N_e} \int \Psi^{N_e}(1, \dots, N_e) \Psi^{N_e-1}(2, \dots, N_e) d2 \dots dN_e. \quad (2.62)$$

2.5 Special points on potential energy surfaces

Within the BO approximation, the nuclear and electronic motions are separated, and by solving the electronic SE, a PES is formed which affects the motion of the nuclei (see Section 2.2). With the help of non-Hermitian transformations like complex scaling, adding a complex absorbing potential or using complex basis functions, resonances can be treated as discrete, square-integrable states with complex energy (see Section 2.4). The CPES of a resonance represents the dependence of the position and the width of a resonance on nuclear coordinates.

In Section 2.2, it was discussed, that adiabatic electronic states can mix due to vibrations, and transition is most probable near intersections of the interacting surfaces. The interaction between different resonances and between a resonance and its parent state plus a free electron can result in interesting phenomena like dissociative electron attachment [8, 9, 11], and can explain electron energy loss or photoelectron spectra [75–77].

The dimensionality of the CPES grows quickly with the size of the system under consideration: the number of nuclear degrees of freedom N is equal to $3N_n - 6$ for nonlinear molecules, and $3N_n - 5$ for linear molecules. This means that studying the CPES can become quite complicated for polyatomic systems. However, there are special points on the CPES, such as minima (equilibrium structures) and surface crossings (see Figure 2.2) that can be used to make predictions for the nuclear motion.

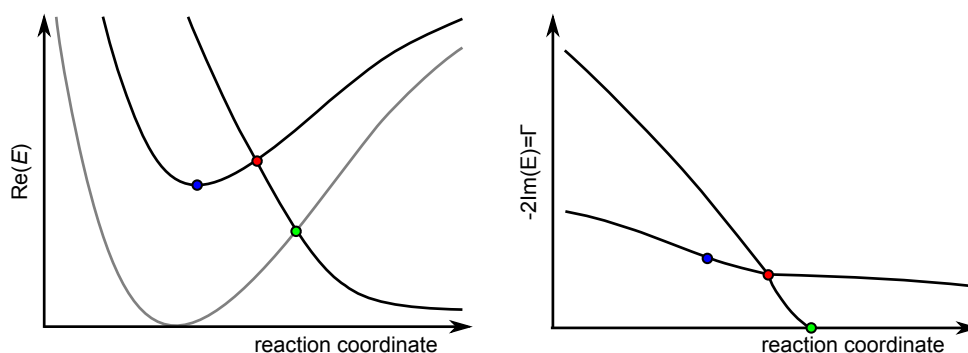


Figure 2.2: Sections of multidimensional (C)PESs corresponding to two metastable states (black curves) and their parent state (gray curve) along a fictional reaction coordinate. Special points on these surfaces are resonance equilibrium structures (blue dot), exceptional points between two resonances (red dot), and crossings between the resonance and its parent state (green dot). After crossing its parent state, the resonance becomes a stable state with zero resonance width.

Molecules trapped in minima can be subject to electron loss for a longer time than those that dissociate. Resonance-resonance crossings, called exceptional points (EPs) [78] increase the probability of nonadiabatic transitions between two states, which can lead to new pathways for deactivation [22, 79]. The position of crossings between a resonance and its parent state is also interesting for deactivation pathways, since, after crossing its parent state the resonance becomes a stable state, and will no longer be subject to autodetachment. This type of crossing is important for estimating the activation energy for DEA routes [80, 81], which can lead to formation of stable anionic fragments. It was proposed [82], that at this type of crossings a low-energy electron can get attached to a neutral molecule with high probability. Nonadiabatic coupling between the anionic resonance state and the parent state + free electron state might also become important in the autoionization process [82–84]. Experiments suggest that this kind of coupling has a noticeable effect on the recorded electron energy loss and photoelectron spectra [75–77].

These special points can be located on multidimensional CPESs efficiently by applying analytic energy gradients (see Section 2.5.2), so it is advantageous if an analytic gradient can be defined for the method to be applied for molecular resonances. It is also important to have a balanced treatment of states, as a small shift of a CPES can affect the position of crossings strongly and can lead to different conclusions about the decay mechanism.

2.5.1 Crossing conditions

The derivative coupling introduced in Section 2.2 enables the transition from one adiabatic electronic state to another. It depends on the inverse of the energy difference of the states (see (2.28)), so when the separation of states is small, there is a high probability of transition. It is thus important to locate points where the surfaces cross. By learning more about the number and the nature of conditions that need to be fulfilled to arrive at a crossing, efficient methods can be constructed for locating intersections.

For the derivation of the crossing conditions of two states, it is advantageous to switch to a (quasi)diabatic basis. In the diabatic basis the nuclear kinetic energy is diagonal and the coupling is through the potential only. Complete diabatization is not possible, but the strongly interacting states can be decoupled from the other states by using a quasidiabatic representation [19, 20]. In the case of two coupled quasidiabatic states, the nuclear kinetic energy is approximately diagonal and the electronic Hamiltonian describes the interaction of the two states

$$\mathbf{H} = \begin{pmatrix} \epsilon_1 & \omega \\ \omega & \epsilon_2 \end{pmatrix}, \quad (2.63)$$

where $\epsilon_{1,2}$ are the diabatic energies and ω is the diabatic coupling between the two states. The eigenvalues of matrix \mathbf{H} are:

$$E_{1,2} = \frac{\epsilon_1 + \epsilon_2}{2} \pm \frac{\sqrt{(\epsilon_1 - \epsilon_2)^2 + 4\omega^2}}{2}. \quad (2.64)$$

In the case of two interacting bound states, the diabatic energies and coupling are real-valued, so the conditions for degeneracy are: $\epsilon_1 - \epsilon_2 = 0$ and $\omega = 0$ [85, 86]. Thus the states can be degenerate in $N - 2$ dimensions, and the degeneracy is lifted in the so called branching plane [87]. This type of crossing is called a conical intersection (CI) due to the double-cone shape of the PESs in the branching plane (Figure 2.3). The energy gap of the two states is linear close to the CI. At the CI only the eigenvalues coalesce, the wave functions of the two states remain orthogonal. The minimum-energy crossing point (MECP) of two interacting states is of special importance in excited state processes, where its accessibility determines the

2.5. SPECIAL POINTS ON POTENTIAL ENERGY SURFACES

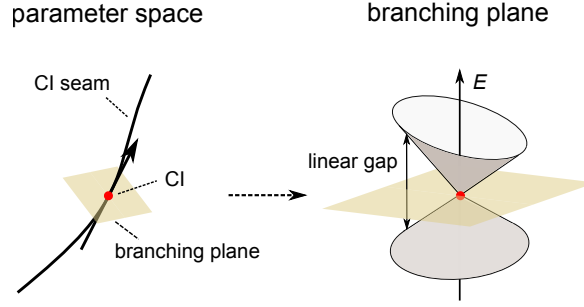


Figure 2.3: Hermitian degeneracy seam of interacting bound states in a 3-dimensional parameter space and behavior of the eigenvalues in the branching plane.

probability of radiationless decay, and its geometry helps in finding the vibrational modes that are most important in the transition [88].

When describing interacting resonances in the non-Hermitian formalism, matrix \mathbf{H} of (2.63) is complex-valued. The degeneracy of real and imaginary parts of the energy is called an exceptional point (EP). At this point, the two conditions that have to be fulfilled [79, 89] are

$$\operatorname{Re}(\sqrt{(\epsilon_1 - \epsilon_2)^2 + 4\omega^2}) = 0, \quad (2.65)$$

$$\operatorname{Im}(\sqrt{(\epsilon_1 - \epsilon_2)^2 + 4\omega^2}) = 0. \quad (2.66)$$

This means that there can be an $N - 2$ dimensional EP seam. From the EP seam, two $N - 1$ dimensional degeneracy seams depart (Figure 2.4): one of the real parts, which is defined by the condition (2.65), and one of the imaginary parts defined by (2.66). The energy gap is now a square-root function of the distance from the EP in its vicinity. Due to the topology of the EP, when encircling the EP, it is possible to arrive at a state different from the initial state [90–92]. For other interesting properties of EPs see, e.g., References [93–97].

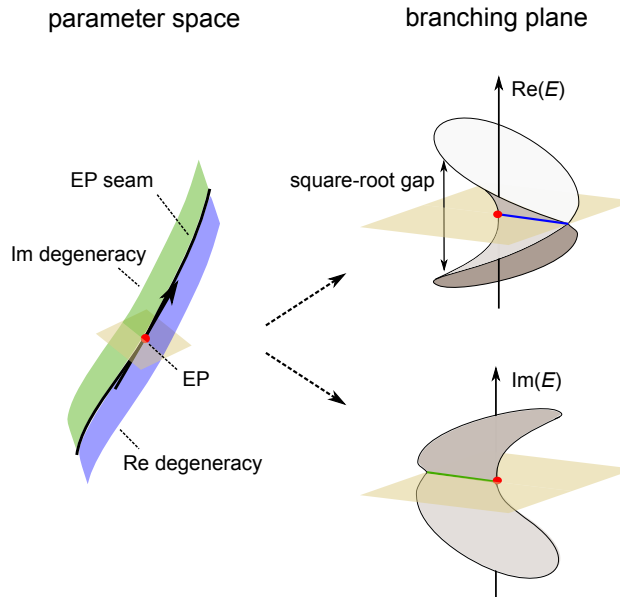


Figure 2.4: Non-Hermitian degeneracy seam of interacting resonances in a 3-dimensional parameter space and behavior of the eigenvalues in the branching plane.

In contrast to a CI of bound states, at an EP the Hamiltonian becomes defective as the two eigenfunctions coalesce. The wave function is self-orthogonal at the EP, thus wave function amplitudes diverge. This behavior can be utilized to check if an EP is in the vicinity by calculating the phase rigidity [98–101], which is the c -norm divided by the regular norm for a given state. In Publication 4 (Section 3.4), the phase rigidity for truncated CAP-EOM-CC methods was defined, and its behavior near EPs was studied. The location of EPs, more specifically the location of the minimum-energy EP (MEEP) and its accessibility is interesting for nonadiabatic processes involving resonances. The nonadiabatic coupling is singular both at CIs and at EPs, so these points act as funnels between (C)PESs. A method for locating EPs and MEEPs for autoionizing resonances was presented in Publication 4 (Section 3.4).

For states that have a different number of electrons, the coupling term ω of (2.63) is zero, and the only condition that has to be fulfilled for a degeneracy is that the energy difference is zero. Non-interacting states thus can be degenerate in $N - 1$ dimensions, and there is one coordinate along which the degeneracy of the states is lifted (see Figure 2.5). The location of crossings between an anionic state and its parent state is important for assessing the probability of a certain stabilization route. The MECP is of special interest, as its structure and energy can provide information about the accessibility of a specific dissociation route, for example. This type of crossing also comes up in the modeling of resonance and parent state + free electron interactions by EOM-CC in Publication 3 (Section 3.3).

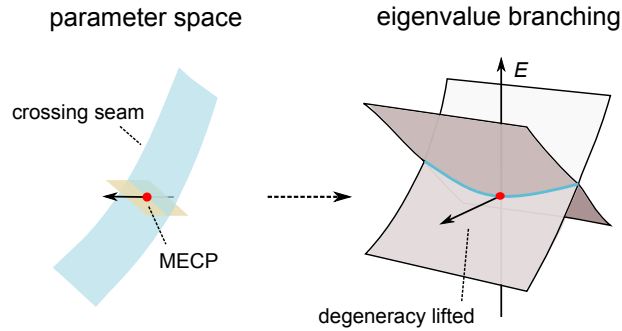


Figure 2.5: Degeneracy seam of non-interacting states in a 3-dimensional parameter space and behavior of the eigenvalues in a plane orthogonal to the crossing seam.

2.5.2 Locating equilibrium structures and surface crossings

To locate equilibrium structures, exceptional points or crossing points on multidimensional surfaces efficiently, gradients of the relevant states are essential. In this section, it is discussed how the gradients can be used to find such points in the case of bound states, and what additional quantities are needed for fast optimization algorithms. Methods for resonances were presented in Publications 1, 3 and 4 (Sections 3.1, 3.3 and 3.4).

The electronic energy is a function of nuclear coordinates and can be expanded around a point \mathbf{R}_0 as

$$E_k(\mathbf{R}) = E_k(\mathbf{R}_0) + \mathbf{G}_k^T(\mathbf{R} - \mathbf{R}_0) + \frac{1}{2}(\mathbf{R} - \mathbf{R}_0)^T \mathbf{H}_k(\mathbf{R} - \mathbf{R}_0) + \dots, \quad (2.67)$$

where \mathbf{G}_k is the gradient vector, that consists of the first derivatives with respect to nuclear coordinates

$$G_{n\alpha}^k = \frac{dE_k}{dR_{n\alpha}}, \quad (2.68)$$

2.5. SPECIAL POINTS ON POTENTIAL ENERGY SURFACES

and \mathbf{H}_k is the Hessian matrix, which consists of second derivatives

$$H_{n\alpha, n'\alpha'}^k = \frac{d^2 E_k}{dR_{n\alpha} dR_{n'\alpha'}}. \quad (2.69)$$

For sake of simplicity we omit the index for electronic states (k) in the following, unless it is essential for understanding a method.

At stationary points \mathbf{G} is zero, and the sign of the eigenvalues of \mathbf{H} can be used to differentiate between minima and saddle points. Equilibrium structures are local minima, here all the eigenvalues of \mathbf{H} are positive, while transition states are first-order saddle points for which \mathbf{H} has one negative eigenvalue.

There are different optimization techniques for locating stationary points, the most well-known is the Newton-Raphson method. In this method, the expansion in (2.67) approximated to second order is differentiated, which yields the Newton-Raphson step $\mathbf{s}^i = \mathbf{R}^{i+1} - \mathbf{R}^i$ in iteration i as

$$\mathbf{s}^i = -(\mathbf{H}^i)^{-1} \mathbf{G}^i = \sum_j^{N_n} \frac{-f_j^i}{b_j^i} \mathbf{u}_j^i, \quad (2.70)$$

where \mathbf{u}_j^i are the eigenvectors and b_j^i are the eigenvalues of the Hessian and f_j^i is the projection of the gradient on the j^{th} eigenvector ($f_j^i = (\mathbf{u}_j^i)^T \mathbf{G}^i$).

The Newton-Raphson method leads to a minimum if the Hessian is positive definite, but the optimization can end up in a transition state if the character of the Hessian changes. To guide the search to where the Hessian has the desired character, shift parameters λ_i can be used

$$\mathbf{s}^i = \sum_j^{N_n} \frac{-f_j^i}{b_j^i - \lambda^i} \mathbf{u}_j^i. \quad (2.71)$$

According to the Eigenvector-Following algorithm [102], which uses the Rational Function approach [103], λ_i are calculated iteratively from

$$\lambda^i = \sum_j^{N_n} \frac{(f_j^i)^2}{b_j^i - \lambda^i}. \quad (2.72)$$

To avoid the calculation of second derivatives, \mathbf{H} is usually approximated in the first step of geometry optimizations, and in the subsequent steps it is updated. An often used updating scheme for minimizations is the Broyden–Fletcher–Goldfarb–Shanno (BFGS) algorithm [104–107]. The Hessian of step $i + 1$ is calculated from the Hessian of the previous step and the current and previous gradients as

$$\mathbf{H}^{i+1} = \mathbf{H}^i + \frac{\Delta \mathbf{G}^i (\Delta \mathbf{G}^i)^T}{(\Delta \mathbf{G}^i)^T \mathbf{s}^i} - \frac{\mathbf{H}^i \mathbf{s}^i (\mathbf{s}^i)^T \mathbf{H}^i}{(\mathbf{s}^i)^T \mathbf{H}^i \mathbf{s}^i}, \quad (2.73)$$

where $\Delta \mathbf{G}^i = \mathbf{G}^{i+1} - \mathbf{G}^i$.

For the location of surface crossings one of the simplest methods is the direct method of Bearpark et al. [108]. According to this method, the MECP can be located by using the gradients (\mathbf{G}_1 and \mathbf{G}_2) and the derivative coupling vector (\mathbf{g}_{12} according to (2.28)) corresponding to the two interacting states.

At a CI, the gradient difference vector $\mathbf{x}_{12} = \mathbf{G}_2 - \mathbf{G}_1$ and \mathbf{g}_{12} span the branching plane (depicted in Figure 2.3). The MECP optimization is done by minimizing the energy difference of the two states and minimizing the energy of the second state in the $(N - 2)$ -dimensional space orthogonal to the $\mathbf{x}_{12} - \mathbf{g}_{12}$ plane simultaneously. The former can be performed by applying a gradient defined as

$$\mathbf{f} = 2(E_2 - E_1) \frac{\mathbf{x}_{12}}{\|\mathbf{x}_{12}\|}, \quad (2.74)$$

which goes to zero when a CI is reached. In order to minimize the energy on the $(N - 2)$ -dimensional CI seam, vectors \mathbf{x}_{12} and \mathbf{g}_{12} are projected out of the gradient of the second state by projector \mathcal{P}

$$\tilde{\mathbf{g}} = \mathcal{P}\mathbf{G}_2. \quad (2.75)$$

The MECP optimization can be done by using the sum of the previously defined gradients

$$\bar{\mathbf{g}} = \mathbf{f} + \tilde{\mathbf{g}} \quad (2.76)$$

in a similar way as \mathbf{G} is used for locating equilibrium structures.

If only a CI on the crossing seam is needed and not necessarily the MECP, it is enough to use gradient \mathbf{f} , the calculation of the derivative coupling and $\tilde{\mathbf{g}}$ are not needed. In the case of crossings between states of different symmetry or multiplicity (depicted in Figure 2.5), the derivative coupling is zero, thus \mathcal{P} needs to project out vector \mathbf{x}_{12} only.

2.6 Analytic energy gradients

In the previous section, it was seen that the first derivatives with respect to nuclear coordinates are needed for locating minima and CIs efficiently on multidimensional PESs. Here computation of the gradient vector for bound states is reviewed, and in Publication 1 (Section 3.1) the calculation of the gradient vector for resonances is discussed.

One approach to calculate gradients is numerical differentiation, which requires the calculation of energies at $6N_n$ displaced geometries. This can mean a lot of single-point energy calculations if the system is large. Analytic differentiation is more efficient, because in this case the derivative is given by an analytic expression that requires only one, though more involved calculation. The implementation of analytic derivatives is usually a larger programming challenge than that of numerical derivatives, but calculations employing analytic derivatives have an overall lower computational cost.

To obtain the elements of the gradient vector, the dependence of the Hamiltonian on nuclear coordinates and the dependence of the wave function on nuclear coordinates through wave function parameters ξ_i have to be considered

$$G_{n\alpha} = \langle \Psi | \frac{\partial \hat{H}}{\partial R_{n\alpha}} | \Psi \rangle + 2 \sum_i \langle \Psi | \hat{H} | \frac{\partial \Psi}{\partial \xi_i} \rangle \frac{\partial \xi_i}{\partial R_{n\alpha}}. \quad (2.77)$$

The dependence on nuclear coordinates can be explicit as in the Hamiltonian, and in basis functions or implicit as in MO coefficients and CC amplitudes. The derivatives of Gaussian basis functions are straightforward to calculate, and there are different schemes for calculating one- and two-electron integral derivatives efficiently [109]. Variational parameters do not contribute to the gradient as for them $\langle \Psi | \hat{H} | \frac{\partial \Psi}{\partial \xi_i} \rangle = 0$ holds, but the derivatives of non-variational parameters contribute. The calculation of the derivatives of non-variational parameters can be replaced by solving a perturbation-independent linear equation according to the Z-vector method [110]. This can be demonstrated by employing the method of Lagrange multipliers [111–113]. According to this method, the local extrema of a function subject to certain constraints can be found as a stationary point of the Lagrangian L , which is variational in all parameters.

$$\frac{dE(R_{n\alpha}, \xi_i)}{dR_{n\alpha}} = \frac{\partial L(R_{n\alpha}, \xi_i, \lambda_i)}{\partial R_{n\alpha}} \quad (2.78)$$

2.6. ANALYTIC ENERGY GRADIENTS

The Lagrangian is built by adding the constraints $g_i = 0$ multiplied by Lagrange multipliers λ_i to the function to be optimized

$$L(R_{n\alpha}, \xi_i, \lambda_i) = E(R_{n\alpha}, \xi_i) + \sum_i \lambda_i g_i(R_{n\alpha}, \xi_i) \quad (2.79)$$

The Lagrange multipliers are determined by making the Lagrangian stationary with respect to ξ_i

$$\frac{\partial L}{\partial \xi_i} = 0, \quad \text{for all } i. \quad (2.80)$$

This way the calculation of the derivatives of non-variational parameters for the gradient is avoided, and only the Lagrange multipliers have to be determined, which are independent of the perturbation. According to the $2n + 1$ rule, to calculate the $(2n + 1)^{\text{th}}$ energy derivative, it is sufficient to calculate the n^{th} derivative of the parameters, while the n^{th} derivative of Lagrange multipliers appears only at order $2n + 2$ [111].

In the following sections the Lagrange formulation of CC and EOM-CC gradients is shown. The modifications that are needed for the CAP-EOM-CC gradient are presented in Publication 1 (Section 3.1).

2.6.1 Coupled-cluster analytic gradient

To minimize the CC energy (2.40) under multiple constraints, the following Lagrangian can be used

$$L_{CC} = \langle \Phi_{\text{HF}} | \bar{H} | \Phi_{\text{HF}} \rangle + \sum_n \lambda_n \langle \Phi_n | \bar{H} | \Phi_{\text{HF}} \rangle + \sum_a \sum_i Z_{ai} \sum_{\mu\nu} C_{\mu a}^* F_{\mu\nu} C_{\nu i} \\ + \sum_{pq} I_{pq} \left(\sum_{\mu\nu} C_{\mu p}^* S_{\mu\nu} C_{\nu q} - \delta_{pq} \right). \quad (2.81)$$

The first constraint that appears in (2.81) is that the CC equations (2.37) have to be fulfilled. The corresponding Lagrange multipliers λ_n can be calculated by making the Lagrangian stationary with respect to all CC amplitudes

$$\frac{\partial L_{CC}}{\partial t_m} = 0 \quad \text{for all } m, \quad (2.82)$$

which yields the so-called Λ equations

$$\langle \Phi_{\text{HF}} | (1 + \hat{\Lambda})(\bar{H} - E_{CC}) | \Phi_m \rangle = 0 \quad \text{for all } m, \quad (2.83)$$

where the de-excitation operator $\hat{\Lambda}$ is defined as

$$\langle \Phi_{\text{HF}} | \hat{\Lambda} = \sum_n \lambda_n \langle \Phi_n |. \quad (2.84)$$

The CC energy is not stationary with respect to orbital rotations, so additional constraints need to be introduced to achieve orbital relaxation. These additional constraints are the Brillouin condition and the orthonormality condition of the MOs (second and third constraints in (2.81)).

The changes of the MO coefficients with nuclear coordinates can be parametrized by

$$\frac{\partial C_{\mu p}}{\partial R_{n\alpha}} = \sum_q C_{\mu q} \frac{\partial U_{qp}}{\partial R_{n\alpha}}, \quad (2.85)$$

and the Lagrange multipliers I_{pq} and Z_{ai} are determined by requiring the derivatives of L with respect to all elements of \mathbf{U} to be zero

$$\frac{\partial L_{CC}}{\partial U_{qp}} = 0, \quad \text{for all } p \text{ and } q. \quad (2.86)$$

These conditions yield the Z-vector equations for Z_{ai} .

Following (2.78), the gradient vector can be written as

$$\begin{aligned}
 G_{n\alpha} &= \frac{\partial L}{\partial R_{n\alpha}} = \langle \Phi_{\text{HF}} | (1 + \Lambda) e^{-\hat{T}} \hat{H}^x e^{\hat{T}} | \Phi_{\text{HF}} \rangle \\
 &+ \sum_a \sum_i Z_{ai} \sum_{\mu\nu} C_{\mu a}^* \left(\frac{\partial h_{\mu\nu}}{\partial R_{n\alpha}} + \sum_{\sigma\rho} D_{\sigma\rho}^{\text{HF}} \frac{\partial \langle \mu\sigma || \nu\rho \rangle}{\partial R_{n\alpha}} \right) C_{\nu i} \\
 &+ \sum_{pq} I_{pq} \sum_{\mu\nu} C_{\mu p}^* \frac{\partial S_{\mu\nu}}{\partial R_{n\alpha}} C_{\nu q}.
 \end{aligned} \tag{2.87}$$

where \hat{H}^x is the derivative of the Hamiltonian that does not include contributions from orbital relaxation. This formula does not include derivatives of amplitudes, coefficients or Lagrange multipliers [114], in accordance with the $2n + 1$ and $2n + 2$ rules [111]. The gradient can be rewritten as the contraction of density matrices with integral derivatives [115]

$$G_{n\alpha} = \sum_{\mu\nu} D_{\mu\nu} \frac{\partial h_{\mu\nu}}{\partial R_{n\alpha}} + \sum_{\mu\nu\sigma\rho} \Gamma_{\mu\nu\sigma\rho} \frac{\partial \langle \mu\sigma || \nu\rho \rangle}{\partial R_{n\alpha}} + \sum_{\mu\nu} I_{\mu\nu} \frac{\partial S_{\mu\nu}}{\partial R_{n\alpha}} + \frac{\partial V_{\text{nn}}}{\partial R_{n\alpha}}, \tag{2.88}$$

where D is the effective one-electron density matrix, Γ is the two-electron density matrix, and I is the generalized energy-weighted density matrix, all expressed in the basis of AOs. Expression (2.88) is general for HF, MPn and CC methods, and the difference between methods manifests itself only in the definition of the density matrices. Detailed expressions for CCSD gradients are given in References [116] and [117].

In summary, to calculate the CC gradient, the MO coefficients and CC amplitudes are determined, then the Λ and Z-vector equations are solved. This enables the construction of the density matrices, which are then transformed to the AO basis, and finally they are contracted with integral derivatives. The computational cost for solving the Λ -equations is comparable to the cost of solving the CC equations, while the costs of computing the density matrices and solving the Z-vector equations are much smaller [117], thus a CC gradient calculation costs approximately twice as much as an energy calculation.

2.6.2 Equation-of-motion coupled-cluster analytic gradient

The EOM-CC method is bivariational for r and l amplitudes, but, just like the CC method, it is not variational for t amplitudes and MO coefficients. The EOM-CC Lagrangian can be written as

$$\begin{aligned}
 L &= \langle \Phi_{\text{HF}} | \hat{L} \bar{H} \hat{R} | \Phi_{\text{HF}} \rangle - \theta (\langle \Phi_{\text{HF}} | \hat{L} \hat{R} | \Phi_{\text{HF}} \rangle - 1) + \sum_n \zeta_n \langle \Phi_n | \bar{H} | \Phi_{\text{HF}} \rangle + \sum_a \sum_i Z_{ai} \sum_{\mu\nu} C_{\mu a}^* F_{\mu\nu} C_{\nu i} \\
 &+ \sum_{pq} I_{pq} \left(\sum_{\mu\nu} C_{\mu p}^* S_{\mu\nu} C_{\nu q} - \delta_{pq} \right),
 \end{aligned} \tag{2.89}$$

where the first term is the EOM-CC energy and the second term comes from the biorthonormality condition. The Lagrangian is stationary with respect to r and l amplitudes if $\theta = E^{\text{EOM}}$. The gradient requires calculation of both right and left states. In line with the $2n + 1$ rule, derivatives of t amplitudes are not needed, just a linear equation has to be solved [118] for ζ_n , analogous to the Λ equations (2.83). The gradient can be written in the form (2.88), with density matrices determined as given in Reference [119]. Gradient formulas and implementations were presented for EE, IP, and EA variants [38, 120].

3 Results

In this chapter, the main results of this PhD work are presented. A short introduction and summary is given before presenting each published article. The corresponding Supporting Information is given in Chapter 5 for each article.

All methods and applications presented in these articles depend upon the analytic CAP-EOM-CC gradient presented in Publication 1 (Section 3.1). The availability of analytic gradients opens up many possibilities to study the CPES of resonances. In this and the subsequent publication (Section 3.2), it was shown how the real part of the gradient can be used to locate equilibrium structures of resonances, and what accuracy can be expected with the approximate methods CAP-EOM-CCSD and CAP-EOM-CCSD(2) in calculating equilibrium structures and adiabatic electron affinities. Different diffuse basis sets were also investigated in order to come up with an affordable variant that performs well for resonances.

The real part of the gradient is also useful for locating crossings between the real parts of CPESs, as Publication 3 (Section 3.3) demonstrates. An interesting application is doing a preliminary optimization of the MECP between anionic and neutral states, which is then completed by a regular EOM-CC optimization. This can be used to verify the accessibility of DEA pathways [80, 81], and for understanding electron energy loss spectra [75, 76, 82, 83].

In Publication 4 (Section 3.4), it was shown that the complex-valued gradient can be used to locate non-Hermitian degeneracies, where both real and imaginary parts of the energies become degenerate. The location of EPs and MEEPs is important for modeling nonadiabatic processes, because the nonadiabatic coupling is large nearby, and it is singular at the EP.

EPs might also cause peculiar behavior of the states, as is known for other dissipative systems [90, 121], and so they have to be further investigated to assess their impact on processes involving autoionizing states. Another promising project is the calculation of derivative couplings between resonances, which also utilizes analytic gradients. The coupling as a function of nuclear configuration is crucial for simulating spectra and modelling multistate phenomena like DEA. This project is shortly discussed in Section 3.5.

Apart from the methodological developments, the systems chosen for demonstrative and benchmark calculations are of interest themselves. Formaldehyde, formic acid, hydrogen cyanide and acrylonitrile are present in interstellar medium [122–125], so their reactions with free electrons are interesting for understanding interstellar chemical evolution. Chloroethylene is a model system for biologically relevant halogenated substances that can be used as sensitizers in radiation therapy [10]. Chloro-substituted ethylenes are also of special interest because they are common pollutants [126] that need to be dehalogenated to decrease their toxicity [127].

3.1 Analytic gradients for complex absorbing potential methods

This article lays the foundation of the methods presented in this and subsequent publications for the optimization of equilibrium structures and crossings of resonances. The analytic gradient can be used (as described in Section 2.5.2) to perform geometry optimization of molecules that are too large to study by scans of the CPES, and in this way it enables new applications of the CAP-EOM-CC method. The analytic gradient formula presented in this article is general for HF, MPn and CC methods with a box-type quadratic CAP, but extension to other types of CAP is also possible. Implementations of analytic gradients for CAP-HF, CAP-CCSD, CAP-EOM-CCSD and CAP-EOM-CCSD(2) methods, for the EE, EA and IP variants of the EOM method, were presented in this publication and in Publication 2 (Section 3.2). Up to date these are the only methods that yield the position and width of resonances simultaneously and have analytic gradients implemented, and in this way they are a big step forward in investigating processes involving resonance states of polyatomic molecules.

The article shows that the advantage of the CAP-EOM-CC method is not only that it usually gives smooth and consistent CPESs, but also that the simple form of the Hamiltonian enables analytic differentiation of the energy, when considering CAP parameters as slowly changing. The analytic gradients of regular CC and EOM-CC methods are well-known (see Sections 2.6.1 and 2.6.2) and available in many quantum chemistry packages. The complex Hamiltonian in the CAP version of these methods results in complex-valued density matrices, which are calculated in a straightforward manner [62]. The back-transformation of density matrices from MO to AO basis involves the complex-valued MO coefficient matrix, which increases the prefactor of the computational cost of this step, but does not change the scaling. A big advantage of CAP methods in the implementation of the gradient is that AO integrals, and thus integral derivatives as well, are real, so only the adequate parts of the complex AO density matrices need to be considered for calculating the real and imaginary gradients. In contrast, for CBF methods, the implementation of analytic energy gradients is expected to be significantly more complicated, as integral derivatives involving complex basis functions need to be evaluated. With the direct CS method, as discussed in Section 2.4, already the construction of a CPES is difficult.

The dependence of the CAP on nuclear coordinates results in two extra terms in the gradient. These are easily evaluated numerically, which also enables future extensions to other forms of CAP. The indirect dependence of the energy on nuclear coordinates through the CAP strength and box size parameters is not taken into account in the analytic gradient, and a scheme including regular updating of the parameters is proposed. This provides a consistent way of choosing the parameters.

This publication presents only the real part of the gradient, whose application is straightforward; it can be used in a similar way as the energy gradient of bound states (see Section 2.5.2), e.g., for locating equilibrium structures and crossings between real parts of CPESs. An application of the latter is the initial optimization of resonance – parent state crossings (Publication 3, Section 3.3). The imaginary part of the gradient describes the dependence of the resonance width on nuclear coordinates and it proves to be essential for locating EPs (Paper 4, Section 3.4), which act as funnels between resonance states, like CIs do between bound states.



Communication: Analytic gradients for the complex absorbing potential equation-of-motion coupled-cluster method

Zsuzsanna Benda and Thomas-C. Jagau

Department of Chemistry, University of Munich (LMU), D-81377 Munich, Germany

(Received 27 November 2016; accepted 3 January 2017; published online 18 January 2017)

The general theory of analytic energy gradients is presented for the complex absorbing potential equation-of-motion coupled-cluster (CAP-EOM-CC) method together with an implementation within the singles and doubles approximation. Expressions for the CAP-EOM-CC energy gradient are derived based on a Lagrangian formalism with a special focus on the extra terms arising from the presence of the CAP. Our implementation allows for locating minima on high-dimensional complex-valued potential energy surfaces and thus enables geometry optimizations of resonance states of polyatomic molecules. The applicability of our CAP-EOM-CC gradients is illustrated by computations of the equilibrium structures and adiabatic electron affinities of the temporary anions of formaldehyde, formic acid, and ethylene. The results are compared to those obtained from standard EOM-CC calculations and the advantages of CAP methods are emphasized. *Published by AIP Publishing.* [<http://dx.doi.org/10.1063/1.4974094>]

Electron attachment to molecules with negative vertical electron affinity (VEA) leads to the formation of temporary anions that can decay through autodetachment and often exhibit distinctly different properties and reactivity patterns than the parent neutral molecules.^{1,2} The so opened uncommon reaction channels play a role in unwanted processes such as radiative DNA damage^{3,4} but can also be exploited productively, for example, in electron-induced reactions.^{5–7} These phenomena and the underlying physical mechanisms such as dissociative electron attachment^{1,8} or interatomic Coulombic decay⁹ cannot be understood in a fixed-nuclei picture but require to take into account the coupling between electronic and nuclear degrees of freedom. The importance of nuclear motion for the understanding of temporary anions is also evident in photodetachment,^{10,11} electron transmission,^{12,13} and electron-impact spectra^{14–16} that feature vibrational structure and thereby allow for the determination of adiabatic electron affinities (AEAs).

The theoretical treatment of temporary anions is challenging because they belong to the continuum and cannot be associated with discrete eigenstates in the Hermitian domain of the molecular Hamiltonian.¹⁷ By means of the Siegert formalism,^{17–19} it is, however, possible to associate temporary anions with adiabatic resonance states with complex energy. This allows for a characterization in analogy to bound states and, in particular, the construction of complex-valued potential energy surfaces (CPESs)²⁰ by invoking the Born-Oppenheimer approximation. The real part of a CPES can be interpreted similarly to the PES of a bound state, whereas the imaginary part yields the local decay rate as a function of molecular structure.^{20–22}

CPESs of several diatomic and triatomic temporary anions, such as N_2^- ,^{23–29} H_2O^- ,³⁰ and CO_2^- ,³¹ have been studied previously, but little is known about the CPESs of polyatomic species. This is because the efficient determination of minima, transition states, conical intersections, etc. on

high-dimensional CPES is feasible only by means of analytical gradients, which have not been available so far for any method for resonance states. Since analytical gradients have been derived and implemented for numerous bound-state electronic-structure methods, including Hartree-Fock (HF),³² coupled-cluster (CC),^{33,34} and equation-of-motion (EOM)-CC theory,³⁵ a possible solution is to apply these methods to resonances. This has been done, for example, for the benzene radical anion³⁶ and the cyclooctatetraene dianion³⁷ but is not satisfying as the metastable nature of the resonance state is neglected entirely.

In this Communication, we present the theory of analytic gradients for the complex absorbing potential (CAP)-EOM-CC method,^{38–41} which enables the determination of equilibrium structures of polyatomic temporary anions. While Siegert energies can be obtained using different techniques such as straight complex scaling (CS),^{42–44} exterior scaling (ES),⁴⁵ complex basis functions (CBF),^{46,47} stabilization methods,^{48,49} and CAPs^{50,51} that can be further combined with different electronic-structure methods, CAP-EOM-CC holds several distinct advantages: First, and in contrast to ES and CBF approaches, evaluation of the energy gradient does not require non-standard two-electron integral derivatives. Second, the wave functions of a temporary anion and its parent neutral state are obtained as eigenfunctions of the same Hamiltonian in CAP-EOM-CC, which ensures that the imaginary part of a CPES is zero if and only if its real part is below the PES of the parent neutral state.²⁹ EOM-CC also offers further advantages such as an unbiased description of the target states by taking account of dynamical and non-dynamical electron correlation at once.

In CAP methods, a purely imaginary potential is added to the usual molecular Hamiltonian \mathcal{H} , which leads to a non-Hermitian Hamiltonian,

$$\mathcal{H}(\eta) = \mathcal{H} - i\eta W. \quad (1)$$

Here, η is the CAP strength parameter and W is in the following chosen to be of the form:

$$W = \sum_{\alpha} W_{\alpha}, \quad \alpha = x, y, z, \quad (2)$$

$$W_{\alpha} = \begin{cases} 0 & \text{if } |r_{\alpha} - o_{\alpha}| \leq r_{\alpha}^0, \\ (|r_{\alpha} - o_{\alpha}| - r_{\alpha}^0)^2 & \text{if } |r_{\alpha} - o_{\alpha}| > r_{\alpha}^0, \end{cases} \quad (3)$$

with r_{α}^0 as the box size parameters and the vector $o = (o_x, o_y, o_z)$ as the origin of the CAP. In our computational protocol, we choose r_{α}^0 as the spatial extent of the wave function of the neutral molecule ($\sqrt{\langle \alpha^2 \rangle}$)⁴⁰ and o as the center of nuclear charges, that is,

$$o_{\alpha} = \frac{\sum_k R_{k,\alpha} Z_k}{\sum_k Z_k}, \quad (4)$$

where $R_{k,\alpha}$ and Z_k are the nuclear coordinates and nuclear charges, respectively. By this choice of o we ensure that the molecule is not displaced relative to the CAP during a geometry optimization, which could happen otherwise if o was defined independently of the nuclear coordinates. Note that the molecule can still rotate relative to the CAP unless this would break spatial symmetry.⁵²

Inserting Eq. (1) into the Schrödinger equation leads to a non-Hermitian eigenvalue problem, from whose complex

eigenvalues $E = E_R - i\Gamma/2$ the resonance positions E_R and widths Γ are obtained. In CAP-EOM-CC, the resonance wave function is parametrized as $|\Psi\rangle = R e^T |\Phi_{\text{HF}}\rangle$, where $|\Phi_{\text{HF}}\rangle$ is the CAP-HF wave function of the reference state that we choose as the ground state of the neutral molecule, T is the cluster operator, and R creates the target states. For temporary anions, the CAP-EOM-EA-CC variant is employed, where R describes the attachment of an electron to the neutral molecule. T and R are defined and determined in analogy to standard EOM-CC theory,^{53–55} but we use parentheses instead of chevrons to indicate the c-product.^{56,57} When $|\Psi\rangle$ is represented in a complete basis, the energy calculated with the CAP corresponds to the exact resonance energy in the limit $\eta \rightarrow 0$.⁵¹ In a finite basis set, however, an optimal finite η_{opt} exists that minimizes the error introduced by the CAP. η_{opt} is usually determined based on perturbation theory by minimizing the expression $|\eta dE/d\eta|$.⁵¹

To derive an expression that allows for the efficient evaluation of the CAP-EOM-CC energy gradient, we employ the Lagrangian technique.^{58,59} Following the same steps as in standard CC gradient theory, we finally arrive at the following expression for the Lagrangian in the atomic-orbital (AO) basis that is valid for any CAP-CC or CAP-EOM-CC model in which the CAP is introduced at the HF level:

$$\begin{aligned} \mathcal{L} = & \sum_{\mu\nu} D_{\mu\nu}^{\text{HF}} (h_{\mu\nu} - i\eta W_{\mu\nu}) + \frac{1}{2} \sum_{\mu\nu\sigma\rho} D_{\mu\nu}^{\text{HF}} D_{\sigma\rho}^{\text{HF}} \langle \mu\sigma || \nu\rho \rangle + \sum_{\mu\nu} I_{\mu\nu}^{\text{HF}} S_{\mu\nu} \\ & + \sum_{\mu\nu} D_{\mu\nu}^{\text{CC}} (f_{\mu\nu} - i\eta W_{\mu\nu}) + \sum_{\mu\nu\sigma\rho} \Gamma_{\mu\sigma\nu\rho}^{\text{CC}} \langle \mu\sigma || \nu\rho \rangle + \sum_{\mu\nu} I_{\mu\nu}^{\text{CC}} S_{\mu\nu} + \sum_{\alpha} \lambda_{\alpha} \left(\frac{\sum_k R_{k,\alpha} Z_k}{\sum_k Z_k} - o_{\alpha} \right) + V_{\text{nuc}}. \end{aligned} \quad (5)$$

Here, $h_{\mu\nu}$, $f_{\mu\nu}$, and $S_{\mu\nu}$ are the elements of the one-electron Hamiltonian, the Fock matrix, and the overlap matrix, $\langle \mu\sigma || \nu\rho \rangle$ denotes antisymmetrized two-electron integrals,⁶⁰ and V_{nuc} is the nuclear repulsion energy. Whereas all these quantities are real-valued, the effective one-electron, two-electron, and generalized energy-weighted density matrices D , Γ ,⁶¹ and I are complex-valued. Quantities labeled with superscripts ‘‘HF’’ and ‘‘CC’’ refer to contributions due to the response of the CAP-HF and the CAP-CC/CAP-EOM-CC wave function, respectively. The expressions for the latter quantities depend on the employed CC/EOM-CC model with no modifications required due to the CAP.^{34,35} We note that the CAP-HF Lagrangian is obtained from Eq. (5) by setting all ‘‘CC’’ quantities to zero.

Eq. (5) includes two kinds of extra terms compared to the regular CC/EOM-CC Lagrangian: The contribution of the CAP to the energy ($-i\eta \sum_{\mu\nu} (D_{\mu\nu}^{\text{HF}} + D_{\mu\nu}^{\text{CC}}) W_{\mu\nu}$) and an extra constraint to account for the dependence of the CAP origin on the nuclear coordinates. To obtain this latter term, Eq. (4) is rearranged and multiplied with Lagrange multipliers λ_{α} . By requiring \mathcal{L} to be stationary with respect to o , we obtain

$$\lambda_{\alpha} = -i\eta \sum_{\mu\nu} (D_{\mu\nu}^{\text{HF}} + D_{\mu\nu}^{\text{CC}}) \left(\frac{\partial W_{\alpha}}{\partial o_{\alpha}} \right)_{\mu\nu}, \quad (6)$$

$$\frac{\partial W_{\alpha}}{\partial o_{\alpha}} = \begin{cases} 0, & \text{if } |r_{\alpha} - o_{\alpha}| \leq r_{\alpha}^0, \\ -2(r_{\alpha} - o_{\alpha} - r_{\alpha}^0), & \text{if } (r_{\alpha} - o_{\alpha}) > r_{\alpha}^0, \\ 2(-r_{\alpha} + o_{\alpha} - r_{\alpha}^0), & \text{if } (r_{\alpha} - o_{\alpha}) < -r_{\alpha}^0, \end{cases} \quad (7)$$

where we exploit that only the terms containing the CAP or the CAP origin depend explicitly on o in Eq. (5).

In addition to the CAP origin, \mathcal{L} also depends on the box size parameters and the CAP strength. Since η_{opt} and r_{α}^0 in turn depend on the nuclear coordinates, further constraints should be included in \mathcal{L} in principle. However, in our current computational protocol, which is described further below, we keep η_{opt} and r_{α}^0 constant while optimizing the geometry so that there is no need for additional constraints.

An element of the gradient vector $dE/dR_{n,\alpha}$ corresponding to nucleus n and $\alpha = x, y, z$ can then be obtained by taking the derivative of Eq. (5) and bearing in mind the $2n + 1$ and $2n + 2$ rules.⁶² For locating minima on the real part of a CPES, only the real part of the gradient is needed. Since all integral derivatives are real-valued, this yields the following general expression for the various CAP-CC and CAP-EOM-CC methods:

$$\begin{aligned} \operatorname{Re}\left(\frac{dE}{dR_{n,\alpha}}\right) &= \sum_{\mu\nu} \left[\operatorname{Re}(D_{\mu\nu}^{\text{HF}}) + \operatorname{Re}(D_{\mu\nu}^{\text{CC}}) \right] \frac{\partial h_{\mu\nu}}{\partial R_{n,\alpha}} + \eta \sum_{\mu\nu} \left[\operatorname{Im}(D_{\mu\nu}^{\text{HF}}) + \operatorname{Im}(D_{\mu\nu}^{\text{CC}}) \right] \left[\frac{\partial W_{\mu\nu}}{\partial R_{n,\alpha}} + \frac{Z_n}{\sum_k Z_k} \left(\frac{\partial W_\alpha}{\partial \sigma_\alpha} \right)_{\mu\nu} \right] \\ &+ \sum_{\mu\nu\sigma\rho} \left[\frac{1}{2} \operatorname{Re}(D_{\mu\nu}^{\text{HF}}) \operatorname{Re}(D_{\sigma\rho}^{\text{HF}}) - \frac{1}{2} \operatorname{Im}(D_{\mu\nu}^{\text{HF}}) \operatorname{Im}(D_{\sigma\rho}^{\text{HF}}) + \operatorname{Re}(D_{\mu\nu}^{\text{CC}}) \operatorname{Re}(D_{\sigma\rho}^{\text{HF}}) - \operatorname{Im}(D_{\mu\nu}^{\text{CC}}) \operatorname{Im}(D_{\sigma\rho}^{\text{HF}}) \right. \\ &\left. + \operatorname{Re}(\Gamma_{\mu\nu\sigma\rho}^{\text{CC}}) \right] \frac{\partial \langle \mu\sigma || \nu\rho \rangle}{\partial R_{n,\alpha}} + \sum_{\mu\nu} \left[\operatorname{Re}(I_{\mu\nu}^{\text{HF}}) + \operatorname{Re}(I_{\mu\nu}^{\text{CC}}) \right] \frac{\partial S_{\mu\nu}}{\partial R_{n,\alpha}} + \frac{\partial V_{\text{nuc}}}{\partial R_{n,\alpha}} \end{aligned} \quad (8)$$

where the derivative of the Fock matrix element $f_{\mu\nu} = h_{\mu\nu} + \sum_{\sigma\rho} D_{\sigma\rho}^{\text{HF}} \langle \mu\sigma || \nu\rho \rangle$ has been split into a one-electron and a two-electron contribution. The corresponding CAP-HF expression is again obtained by setting all ‘‘CC’’ quantities to zero. Note that even though only the real part of the two-electron density matrix Γ^{CC} is needed, this quantity is calculated using complex algebra in the molecular orbital (MO) basis and then back-transformed to the AO basis using complex MO coefficients. This increases the cost of CAP-CC/CAP-EOM-CC gradients considerably compared to the CAP-free case. However, the formal scaling of every CAP method is the same as that of the corresponding real-valued method.

Eq. (8) illustrates that the computation of the energy gradient for CAP methods requires the evaluation of two additional derivatives compared to standard gradient theory: $\partial W_{\mu\nu} / \partial R_{n,\alpha}$ and $(\partial W_\alpha / \partial \sigma_\alpha)_{\mu\nu}$. Explicit expressions for the latter term are given in Eq. (7), while the former term becomes

$$\frac{\partial W_{\mu\nu}}{\partial R_{n,\alpha}} = \frac{\partial (W_x)_{\mu\nu}}{\partial R_{n,\alpha}} + \frac{\partial (W_y)_{\mu\nu}}{\partial R_{n,\alpha}} + \frac{\partial (W_z)_{\mu\nu}}{\partial R_{n,\alpha}}, \quad (9)$$

$$\frac{\partial (W_x)_{\mu\nu}}{\partial R_{n,\alpha}} = \left\langle \frac{\partial \chi_\mu}{\partial R_{n,\alpha}} \middle| W_x \middle| \chi_\nu \right\rangle + \left\langle \chi_\mu \middle| W_x \middle| \frac{\partial \chi_\nu}{\partial R_{n,\alpha}} \right\rangle \quad (10)$$

with χ_μ, χ_ν as standard Gaussian basis functions.⁶⁰ Eqs. (7) and (10) are evaluated numerically in our implementation in the same way as detailed in Ref. 40 for $W_{\mu\nu}$.

CAP-CC and CAP-EOM-EA-CC gradients have been implemented within the singles and doubles (SD) approximation into the Q-Chem program package.⁶³ In addition, our implementation allows for the evaluation of restricted and unrestricted CAP-HF gradients. Spatial symmetry is exploited and the libtensor library⁶⁴ is used for operations on high-dimensional tensors. The implementation has been verified by means of numerical differentiation. Currently, the implicit dependence of E on $R_{n,\alpha}$ through η_{opt} and r_α^0 is not considered in the expression for the gradient (Eq. (8)), instead we use the following procedure for geometry optimizations:

1. Determine $\sqrt{\langle \alpha^2 \rangle}$ of the neutral molecule.
2. Find η_{opt} for $r_\alpha^0 = \sqrt{\langle \alpha^2 \rangle}$.
3. Optimize the geometry while leaving $\eta = \eta_{\text{opt}}$ and r_α^0 unchanged.
4. Go to 1 until $\sqrt{\langle \alpha^2 \rangle}$ and η_{opt} are converged.

Updating the box size parameters is especially important if the molecule rotates in the box during geometry optimization. If this is not the case, re-optimizing the geometry with updated CAP parameters typically entails only small structural changes.

In the following, we apply the CAP-EOM-EA-CCSD method for geometry optimizations of the anionic resonance states of CH_2O , HCOOH , and C_2H_4 and determine the corresponding AEAs and resonance widths. The aug-cc-pVDZ+3s3p(A) basis set⁶⁵ from Ref. 40 is used in all calculations. This basis is diffuse enough to represent the coupling of the resonance to the continuum and hence sufficient to illustrate the differences between CAP-including and CAP-free gradient calculations, which is the focus of our Communication. A quantitative comparison to experimental values would demand the use of a triple- ζ or quadruple- ζ basis as will be discussed in more detail further below. Values for the parameters r_α^0 and η_{opt} are compiled in the [supplementary material](#).

Changes in the box size are related to structural differences between the neutral molecule and the anion. In the case of CH_2O , the C=O bond length differs significantly between the neutral and anionic equilibrium structures (1.215 Å vs. 1.286 Å), whereas the differences in the remaining geometrical parameters are negligible (see the [supplementary material](#)). This is reflected in the large change in r_z^0 compared to the changes in r_x^0 and r_y^0 . The geometrical change can be explained qualitatively by the π^* character of the corresponding Dyson orbital^{66,67} depicted in Figure 1(a). Note that the anionic equilibrium structure is planar and belongs to the C_{2v} point group, i.e., electron attachment does not induce a lowering of the molecular symmetry.

In the cases of HCOOH and C_2H_4 , non-planar distortion of the molecule is observed upon electron attachment in addition to lengthening of the C–O and C–C bonds. For formic acid, the C–O bond lengths change from 1.208 Å and 1.354 Å to 1.276 Å and 1.451 Å, while for ethylene, the C–C bond length changes from 1.348 Å to 1.439 Å, which can again be explained by the π^* character of the corresponding Dyson orbitals (Figures 1(b) and 1(c)). The differences in the other bond lengths are very small (see the [supplementary material](#)). The equilibrium structure of HCOOH^- is of C_1 symmetry compared to C_s for the neutral molecule, while

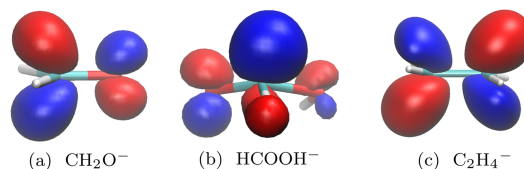


FIG. 1. Real parts of CAP-EOM-EA-CCSD Dyson orbitals for electron attachment to CH_2O^- , HCOOH^- , and C_2H_4^- . Computed with the aug-cc-pVDZ+3s3p(A) basis set at the equilibrium structures of the respective resonant anions.

TABLE I. Theoretical and experimental values for the vertical and adiabatic electron affinities (VEA and AEA), vertical detachment energies (VDE), and resonance widths (Γ) of formaldehyde, formic acid, ethylene, and the corresponding anions. Γ_0 is the resonance width at the neutral equilibrium structure and Γ_{res} is that at the resonance equilibrium structure. The CAP-EOM-EA-CCSD/aug-cc-pVDZ+3s3p(A) method was employed in all calculations. All values are given in eV.

		VEA	VDE	AEA	Γ_0	Γ_{res}
CH ₂ O ⁻	Calc.	-1.372	-0.837	-1.019	0.353	0.213
	Expt.	-0.86 ⁶⁹	...	-0.65 ⁶⁹	0.2-0.4 ⁶⁹	
HCOOH ⁻	Calc.	-2.325	-0.482	-1.481	0.252	0.126
	Expt.	-1.73 ⁷⁰	...	-1.3 ⁷¹	...	
C ₂ H ₄ ⁻	Calc.	-2.228	-1.654	-2.039	0.450	0.307
	Expt.	-1.76 ⁷²	...	-1.55 ⁷³	0.3-0.7 ⁷²	

that of C₂H₄⁻ belongs to the C_{2h} point group compared to D_{2h} for the neutral molecule. For the anion of ethylene, symmetry lowering from D_{2h} to C_{2h} has also been predicted by HF calculations using very small bases and was rationalized in terms of $\sigma^*-\pi^*$ mixing.⁶⁸ η_{opt} values for CH₂O⁻ and HCOOH⁻ are significantly smaller at the equilibrium structure of the resonance than at that of the neutral molecule, while this decrease is less pronounced for C₂H₄⁻.

The calculated VEAs and AEAs and vertical detachment energies (VDE) along with the resonance widths at the neutral equilibrium (Γ_0) and at the resonance equilibrium structure (Γ_{res}) are listed in Table I. For all molecules, AEA is significantly lower than VEA in terms of absolute values; the effect of structural relaxation amounts to 0.85 eV for HCOOH⁻, 0.35 eV for CH₂O⁻, and 0.19 eV for C₂H₄⁻. Remarkably, experimental results⁶⁹⁻⁷³ also suggest a larger relaxation energy for HCOOH⁻ than for the other two anions.

The quantitative comparison to experiment is difficult due to the incomplete basis set, the perturbation due to the CAP, the truncation of the CC expansion, and the neglect of the zero-point vibrational energy. Also, the experimental determination of VEA is problematic.¹³ The calculated absolute values for VEA are typically 0.5 eV higher than the corresponding experimental values. This discrepancy can be largely attributed to the first two effects: CAP-EOM-EA-CCSD calculations for C₂H₄⁻ using the aug-cc-pVQZ+3s3p3d(C) basis set yielded VEA values 0.24 eV lower than aug-cc-pVDZ+3s3p(A) and a first-order correction for the CAP perturbation lowered the

energy further by 0.08 eV.⁴⁰ Similar effects can be anticipated for the AEA values as well.

Table I shows that Γ_{res} is smaller than Γ_0 for all three molecules. This is a general feature of temporary anions because VDE is always smaller than VEA. When the energy difference between an anionic resonance and the parent neutral state becomes smaller, the resonance width has to decrease and, if the two PES cross, it has to become zero as the resonance turns into a stable state.²⁹

To demonstrate the advantages of a geometry optimization including a CAP over an approach that treats the resonance as a bound state, we carried out CAP-free EOM-EA-CCSD calculations for C₂H₄⁻ using a variety of basis sets. This is documented in Table II.

Using the cc-pVDZ basis set, the lowest EOM-EA-CCSD root resembles the resonance state and a bent equilibrium structure of C_{2h} symmetry is obtained for the anion. However, the AEA is overestimated by 0.9 eV. As we enlarge the basis set, more and more continuum states appear in the spectrum, making it harder to associate a single state with the resonance.^{74,75} Already for aug-cc-pVDZ, the lowest root has continuum character describing C₂H₄+e⁻ rather than C₂H₄⁻, which is reflected in the optimized geometrical parameters R(CC) = 1.351 Å and $\angle(\text{HCCH}) = 180.0^\circ$. As Table II shows, it is still possible to identify resonance-like higher-lying roots in the larger bases, but even so, their equilibrium structures differ qualitatively from that obtained in the presence of the CAP: regular EOM-EA-CCSD predicts a planar equilibrium structure and a too short C—C bond length using the aug-cc-pVDZ and aug-cc-pVDZ+3s3p(A) basis sets.

This clearly shows that although states with properties similar to the resonance can be found with bound-state approaches, this is an artifact of discretizing the continuum by means of small basis sets and valid results are not guaranteed. In contrast, in the presence of a CAP, the resonance state is usually one of the lowest-lying roots also in larger bases and the determination of the equilibrium structure and the AEA is straightforward.

In sum, we have derived and implemented analytic gradients for CAP-HF, CAP-CCSD, and various CAP-EOM-CCSD methods and proposed a procedure for the geometry optimization of temporary anions. Equilibrium structures and adiabatic electron affinities of the anions of formaldehyde, formic acid, and ethylene have been determined for the first time using CAP methods, and the advantages

TABLE II. Equilibrium structures for neutral C₂H₄ (0) computed with CCSD and the resonant anion C₂H₄⁻ (res) computed with regular and CAP-augmented EOM-EA-CCSD using different basis sets. AEAs and the followed root (of A_g symmetry in the C_{2h} point group) in the EOM-EA-CCSD eigenvalue equation are also listed.

Basis	R(CC)/Å		$\angle(\text{HCCH})/\text{deg}$		AEA/eV	Root
	0	Res	0	Res		
cc-pVDZ ^a	1.345	1.456	0.0	48.7	-2.941	1
aug-cc-pVDZ ^a	1.348	1.418	0.0	0.0	-1.923	2
aug-cc-pVDZ+3s3p(A) ^a	1.348	1.405	0.0	0.1	-1.983	7
aug-cc-pVDZ+3s3p(A) ^b	1.348	1.439	0.0	26.6	-2.039	2

^aWithout CAP.

^bIncluding CAP.

over applying bound-state methods have been illustrated. The present work represents a key step towards modeling nuclear motion in processes involving electronic resonances. We plan to generalize our current implementation to other types of resonances and different electronic-structure methods.

See [supplementary material](#) for the coordinates of all optimized molecular structures in Z-matrix format, CAP box sizes, and optimal CAP strengths.

This work has been supported by the Fonds der Chemischen Industrie through a Ph.D. fellowship to Z.B. and a Liebig fellowship to T.-C.J. We thank Professor Christian Ochsenfeld for support and hospitality at LMU Munich.

- ¹J. M. Herbert, *Rev. Comput. Chem.* **28**, 391 (2015).
- ²T.-C. Jagau, K. B. Bravaya, and A. I. Krylov, "Extending quantum chemistry of bound states to electronic resonances," *Annu. Rev. Phys. Chem.* (published online).
- ³B. Boudaiffa, P. Cloutier, D. Hunting, M. A. Huels, and L. Sanche, *Science* **287**, 1658 (2000).
- ⁴J. Simons, *Acc. Chem. Res.* **39**, 772 (2006).
- ⁵G. Dujardin, R. E. Walkup, and P. Avouris, *Science* **255**, 1232 (1992).
- ⁶D. Davis, V. P. Vysotskiy, Y. Sajeev, and L. S. Cederbaum, *Angew. Chem., Int. Ed.* **50**, 4119 (2011).
- ⁷A. Studer and D. P. Curran, *Nat. Chem.* **6**, 765 (2014).
- ⁸C. R. Arumainayagam, H.-L. Lee, R. B. Nelson, D. R. Haines, and R. P. Gunawardane, *Surf. Sci. Rep.* **65**, 1 (2010).
- ⁹R. Santra, J. Zobeley, L. S. Cederbaum, and N. Moiseyev, *Phys. Rev. Lett.* **85**, 4490 (2000).
- ¹⁰D. B. Dao and R. Mabbs, *J. Chem. Phys.* **141**, 154304 (2014).
- ¹¹T.-C. Jagau, D. B. Dao, N. S. Holtgrewe, A. I. Krylov, and R. Mabbs, *J. Phys. Chem. Lett.* **6**, 2786 (2015).
- ¹²P. D. Burrow, J. A. Michejda, and K. D. Jordan, *J. Chem. Phys.* **86**, 9 (1987).
- ¹³K. D. Jordan and P. D. Burrow, *Chem. Rev.* **87**, 557 (1987).
- ¹⁴K. Regeta and M. Allan, *Phys. Rev. Lett.* **110**, 203201 (2013).
- ¹⁵K. Regeta and M. Allan, *J. Chem. Phys.* **142**, 184307 (2015).
- ¹⁶K. Regeta and M. Allan, *Phys. Rev. A* **91**, 012707 (2015).
- ¹⁷N. Moiseyev, *Non-Hermitian Quantum Mechanics* (Cambridge University Press, Cambridge, UK, 2011).
- ¹⁸G. Gamov, *Z. Phys.* **51**, 204 (1928).
- ¹⁹A. J. F. Siegert, *Phys. Rev.* **56**, 750 (1939).
- ²⁰S. Klaiman and N. Moiseyev, *J. Phys. B* **42**, 044004 (2009).
- ²¹T. Sommerfeld and H.-D. Meyer, *J. Phys. B* **35**, 1841 (2002).
- ²²Note that these considerations hold for well-separated resonances sufficiently far away from the threshold, which are the focus of the present work. A more involved description is required for treating overlapping resonance states. Also, near the threshold a description in terms of the energy-dependent non-local width from the Feshbach formalism is recommended.
- ²³D. T. Birtwistle and A. Herzenberg, *J. Phys. B* **4**, 53 (1971).
- ²⁴J. G. Lauderdale, C. W. McCurdy, and A. U. Hazi, *J. Chem. Phys.* **79**, 2200 (1983).
- ²⁵B. Nestmann and S. D. Peyerimhoff, *J. Phys. B* **18**, 4309 (1985).
- ²⁶M. Honigmann, R. J. Buenker, and H.-P. Liebermann, *J. Chem. Phys.* **125**, 234304 (2006).
- ²⁷A. Ghosh, A. Karne, S. Pal, and N. Vaval, *Phys. Chem. Chem. Phys.* **15**, 17915 (2013).
- ²⁸M. F. Falcetta, L. A. Di Falco, D. S. Ackerman, J. C. Barlow, and K. D. Jordan, *J. Phys. Chem. A* **118**, 7489 (2014).
- ²⁹T.-C. Jagau and A. I. Krylov, *J. Phys. Chem. Lett.* **5**, 3078 (2014).
- ³⁰D. J. Haxton, C. W. McCurdy, and T. N. Rescigno, *Phys. Rev. A* **75**, 012710 (2007).
- ³¹T. Sommerfeld, H.-D. Meyer, and L. S. Cederbaum, *Phys. Chem. Chem. Phys.* **6**, 42 (2004).
- ³²P. Pulay, *Mol. Phys.* **17**, 197 (1969).
- ³³A. C. Scheiner, G. E. Scuseria, J. E. Rice, T. J. Lee, and H. F. Schaefer, *J. Chem. Phys.* **87**, 5361 (1987).
- ³⁴J. Gauss, J. F. Stanton, and R. J. Bartlett, *J. Chem. Phys.* **95**, 2623 (1991).
- ³⁵J. F. Stanton, *J. Chem. Phys.* **99**, 8840 (1993).
- ³⁶A. Bazanté, E. R. Davidson, and R. J. Bartlett, *J. Chem. Phys.* **142**, 204304 (2015).
- ³⁷A. Yu. Sokolov, D. B. Magers, J. I. Wu, W. D. Allen, P. v. R. Schleyer, and H. F. Schaefer, *J. Chem. Theory Comput.* **9**, 4436 (2013).
- ³⁸A. Ghosh, N. Vaval, and S. Pal, *J. Chem. Phys.* **136**, 234110 (2012).
- ³⁹T.-C. Jagau, D. Zuev, K. B. Bravaya, E. Epifanovsky, and A. I. Krylov, *J. Phys. Chem. Lett.* **5**, 310 (2014).
- ⁴⁰D. Zuev, T.-C. Jagau, K. B. Bravaya, E. Epifanovsky, Y. Shao, E. Sundstrom, M. Head-Gordon, and A. I. Krylov, *J. Chem. Phys.* **141**, 024102 (2014).
- ⁴¹D. Zuev, T.-C. Jagau, K. B. Bravaya, E. Epifanovsky, Y. Shao, E. Sundstrom, M. Head-Gordon, and A. I. Krylov, *J. Chem. Phys.* **143**, 149901 (2015).
- ⁴²J. Aguilar and J. M. Combes, *Commun. Math. Phys.* **22**, 269 (1971).
- ⁴³E. Balslev and J. M. Combes, *Commun. Math. Phys.* **22**, 280 (1971).
- ⁴⁴B. Simon, *Commun. Math. Phys.* **27**, 1 (1972).
- ⁴⁵B. Simon, *Phys. Lett. A* **71**, 211 (1979).
- ⁴⁶C. W. McCurdy and T. N. Rescigno, *Phys. Rev. Lett.* **41**, 1364 (1978).
- ⁴⁷N. Moiseyev and C. Corcoran, *Phys. Rev. A* **20**, 814 (1979).
- ⁴⁸A. U. Hazi and H. S. Taylor, *Phys. Rev. A* **1**, 1109 (1970).
- ⁴⁹M. Nestmann and S. D. Peyerimhoff, *J. Phys. B* **18**, 615 (1985).
- ⁵⁰G. Jolicard and E. J. Austin, *Chem. Phys. Lett.* **121**, 106 (1985).
- ⁵¹U. V. Riss and H.-D. Meyer, *J. Phys. B* **26**, 4503 (1993).
- ⁵²This undesired behavior can be corrected by recalculating $\sqrt{\alpha^2}$ and updating the box size parameters during a geometry optimization. We note that an alternative would be the use of a spherically symmetric CAP as rotation of the molecule would not affect the results in this case. Assessing the performance of spherical CAPs will be the subject of future work.
- ⁵³J. F. Stanton and R. J. Bartlett, *J. Chem. Phys.* **98**, 7029 (1993).
- ⁵⁴M. Nooijen and R. J. Bartlett, *J. Chem. Phys.* **102**, 3629 (1995).
- ⁵⁵I. Shavitt and R. J. Bartlett, *Many-Body Methods in Chemistry and Physics: MBPT and Coupled-Cluster Theory* (Cambridge University Press, Cambridge, UK, 2009).
- ⁵⁶N. Moiseyev, P. R. Certain, and F. Weinhold, *Mol. Phys.* **36**, 1613 (1978).
- ⁵⁷Since the CAP-augmented Hamiltonian $\mathcal{H}(i\eta)$ is not Hermitian but complex symmetric, the proper scalar product needs to be replaced by the c-product in all equations. The difference is that the bra state is not complex conjugated.
- ⁵⁸T. Helgaker and P. Jørgensen, *Adv. Quantum Chem.* **19**, 183 (1988).
- ⁵⁹P. G. Szalay, *Int. J. Quantum Chem.* **55**, 151 (1995).
- ⁶⁰Note that because the AOs are real valued the c-product metric coincides with the usual metric. We chose to keep chevrons in order to avoid confusion between Dirac and Mulliken notation for the two-electron integrals.
- ⁶¹Note that Γ denotes both the resonance width and the two-electron density matrix in this Communication, which is unfortunate, but in our opinion preferable to introducing non-standard notation for either quantity. The meaning is always clear from the context.
- ⁶²P. Jørgensen and T. Helgaker, *J. Chem. Phys.* **89**, 1560 (1988).
- ⁶³Y. Shao, Z. Gan, E. Epifanovsky, A. T. B. Gilbert, M. Wormit *et al.*, *Mol. Phys.* **113**, 184 (2015).
- ⁶⁴E. Epifanovsky, M. Wormit, T. Kuš, A. Landau, D. Zuev, K. Khistyayev, P. Manohar, I. Kaliman, A. Dreuw, and A. I. Krylov, *J. Comput. Chem.* **34**, 2293 (2013).
- ⁶⁵In this basis set, the standard aug-cc-pVDZ basis set is supplemented by 3 additional even tempered diffuse s and p functions each at all atoms except hydrogen.
- ⁶⁶J. Linderberg and Y. Öhrn, *Propagators in Quantum Chemistry* (Academic, London, 1973).
- ⁶⁷T.-C. Jagau and A. I. Krylov, *J. Chem. Phys.* **144**, 054113 (2016).
- ⁶⁸M. N. Paddon-Row, N. G. Rondan, K. N. Houk, and K. D. Jordan, *J. Am. Chem. Soc.* **104**, 1143 (1982).
- ⁶⁹P. D. Burrow and J. A. Michejda, *Chem. Phys. Lett.* **42**, 223 (1976).
- ⁷⁰K. Afllatooni, B. Hitt, G. A. Gallup, and P. D. Burrow, *J. Chem. Phys.* **115**, 6489 (2001).
- ⁷¹M. Tronc, M. Allan, and F. Edard, in *Abstract of Contributed Papers, XVII ICPEAC* (North Holland, Amsterdam, 1987), p. 335.
- ⁷²L. Sanche and G. J. Schulz, *J. Chem. Phys.* **58**, 479 (1973).
- ⁷³P. D. Burrow and K. D. Jordan, *Chem. Phys. Lett.* **36**, 594 (1975).
- ⁷⁴E. Epifanovsky, I. Polyakov, B. Grigorenko, A. Nemukhin, and A. I. Krylov, *J. Chem. Theory Comput.* **5**, 1895 (2009).
- ⁷⁵K. B. Bravaya, D. Zuev, E. Epifanovsky, and A. I. Krylov, *J. Chem. Phys.* **138**, 124106 (2013).

3.2 Structure optimization of temporary anions

This publication focuses on applications of the CAP-EOM-CC analytic gradient for structure optimization of resonances. Choosing the right basis set is a very important part of CAP-EOM-CC calculations, as according to previous studies on vertical quantities [62], the basis set can affect the quality of the results considerably. However, although a large and diffuse basis set might produce more reliable results, in applications a compromise has to be made between accuracy and affordability. For this reason, it was investigated how double- and triple- ζ basis sets with different number and type of diffuse functions influence the optimized structural parameters, vertical and adiabatic electron affinities and resonance widths.

An implementation of the CAP-EOM-CCSD(2) gradient, and benchmark calculations, where CAP-EOM-CCSD and CAP-EOM-CCSD(2) results were compared for different basis sets and various anionic resonances, were also presented in this publication.

A disadvantage of using a box-shaped CAP, a problem already mentioned in Publication 1 (Section 3.1), is that the orientation of the molecule relative to the box is usually not unambiguous, thus in some cases the molecule might rotate relative to the box during optimization. In this article, the impact the relative orientation of the molecule and the CAP has on the energy was investigated. It was shown that by updating the box size parameters, these effects can be moderated.

During a geometry optimization, it can happen that the optimal value of the CAP strength parameter changes abruptly with the geometry. This is because at some geometries multiple parameter values fulfill the requirement (2.58), and at other geometries none do. The disappearance of a certain minimum of (2.58) can influence the smoothness of the CPES, which is discussed in Publication 3 (Section 3.3).

Geometry optimizations of anionic resonances of acrylonitrile, methacrylonitrile and unsaturated hydrocarbons up to 1,3,5-hexatriene, something that was previously impossible with methods for metastable states, were also presented in this publication. CAP-EOM-CCSD and CAP-EOM-CCSD(2) results with a double- ζ basis set have a somewhat high deviation (0.2-0.5 eV) from experimental electron affinities, but trends in electron affinity and resonance width usually correlate well with experiments. For example, the calculated energy difference between the $2\pi^*$ states of *cis*- and *trans*-1,3,5-hexatriene (0.58-0.61 eV) is in very good agreement with the experimental value (0.55 eV). Using a triple- ζ basis set, and an approximate zero-point vibrational energy correction extracted from Reference [75] can bring the deviation between calculation and experiment under 0.1 eV for the adiabatic electron affinity of acrylonitrile. Structural differences between the resonance and its parent neutral state for acrylonitrile and methacrylonitrile were analyzed, and connections with peaks of the measured electron energy loss spectra [75, 76] were suggested.

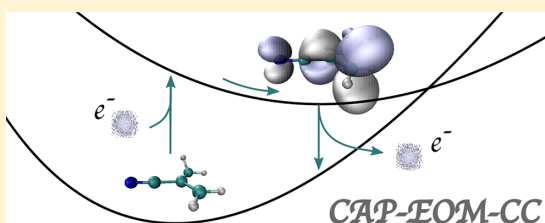
Structure Optimization of Temporary Anions

Zsuzsanna Benda,* Kerstin Rickmeyer, and Thomas-C. Jagau*[✉]

Department of Chemistry, University of Munich (LMU), D-81377 Munich, Germany

^S Supporting Information

ABSTRACT: We determine equilibrium structures, adiabatic electron affinities, and resonance widths of various temporary anions to benchmark the complex absorbing potential equation-of-motion coupled-cluster (CAP-EOM-CC) method. The second-order approximation to CAP-EOM-CC with singles and doubles (SD) excitations is found to yield slightly lower resonance positions and widths than full CAP-EOM-CCSD. The basis set dependence of adiabatic resonance positions and widths is similar to that of the vertical quantities. We demonstrate the usefulness of structure optimizations of temporary anions by two examples. For the anions of acrylonitrile and methacrylonitrile, we observe good agreement for the adiabatic electron affinities and structural changes between our theoretical results and two-dimensional electron-energy loss spectra. For the unsaturated hydrocarbons ethylene, 1,3-butadiene, and *cis*- and *trans*-1,3,5-hexatriene, the agreement between theory and electron transmission spectroscopy is good for the lower-lying π^* resonances, while our results for the $3\pi^*$ resonance of *trans*-hexatriene suggest a shortcoming of the method or reinterpretation of the corresponding electron transmission spectrum. The experimentally determined difference between the electron affinities of the *cis* isomer and the *trans* isomer of hexatriene are reproduced well by CAP-EOM-EA-CCSD and CAP-EOM-EA-CCSD(2).



1. INTRODUCTION

Molecular anions play a key role in many chemical processes such as electron transfer or bond breaking through dissociative electron attachment.¹ Since the extra electron changes the bonding pattern, molecular properties and chemical reactivity of anions and their parent neutral species can differ substantially. The comprehensive theoretical characterization of molecular anions requires one to take into account nuclear motion. In the case of bound anions, that is, when the anion is lower in energy than the ground state of the neutral molecule, standard electronic-structure methods can be employed for investigating the potential energy surfaces (PES) of the relevant anionic and neutral electronic states and identifying special points such as equilibrium structures and transition states.

In contrast, anions that are above the neutral ground state are electronic resonances and subject to autodetachment.¹ Resonances cannot be represented as stationary states in the Hermitian domain of the molecular Hamiltonian and are, therefore, not amenable to bound-state electronic-structure calculations. However, in the non-Hermitian domain, they can be associated with quasistationary states with complex energy,^{2,3}

$$E = E_R - i\Gamma/2 \quad (1)$$

with E_R as the resonance position and Γ as the resonance width. Hence, complex-valued PES (CPES)⁴ can be constructed for an anion at molecular structures where it is not bound but of temporary nature. CPES can be experimentally probed, for example, in electron impact,^{5–7} electron trans-

mission,^{8–10} and photodetachment¹¹ experiments. Temporary anions can be observed as resonances in such spectra with the spectral width corresponding to their inverse lifetime. When the resonance is sufficiently long-lived compared to the time scale of nuclear motion, vibrational bands can appear in the spectrum, and if the Franck–Condon overlap is sufficiently large, the adiabatic electron affinity (AEA) can be determined. The interpretation of these experiments calls for reliable computational methods that are able to locate minimum-energy structures of polyatomic temporary anions.

Recently, we derived an expression for the analytic energy gradient for complex absorbing potential equation-of-motion coupled-cluster (CAP-EOM-CC) methods.¹² This makes CAP-EOM-CC the only method for electronic resonances that has analytic gradients and thus can be used to optimize systems larger than the diatomic and triatomic molecules previously optimized by constructing full-dimensional PES through single-point energy calculations. In our previous publication,¹² we performed structure optimizations of several small temporary anions consisting of 4–6 atoms. In this article, we apply CAP gradients to larger systems and investigate the performance of different basis sets and approximations to the many-body treatment in EOM-CC.

In CAP methods,^{13–17} the Hamiltonian is the sum of the usual molecular Hamiltonian \mathcal{H} and the CAP. In our case, the CAP is a purely imaginary potential multiplied by the strength parameter η :

Received: February 5, 2018

Published: June 8, 2018

$$\mathcal{H}(\eta) = \mathcal{H} - i\eta W \quad (2)$$

$$W = \sum_{\alpha} W_{\alpha}, \quad \alpha = x, y, z \quad (3)$$

$$W_{\alpha} = \begin{cases} 0 & \text{if } |r_{\alpha} - o_{\alpha}| \leq r_{\alpha}^0 \\ (|r_{\alpha} - o_{\alpha}| - r_{\alpha}^0)^2 & \text{if } |r_{\alpha} - o_{\alpha}| > r_{\alpha}^0 \end{cases} \quad (4)$$

Throughout the article, the box size parameters r_{α}^0 are chosen as the spatial extent of the wave function of the parent neutral state ($\sqrt{\langle R^2 \rangle_0}$) in the x , y , and z directions¹⁸ unless stated otherwise. The CAP origin o is chosen as the center of nuclear charges.¹²

The operator $\mathcal{H}(\eta)$ from eq 2 has complex eigenvalues according to eq 1. In a complete basis, one would obtain the exact resonance position and width with an infinitesimally small η ,¹³ but in a finite basis set, the limit $\eta \rightarrow 0$ is not meaningful, and one has to use a finite η , which introduces a perturbation of the system. Riss and Meyer proposed¹³ that an optimal value of η (η_{opt}) can be determined by minimizing $|\eta \, dE/d\eta|$. However, η_{opt} is not well-defined as this expression often has multiple minima. In particular, the position and number of minima in $|\eta \, dE/d\eta|$ can be different at different geometries and disappearing minima can cause discontinuities in the CPES of the resonance.

As shown in ref 19, the stabilization of the resonance can be seen also from the convergence of the spatial extent of the resonance wave function, $\sqrt{\langle R^2 \rangle_r}$. From the η values corresponding to minima of $|\eta \, dE/d\eta|$, we choose the smallest one for which both real and imaginary parts of $\sqrt{\langle R^2 \rangle_r}$ are stable with respect to a further increase of η .

For structure optimization, we then follow the procedure proposed in ref 12, which involves repeated updating of the parameters η_{opt} and r_{α}^0 :

1. Determine $\sqrt{\langle \alpha^2 \rangle_0}$ of the neutral molecule.
2. Find η_{opt} for $r_{\alpha}^0 = \sqrt{\langle \alpha^2 \rangle_0}$.
3. Optimize the geometry while leaving $\eta = \eta_{\text{opt}}$ and r_{α}^0 unchanged.
4. Go to step 1 and repeat until $\sqrt{\langle \alpha^2 \rangle_0}$ and η_{opt} are converged.

In most cases, this procedure entails only moderate changes in η_{opt} and r_{α}^0 and provides a smooth path from the equilibrium structure of the parent neutral state to that of the resonant anion. However, we encountered some cases in which an abrupt change in η_{opt} could not be avoided as will be discussed in section 2.2.

Instead of minimizing $|\eta \, dE/d\eta|$ for the determination of η_{opt} , one can also minimize a deperturbed complex energy $E - \eta \, dE/d\eta$ ^{13,19} or perform analytic continuation using Padé approximants²⁰ to reach the limit $\eta \rightarrow 0$. Although these approaches may lead to improved resonance positions and widths, they share the property that the final energy is not obtained as an eigenvalue of an approximate Schrödinger equation rendering the formulation of the corresponding gradient theories more involved.

The CAP method has been successfully combined with various electronic-structure methods including density-functional theory,²¹ algebraic diagrammatic construction,^{22,23}

multireference configuration interaction,^{24,25} multiconfigurational quasidegenerate perturbation theory,²⁶ symmetry-adapted-cluster configuration interaction²⁷ (SAC-CI), and EOM-CC.^{18,28} We derived analytic gradients for the excitation energy (EE),²⁹ electron attachment (EA),³⁰ and ionization potential (IP)³¹ variants of CAP-EOM-CC and implemented them within the singles and doubles (CCSD) approximation in Q-Chem,³² release 5.0.

In this work, we extend our implementation to the CAP-EOM-CCSD(2) family of methods. EOM-CCSD(2),³³ also called EOM-MP2, is an approximation to EOM-CCSD that arises from a perturbative analysis of the EOM-CCSD similarity-transformed Hamiltonian and uses an MP2 reference state in the EOM procedure. The working equations of the EOM-CCSD(2) energy calculation are identical to EOM-CCSD, while the expressions for some density matrix elements differ slightly and the Z equations that determine the amplitude response become trivial. The computational cost of energy and gradient calculations with the EA and IP variants of EOM-CCSD(2) is reduced compared to EOM-CCSD because all iterative procedures scale as N^5 . In contrast, the EE variant scales as N^6 , and no reduction of scaling is achieved.

For bound states, it was demonstrated^{34,35} that the EOM-EE-CCSD(2) method has an accuracy comparable to EOM-EE-CCSD. The performance of EOM-EE-CCSD(2) depends on the basis set, and the standard deviation of the excitation energy difference from higher order methods (EOM-EE-CCSDT and CC3 linear response theory) is larger for EOM-EE-CCSD(2) than for EOM-EE-CCSD.

Here, we use the EA variants of CAP-EOM-CCSD and CAP-EOM-CCSD(2) to determine resonance positions and widths of temporary anions as well as their equilibrium structures. In all calculations of the resonance states, the CAP is introduced at the Hartree–Fock (HF) level. The optimization of the parent neutral molecules is done at the CCSD and MP2 levels. In both schemes, a temporary anion and its parent neutral state are obtained as eigenstates of the same Hamiltonian ensuring consistency between the real and imaginary parts of the CPES.³⁶

Figure 1 describes the quantities that are used throughout the article for describing temporary anions. The vertical electron affinity (VEA) is calculated as the difference between the energy of the neutral ground state and the real part of the energy of the resonance, both calculated at the equilibrium structure of the neutral species, whereas the vertical detachment energy (VDE) is the same energy difference evaluated at the equilibrium structure of the resonance. We calculate the adiabatic electron affinity (AEA) as the difference between the energy of the neutral ground state at the neutral equilibrium structure and the real part of the resonance energy evaluated at the resonance equilibrium structure neglecting vibrational energy contributions. Γ_0 is the resonance width determined at the neutral equilibrium structure, whereas Γ_r is calculated at the resonance equilibrium structure.

The rest of the article is structured as follows. In section 2, we examine how the size and diffuseness of the basis set affect equilibrium structures, electron affinities, and resonance widths. CAP-EOM-EA-CCSD(2) is compared against CAP-EOM-EA-CCSD for various molecules and basis sets, and rotation of the molecule relative to the CAP is also investigated. In section 3, we use the CAP-EOM-EA-CCSD and -CCSD(2) methods to study experimentally observed phenomena: the electron energy loss spectra of acrylonitrile

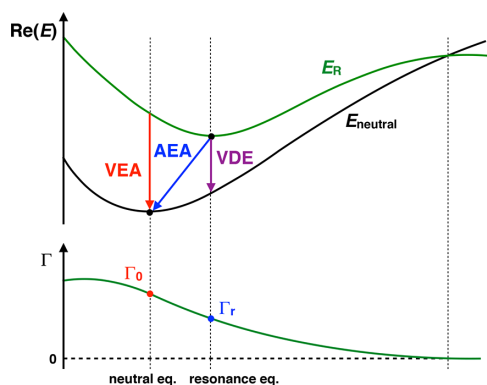


Figure 1. Schematic drawing of the CPES of a temporary anion (green) and the PES of its stable neutral parent state (black). The black dots correspond to the minima of the E_R and the E_{neutral} curves and thus define the resonance and neutral equilibrium structures. The quantities used in the article for the description of temporary anions, vertical and adiabatic electron affinity, vertical detachment energy, and the resonance widths Γ_0 and Γ_r are also shown in the figure.

and methacrylonitrile and trends in the positions and lifetimes of the temporary anions of ethylene, 1,3-butadiene, and *cis*- and *trans*-1,3,5-hexatriene. Section 4 provides our concluding remarks.

2. BENCHMARK CALCULATIONS

2.1. Basis Set Effects. The calculation of anions, bound and resonant, requires in general very diffuse basis sets due to the extension of the wave function. When studying resonances with CAP methods, the basis set in addition needs to describe the regions where the CAP is active. A problem with such highly diffuse basis sets is that linear dependencies can occur, which can be projected out of the basis set but can still lead to discontinuities in the PES during a geometry optimization. Also, a CAP gradient calculation is more costly than the corresponding regular gradient calculation because of the need to handle complex density matrices.¹² These peculiarities motivate the search for an optimal basis set, which is diffuse enough to describe the resonance properly yet small enough to enable calculations beyond model systems and avoid linear dependency problems.

We tested several basis sets on the π^* resonances of CH_2O , C_2H_4 , and HCOOH for which we presented initial results in ref 12. In these calculations, the standard aug-cc-pVDZ and aug-cc-pVTZ basis sets³⁷ were augmented by different types and numbers of extra diffuse functions on the heavy atoms, following the augmentation scheme “A” described in ref 18. In the following, we use shorthand notations for the basis sets, with -DZ and -TZ standing for aug-cc-pVDZ and aug-cc-pVTZ, and the suffixes, for example +3p3d, specifying the number and type of extra diffuse functions (three p-type and three d-type functions in this case).

Figure 2 shows C=O and C=C bond lengths for these three temporary anions. The corresponding VEA and AEA values and resonance widths are given in Figure 3, while η_{opt} values for the various molecule–basis combinations are given in the Supporting Information. Results for CH_2O show that the smallest basis, -DZ without further augmentation, is already able to capture the resonance, but the calculated EAs and Γ s (VEA = -1.73 eV, AEA = -1.39 eV, $\Gamma_0 = 0.51$ eV, $\Gamma_r = 0.47$

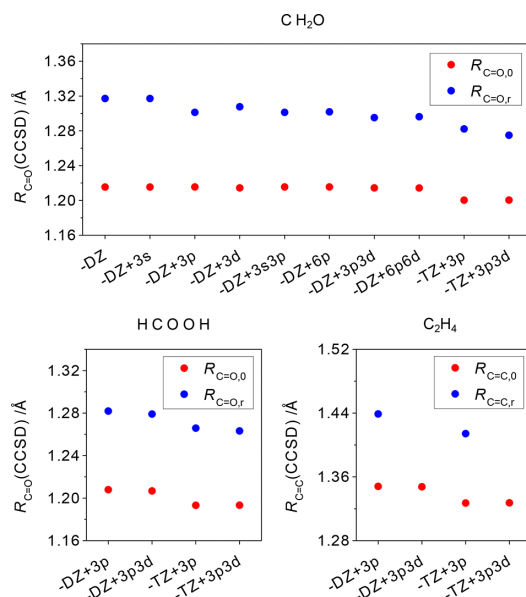


Figure 2. C=O and C=C equilibrium bond lengths of CH_2O , HCOOH , and C_2H_4 and the corresponding temporary anions obtained using various basis sets. Structures of temporary anions computed with CAP-EOM-EA-CCSD and those of neutral molecules with CCSD.³⁸

eV) differ considerably from the experimental values (VEA = -0.86 eV, AEA = -0.65 eV, Γ in the range of 0.2 – 0.4 eV).⁸ Figure 2 shows that adding extra diffuse functions to the -DZ or -TZ basis sets has practically no effect on the C=O bond length of the neutral molecule (1.215 Å with -DZ and 1.200 Å with -TZ). However, extra diffuse functions can give substantially different VEA and Γ_0 values (Figure 3) if they improve the representation of the resonance. As the extra electron occupies a π^* orbital, the representation improves most when extra p functions are added on the C and O atoms to the standard basis set. In this case the calculated values change significantly: VEA becomes -1.37 eV and Γ_0 goes down to 0.35 eV. The importance of p-functions is also seen from the drastic change in η_{opt} between -DZ (0.035 au) and -DZ+3p (0.005 au). Extra d-functions are not as important as p-functions but also have a significant impact (VEA = -1.31 eV, $\Gamma_0 = 0.37$ eV), while extra s-functions do not have a notable effect on the results as expected from symmetry considerations.

As the description of the resonance improves when p-functions are added, the optimized structure of the resonance also changes (Figure 2). Whereas all basis sets predict a longer C=O equilibrium distance for the resonance than for neutral CH_2O in line with the antibonding character of the π^* orbital, the DZ+3p basis yields a shorter bond distance (1.301 Å) than the -DZ basis set (1.317 Å). The -DZ+3p3d basis yields an even shorter bond distance (1.295 Å) while diffuse s-functions make no impact. Going from double- ζ to triple- ζ also shortens the C=O bond, but here the effect is similar for the anion (0.020 Å) and the neutral molecule (0.015 Å).

The AEA and Γ_r values exhibit a similar basis set dependence as the VEA and Γ_0 values. The 3p3d augmentation results in smaller absolute EA values, larger Γ_0 and smaller Γ_r

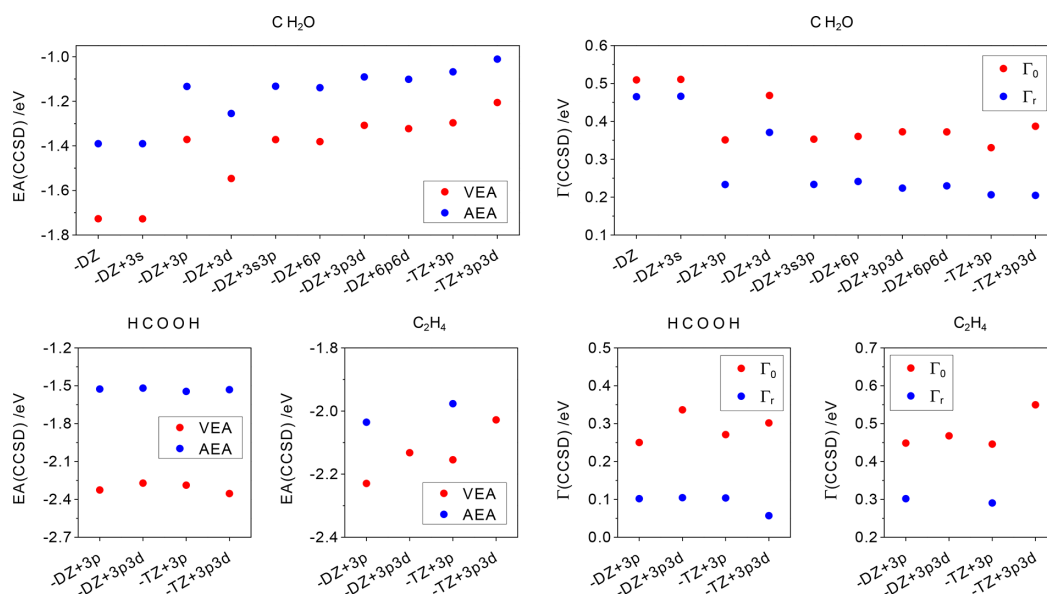


Figure 3. EA and Γ values for the π^* resonances of CH_2O , HCOOH , and C_2H_4 calculated with CAP-EOM-EA-CCSD using various basis sets.³⁸

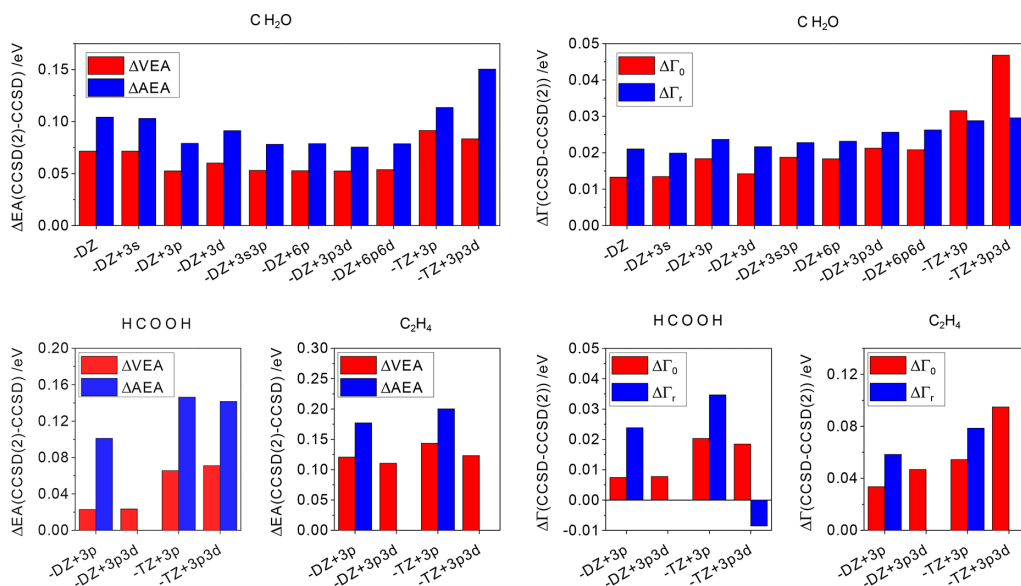


Figure 4. Differences between CAP-EOM-EA-CCSD and CAP-EOM-EA-CCSD(2) results for the EA and Γ values of the π^* resonances of CH_2O , HCOOH , and C_2H_4 calculated using various basis sets.³⁸

values compared to 3p for both double- and triple- ζ basis sets. Including more than three diffuse p- or d-functions, however, changes energies and widths only by about 0.01 eV and the C=O bond distance only by 0.001 Å.

Given these results for CH_2O , we focused on differences between the 3p and 3p3d augmentations and double- and triple- ζ basis sets for C_2H_4 and HCOOH . The lower part of Figure 2 shows that the trends observed for the C=O bond length of CH_2O hold for the other two test cases as well; adding extra d-functions, as well as changing the basis from double- to triple- ζ , results in shorter equilibrium bond lengths

for the resonances. Figure 3 shows that the basis set dependence of the VEA and AEA of HCOOH and C_2H_4 is somewhat different than that of CH_2O . In particular, the AEA of HCOOH changes by less than 0.02 eV when adding extra d-functions or going from double- to triple- ζ .

In conclusion, we find aug-cc-pVDZ+3p to be the smallest basis set that gives qualitatively correct results for energies, widths, and resonance equilibrium structures. The best way to improve it is by adding three extra d-functions or going to a triple- ζ basis if computationally feasible.

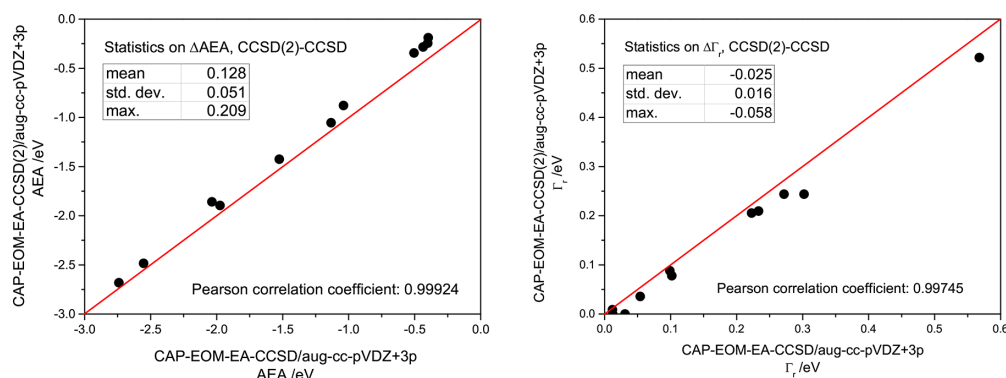


Figure 5. Comparison of AEA and Γ_r values calculated with CAP-EOM-EA-CCSD and CAP-EOM-EA-CCSD(2) using the aug-cc-pVDZ+3p basis set. The investigated resonances are: lowest π^* resonance of formaldehyde, formic acid, acrylonitrile, methacrylonitrile, ethylene, 1,3-butadiene (two states), and *cis*- and *trans*-1,3,5-hexatriene (two states).

2.2. Comparison of CAP-EOM-EA-CCSD and -CCSD(2). To check the performance of CAP-EOM-EA-CCSD(2) for EA and Γ values as well as equilibrium structures of resonances, we repeated the calculations presented in section 2.1 with CAP-EOM-EA-CCSD(2). The differences between -CCSD(2) and -CCSD results are plotted in Figure 4.

In general, there is a larger difference between results for the quantities that were calculated after geometry optimization of the resonance (AEA and Γ_r) than for the vertical ones (VEA and Γ_0). This effect is most pronounced for HCOOH calculated with double- ζ bases. Here, the two methods agree within less than 0.03 and 0.01 eV for VEA and Γ_0 , respectively, while the differences in AEA and Γ_r (ca. 0.10 and 0.02 eV) are similar to those observed for CH₂O. Moreover, the calculations on CH₂O show that the differences in VEA and AEA as well as in Γ_0 and Γ_r are similar for all double- ζ basis sets that contain extra diffuse p-functions.

Figure 4 also shows that triple- ζ basis sets lead to a somewhat larger difference between CAP-EOM-EA-CCSD and -CCSD(2) than the corresponding double- ζ basis sets. In the case of the CH₂O molecule, ΔAEA is especially large (ca. 0.15 eV) with the -TZ+3p3d basis set. This is because the η dE/d η expression has local minima at multiple η values and the one minimum chosen to define η_{opt} at the neutral equilibrium structure disappears during the geometry optimization at the -CCSD(2) level. This means that another η dE/d η minimum has to be used to define η_{opt} at the resonance equilibrium structure, which results in substantially different η_{opt} values for the two methods (see Supporting Information). Interestingly, this difference in η_{opt} causes a remarkable peak only for ΔAEA but not for $\Delta \Gamma_r$. The -TZ+3p3d basis set also gives a large $\Delta \Gamma_0$ for CH₂O⁻ (ca. 0.05 eV), which is surprising as η_{opt} values at the equilibrium structure of the neutral molecule are very similar. In the case of C₂H₄, the CCSD(2)-CCSD difference is significantly larger than in the cases of CH₂O and HCOOH for both vertical and adiabatic EA and Γ values (note the different scales in the panels of Figure 4).

Our VEA values for C₂H₄ obtained with the -TZ+3p3d basis set (-2.028 and -1.905 eV for CAP-EOM-EA-CCSD and -CCSD(2)) agree well with those of Falcetta et al.³⁹ who used standard EOM-EA-CCSD and -CCSD(2) in conjunction with the stabilization method. However, the CAP method yields smaller Γ_0 values (0.550 and 0.455 eV) than the stabilization method (0.646 and 0.604 eV). The CAP method behaves in a

similar way compared to the method of complex basis functions (CBF) as calculations for CH₂O⁻ illustrate: Our CAP-EOM-EA-CCSD/aug-cc-pVTZ+3p3d value for VEA (-1.206 eV) agrees well with CBF-EOM-EA-CCSD/aucc-cc-pCVTZ(cm+) (-1.163 eV), but the Γ_0 values differ considerably (0.387 eV vs 0.567 eV).

The comparison of the structures of the three anions shows that CAP-EOM-EA-CCSD(2) yields longer C-C or C-O equilibrium distances for all three resonances than -CCSD; the differences amount to 0.010–0.018 Å. This is in line with the trend for neutral molecules that MP2 usually gives longer equilibrium distances than CCSD.⁴⁰ All C-C and C=O equilibrium bond lengths are compiled in the Supporting Information.

In addition to examining the difference between CAP-EOM-EA-CCSD and -CCSD(2) energies and widths for various basis sets, we also quantified this difference for various π^* resonances using one particular basis set, namely, aug-cc-pVDZ+3p that was established as the smallest trustworthy basis set for such systems in section 2.1. The lowest-energy π^* resonances of formaldehyde, formic acid, acrylonitrile, methacrylonitrile, and ethylene, and the two lowest-energy π^* resonances of 1,3-butadiene and *cis*- and *trans*-1,3,5-hexatriene were investigated for this purpose.

Figure 5 reveals clear linear correlation between AEA and Γ_r values calculated with the two methods. In all cases -CCSD(2) yields smaller AEA (in absolute values) and Γ_r than -CCSD; the mean of the differences is 0.128 eV for AEA and -0.025 eV for Γ_r . The corresponding differences for VEA and Γ_0 are slightly smaller (0.098 eV and -0.020 eV), consistent with the results presented in Figure 4 for various basis sets. The statistics for VEA and Γ_0 are available from the Supporting Information.

In summary, CAP-EOM-EA-CCSD(2) yields results close to CAP-EOM-EA-CCSD; the difference between the two methods grows somewhat when going from double- ζ to triple- ζ basis sets. EA and Γ values calculated with CAP-EOM-EA-CCSD(2) are typically smaller (in absolute values) than those calculated with CAP-EOM-EA-CCSD. As a more complete treatment of electron correlation in general decreases EAs of temporary anions,⁴¹ the counterintuitive performance of CAP-EOM-EA-CCSD(2) is likely due to error cancellation.

2.3. Orientation of the Molecule Relative to the CAP. During geometry optimization, rotation of the molecule in the

CAP box is allowed if it does not break spatial symmetry.¹² This rotation can lead to different η_{opt} , EA, and Γ values. The dependence of resonance energies and widths on the size of the CAP box has been investigated several times,^{18,21,42,43} but rotation with respect to the box has not been studied before.

To check the effect of rotation, we considered the π^* resonance of formic acid at the equilibrium structure of the neutral molecule as an example. This molecule has C_s symmetry, so rotation is only allowed in the x - y plane (molecular plane). To assess the importance of recalculating the box size parameters during a geometry optimization, we carried out two sets of calculations at the CAP-EOM-EA-CCSD(2)/aug-cc-pVDZ+3p level: in the first set, the molecule was rotated around the z -axis by different angles while the box was held fixed, and in the second set, the box size parameters were updated while the molecule was rotated. Since these rotations do not affect $\sqrt{\langle z^2 \rangle_0}$, r_z^0 is the same in all calculations. In the second case (updated box) rotations by 90° result in the same energy and width, while in the first case (fixed box), only rotations by 180° do. The obtained EA and Γ values are plotted in Figure 6.

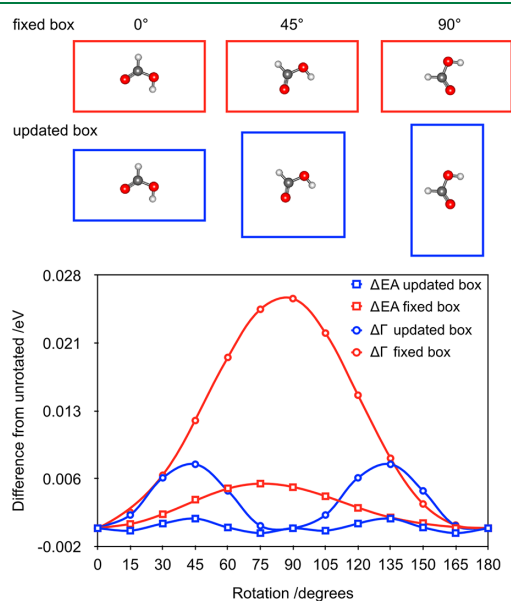


Figure 6. Differences in EA and Γ values arising from rotation of the molecule in a fixed CAP box (red line) and in an updated CAP box (blue line). Calculated at the CAP-EOM-EA-CCSD(2)/aug-cc-pVDZ+3p level and compared to the unrotated case.

Rotating the molecule has little effect on the real part of the energy: in the case of a fixed box, fluctuations smaller than 0.005 eV are observed, which can be reduced to 0.002 eV by updating the box parameters. The resonance width changes more with the rotation angle: for a fixed box, fluctuations can be as large as 0.025 eV, which is around 10% of the absolute value of Γ in the present case. Updating the box reduces the fluctuations to 0.007 eV, which is still more than three times larger than for the real part.

To minimize the impact of such rotations, we suggest to update the box size parameters and recalculate the η_{opt}

parameter during the geometry optimization of a resonance after a minimum has been found. In some cases, when there are large structural changes or the properties of the resonance change drastically during geometry optimization, it may even be necessary to update the box size parameters more frequently.

3. APPLICATIONS

3.1. Acrylonitrile and Methacrylonitrile. Electron energy loss (EEL) spectroscopy on acrylonitrile and methacrylonitrile indicates the presence of three low-lying π^* resonances.⁷ The lowest anionic states of both molecules feature rich vibrational structure in the EEL spectra so that the AEAs corresponding to these states can be determined experimentally.^{6,7} The experimental data suggest that the anion of methacrylonitrile has a considerably shorter lifetime than that of acrylonitrile.

We carried out structure optimizations for the lowest-lying anionic states of acrylonitrile and methacrylonitrile and calculated electron affinities and resonance widths at the neutral and the resonance equilibrium structures with CAP-EOM-EA-CCSD and CAP-EOM-EA-CCSD(2). The results are compiled in Table 1. For acrylonitrile, the vertical

Table 1. Calculated and Experimental Electron Affinities and Resonance Widths for the Lowest π^* Resonances of Acrylonitrile and Methacrylonitrile^a

method	basis	VEA (eV)	AEA (eV)	Γ_0 (eV)	Γ_r (eV)
acrylonitrile					
-CCSD	-DZ+3p	-0.583	-0.397	0.065	0.031
-CCSD(2)	-DZ+3p	-0.409	-0.188	0.048	0.000
-CCSD	-TZ+3p	-0.529	-0.334	0.060	0.022
-CCSD(2)	-TZ+3p	-0.332	-0.108	0.038	0.000
expt ¹⁰			-0.11		
expt ^{6,7}			-0.138		0.014
methacrylonitrile					
-CCSD	-DZ+3p	-0.707	-0.506	0.172	0.054
-CCSD(2)	-DZ+3p	-0.573	-0.344	0.122	0.036
expt ⁷			-0.190		0.100

^aCalculations were done with CAP-EOM-EA-CCSD and -CCSD(2) using the aug-cc-pVDZ+3p and aug-cc-pVTZ+3p basis sets.

quantities (VEA and Γ_0) are similar to those calculated with CAP/SAC-CI and a triple- ζ basis set using a smooth Voronoi potential (VEA ranging from -0.48 to -0.38 eV, $\Gamma_0 = 0.06$ eV).⁴⁴

Our calculations indicate a very small resonance width of acrylonitrile at both the neutral and the resonance equilibrium structure, which agrees with the estimate from experiment. With CAP-EOM-EA-CCSD(2), the anion is vertically stable against electron detachment at its equilibrium structure resulting in zero Γ_r . For methacrylonitrile, Γ_0 and Γ_r enclose the experimental value. The resonance widths Γ_0 of acrylonitrile and methacrylonitrile are calculated to differ by a factor of 2–3 as compared to 7 for the experimental estimates of Γ . We note that a direct comparison of resonance widths from theory and experiment is complicated because the experimental value does not correspond to a particular geometry, but is averaged over the CPES of the resonance.⁴⁵

Structure optimization lowers the electron affinities by approximately 0.2 eV for both molecules and thus brings the results considerably closer to the experimental EA values (see

Table 2. Equilibrium Structures of Acrylonitrile and Methacrylonitrile and Their Anions^a

	neutral				anion			
					CAP-EOM-EA			
	CCSD DZ+3p	MP2 DZ+3p	CCSD 3TZ+3p	MP2 TZ+3p	-CCSD DZ+3p	-CCSD(2) DZ+3p	-CCSD TZ+3p	-CCSD(2) TZ+3p
acrylonitrile								
R_{C_1-N}	1.172	1.188	1.156	1.168	1.193	1.212	1.173	1.193
$R_{C_1-C_2}$	1.452	1.441	1.439	1.421	1.416	1.409	1.393	1.386
$R_{C_2-C_3}$	1.350	1.352	1.334	1.333	1.424	1.431	1.404	1.415
methacrylonitrile								
R_{C_1-N}	1.172	1.189			1.192	1.213		
$R_{C_1-C_2}$	1.459	1.447			1.418	1.408		
$R_{C_2-C_3}$	1.351	1.355			1.415	1.428		
$\angle C_1-C_3-C_2-C_4$	180.0	180.0			176.1	176.2		

^aBond lengths are given in Å, angles in degrees.

Table 1). The remaining deviations from the experimental AEAs are 0.26–0.32 eV for CAP-EOM-EA-CCSD/aug-cc-pVDZ+3p, which is in line with the results from section 2.1 and similar to the error bars of EOM-EA-CCSD for bound anions. With the aug-cc-pVTZ+3p basis, the calculated AEA deviates by 0.20 eV from the EEL value for acrylonitrile. By inclusion of zero-point vibrational energy corrections ($\Delta ZPVE$), the accuracy of theoretical results can be further increased. We estimate $\Delta ZPVE$ using vibrational frequencies of the neutral molecules and the anions calculated by Regeta and Allan at the B3LYP/6-311++G(2df,2p) level.^{6,7} For acrylonitrile, the correction amounts to 0.126 eV and for methacrylonitrile to 0.145 eV. This means that CAP-EOM-EA-CCSD is capable of providing an electron affinity accurate within 0.1 eV when combined with the aug-cc-pVTZ+3p basis set and considering the zero-point vibrational energy correction. However, it seems that CAP-EOM-EA-CCSD(2) is subject to substantial error cancellation, as it gives an AEA within 0.01 eV of the experimental one for methacrylonitrile if $\Delta ZPVE$ is considered, while for acrylonitrile it even overshoots the experimental values.

Structural differences between the neutral molecules and their anions are summarized in Table 2. For acrylonitrile and methacrylonitrile, elongation of the C_2C_3 and the C_1N bonds is observed upon electron attachment, whereas the C_1C_2 bonds shrink. The change of the first bond length is more pronounced (0.06–0.08 Å) than that of the latter two (0.02 Å and 0.03–0.04 Å, respectively). This agrees with the shape of the Dyson orbital⁴⁶ depicted in Figure 7: It is antibonding between C_2 and C_3 and between C_1 and N and bonding between C_1 and C_2 . Also, a larger share of the excess electron density resides on the carbon atoms than on the nitrogen atom. Elongation of the C_1N and C_2C_3 bonds in the temporary anions is also suggested by two-dimensional EEL

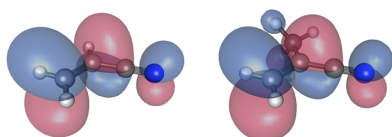


Figure 7. Real parts of the Dyson orbitals of the lowest π^* resonances of acrylonitrile and methacrylonitrile at their equilibrium structures calculated with CAP-EOM-EA-CCSD/aug-cc-pVDZ+3p.

spectra^{6,7} that feature prominent signals of the normal modes that correspond to nuclear motion in these directions.

While acrylonitrile remains planar upon electron attachment, methacrylonitrile has a nonsymmetric resonance equilibrium structure according to our calculations. However, the deflection of the heavy atoms from the molecular plane is small, and it does not entail a significant energy gain illustrating that the CPES of the anion is flat in these directions. In the EEL spectra,⁷ the CCN out-of-plane bending mode appears for both molecules with appreciable intensity, which indicates nuclear motion along this mode upon electron attachment in both cases despite the different equilibrium structure.

In sum, our results for acrylonitrile and methacrylonitrile show that a geometry optimization of the respective anions explains several features of the EEL spectra. Our calculations confirm the experimental AEAs and trends in energies and widths of the two species. It is also clear that a more comprehensive investigation of the anionic CPES beyond the equilibrium structures is necessary to explain all features of the EEL spectra such as the appearance of the out-of-plane bending modes.

3.2. Unsaturated Hydrocarbons. We carried out CAP-EOM-EA-CCSD and -CCSD(2)/aug-cc-pVDZ+3p structure optimizations for the π^* resonance states of ethylene, 1,3-butadiene, and *cis*- and *trans*-1,3,5-hexatriene to investigate trends in resonance positions, resonance widths, and equilibrium structures. The correlation diagrams for EA and Γ are shown in Figure 8; all calculated values are additionally compiled in the Supporting Information.

Experimental AEAs have been reported for all of these states.^{9,47,48} However, the values are of varying quality because vibrational structure is often only weak or not observed at all in the spectra. In the case of ethylene, faint undulations are observed in the electron transmission (ET) spectrum,⁴⁸ but it remains unclear whether the lowest feature corresponds to the 0–0 transition. Therefore, only an upper limit of –1.55 eV was given for the AEA, while the VEA was estimated as –1.74 eV based on the midpoint of the spectral feature. Owing to clear vibrational progression, the interpretation of the ET spectra is easier for the $1\pi^*$ resonance of butadiene: the AEA was established as -0.62 ± 0.05 eV. In contrast, the ET spectrum of the $2\pi^*$ state of butadiene does not feature any vibrational progression, and the experimental estimate of the EA (2.8 eV) is simply the midpoint of the spectral feature.

For *cis*- and *trans*-hexatriene, photoelectron⁴⁹ and optical spectroscopy⁵⁰ show that the three π ionization potentials and

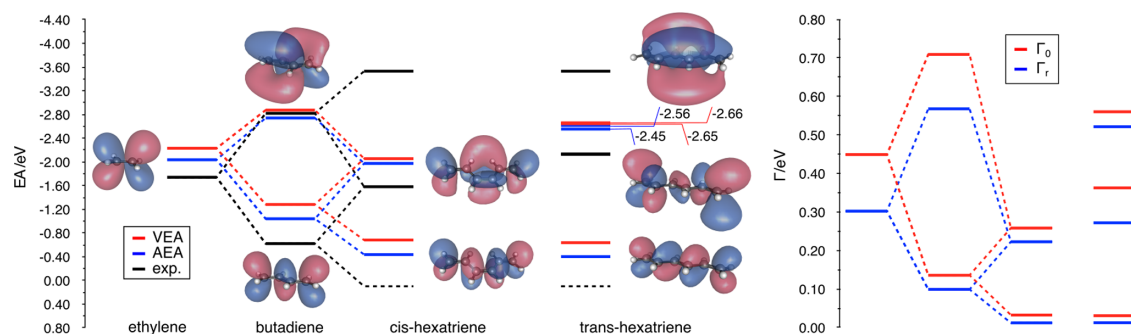


Figure 8. Correlation diagrams of the EA (left panel) and Γ (right panel) values of the π^* resonances of some unsaturated hydrocarbons calculated with CAP-EOM-EA-CCSD/aug-cc-pVDZ+3p. The real parts of the Dyson orbitals at the equilibrium structures of the respective resonances are also displayed in the left panel. The experimental EA values are taken from refs 9 and 47. The dashed energy levels indicate estimates⁹ of the EAs of the lowest anionic states of *cis*- and *trans*-hexatriene, which are bound states according to experiment.

the three π - π^* excitation energies of both isomers are very similar, but trends in the π^* electron affinities are less clear. The $1\pi^*$ state is not seen in the ET spectrum of either isomer and was, therefore, predicted to be stable against electron detachment.⁴⁷ The $2\pi^*$ anion state of the *cis* isomer is considerably lower in energy (1.58 eV) than that of the *trans* isomer (2.13 eV) according to ET spectroscopy, while the $3\pi^*$ anion state was tentatively assigned to structures at 3.53 eV for both isomers.⁴⁷ Vibrational progression could not be observed for any state of hexatriene.

Figure 8 illustrates that the trends in our calculated VEA and AEA values qualitatively agree with most of the experimental observations. Most VEA values calculated with CAP-EOM-EA-CCSD are 0.5–0.6 eV above the experimental values, which is similar to what was observed for smaller molecules.¹² These deviations are only partly due to the small double- ζ basis set. With a triple- ζ basis set, the VEA and AEA values of ethylene and the $1\pi^*$ resonance of butadiene change by only 0.06–0.07 eV. Optimizing the structure of the resonances reduces the EAs of the higher-lying states less (0.08–0.14 eV) than those of the lower-lying states (0.20–0.25 eV). Our best estimates (CAP-EOM-EA-CCSD(2)/aug-cc-pVTZ+3p) for the AEAs of ethylene and butadiene ($1\pi^*$ state) are -1.78 eV and -0.79 eV and deviate by 0.23 and 0.17 eV from the experimental estimates.

Among the higher-lying resonances, for which there is no experimental estimate of AEA, several inconsistencies are observed between theory and experiment: for the $2\pi^*$ state of butadiene, the difference between our CAP-EOM-EA-CCSD/aug-cc-pVDZ+3p value and the experiment is surprisingly small (0.05 eV). With a triple- ζ basis set, we even obtain a VEA slightly below the experimental estimate.

Also, we could not locate the $3\pi^*$ resonance of *cis*-hexatriene. We performed additional calculations using different CAP box sizes and basis sets of double- ζ and triple- ζ quality but found only states with substantial continuum contribution in the energy range below 5 eV. Furthermore, the $3\pi^*$ resonance of *trans*-hexatriene was calculated to lie almost at the same energy as the $2\pi^*$ resonance. These findings may indicate that the current approach is not reliable for the $3\pi^*$ resonances of these molecules. It could also be that the structure at 2.13 eV in the ET spectrum of the *trans*-isomer is caused by the $2\pi^*$ and $3\pi^*$ resonances together, whereas the

signal at 3.5 eV is not due to a π^* valence resonance for any of the isomers.

For the $1\pi^*$ state of both *cis*- and *trans*-hexatriene, our calculations produce negative values for VEA (0.50–0.68 eV) and AEA (0.24–0.44 eV) with fairly small resonance widths Γ_0 and Γ_r of less than 0.03 eV. Only the $1\pi^*$ state of *trans*-hexatriene is found to be vertically bound at its own equilibrium geometry at the CAP-EOM-CCSD(2) level of theory by about 0.004 eV. Semiempirical calculations yielded positive EAs in the range from 0.0 to +0.1 eV,⁹ which agrees with the absence of these states from the ET spectra. Interestingly, SAC-CI calculations⁵¹ also yielded a negative EA for *trans*-hexatriene. Given the deviations between theory and experiment we observed in sections 2.1 and 3.1, the AEAs of these states are likely very small, but a final decision about their signs cannot be made.

The energy difference between the $2\pi^*$ states of *cis*- and *trans*-hexatriene is calculated to be 0.59 eV using the CCSD VEA values, and 0.58 eV using the CCSD AEA values, which illustrates that structural relaxation has a similar effect on these two states. CCSD(2) yields very similar gaps (0.61 and 0.59 eV); thus both methods reproduce the experimental estimate of 0.55 eV for this pair of states well and confirm the assignment of the features in the spectra.

In general, CAP-EOM-EA-CCSD(2) gives lower absolute VEA and AEA values for all hydrocarbons investigated here (see Supporting Information). For the lowest resonances, the CCSD(2)–CCSD difference is 0.12–0.18 eV, which is in line with the results from section 2.2 (Figure 4), but for the higher-lying states of butadiene and hexatriene, this difference is considerably smaller (0.04–0.08 eV).

Even though geometry optimization entails only small energetic changes for the anions of the unsaturated hydrocarbons, their equilibrium structures differ significantly from those of the neutral molecules (see Table 3 and Supporting Information). For the low-lying resonances, the changes reflect the nodal structures of the Dyson orbitals depicted in Figure 8. The elongation of the CC bond in ethylene is consistent with features in ET^{9,48} and EEL spectra^{52–54} that were attributed to vibrational excitation of the C=C stretching mode. Similarly, the elongation of the C₁C₂ bond in the $1\pi^*$ state of butadiene agrees well with the presence of the C=C stretching mode in the ET spectrum.⁴⁸ A weaker feature in the same spectrum was

Table 3. Equilibrium Structures of Ethylene, 1,3-Butadiene, *trans*-1,3,5-Hexatriene, *cis*-1,3,5-Hexatriene, and Their Anions^a

		CCSD/DZ+3p		CAP-EOM-EA-CCSD/DZ+3p		
		neutral		1 π^*	2 π^*	3 π^*
C ₂ H ₄	R _{C-C}	1.348		1.439	—	—
C ₄ H ₆	R _{C1-C2}	1.353		1.410	1.374	—
	R _{C2-C3}	1.473		1.422	1.517	—
<i>trans</i> -C ₆ H ₈	R _{C1-C2}	1.354		1.392	1.388	1.360
	R _{C2-C3}	1.468		1.425	1.487	1.478
	R _{C3-C4}	1.358		1.411	1.362	1.376
<i>cis</i> -C ₆ H ₈	R _{C1-C2}	1.354		1.391	1.385	—
	R _{C2-C3}	1.471		1.427	1.481	—
	R _{C3-C4}	1.361		1.419	1.361	—
		CCSD/TZ+3p		CAP-EOM-EA-CCSD/TZ+3p		
		neutral		1 π^*		
C ₂ H ₄	R _{C-C}	1.327		1.414		
C ₄ H ₆	R _{C1-C2}	1.332		1.389		
	R _{C2-C3}	1.454		1.402		

^aAll bond lengths are given in Å.

tentatively assigned to the C–C stretching mode and may be attributed to the shortening of the C₂C₃ bond.

The trends in the equilibrium structures of the higher-lying anions are less clear due to through-space interactions. Structural changes compared to the neutral species are less pronounced than for the lower-lying resonances and do not exceed 0.04 Å for any CC bond. However, an experimental confirmation of these predictions is difficult since vibrational progression is not observed for the higher-lying states. The equilibrium structures of the ethylene anion and the 2 π^* state of butadiene are reached from the neutral equilibrium structures via slight out-of-plane distortions, whereas symmetry lowering is not observed for the other resonances (for the 3 π^* state of *trans*-hexatriene, we restricted the symmetry to C_{2h} a priori). In both cases, the associated energetic changes are small compared to those due to the symmetry-preserving relaxation of the CC bonds. We add that the experimental data for ethylene neither confirm nor rule out a nonplanar equilibrium structure.^{9,52}

The widths of all resonances but the 1 π^* states of *cis*- and *trans*-hexatriene, which are not observed experimentally, are such that autodetachment happens on the same time scale as nuclear motion or even faster for the higher-lying resonances of butadiene and hexatriene. This is consistent with the weak undulations in the case of ethylene and the complete absence of vibrational features in the latter cases. However, the 2 π^* resonances of the hexatriene isomers are two notable exceptions: Since their resonance widths are calculated to be smaller than those of ethylene, we would expect discernible vibrational progressions in the corresponding ET spectra. We finally note that the changes in Γ upon geometry optimization show the opposite trend as the EAs: the lowering is more pronounced for states that feature a large Γ_0 , that is, the higher-lying ones.

4. CONCLUSIONS

In this article, we have applied the recently developed CAP-EOM-EA-CCSD analytic gradients¹² to the structure optimization of various temporary anions. We conducted bench-

mark calculations on equilibrium structures, vertical and adiabatic electron affinities, and resonance widths using various augmented basis sets and found aug-cc-pVDZ+3p to be the smallest basis set that produces qualitatively correct results for π^* resonances. Using a basis set of triple- ζ quality reduces the adiabatic EAs significantly in accordance with trends established for vertical EAs,¹⁸ whereas the basis set dependence of the resonance widths Γ_r and Γ_0 is weaker and less uniform. The equilibrium structures of the resonant anions show a similar basis set dependence as those of the parent neutral molecules, that is, triple- ζ bases produce somewhat shorter bond distances than double- ζ bases.

We have extended our initial gradient implementation to CAP-EOM-EA-CCSD(2). Electron affinities computed with this method are 0.10–0.13 eV smaller (in absolute values) than those with CAP-EOM-EA-CCSD when using the aug-cc-pVDZ+3p basis and thus, owing to error cancellation, deviate less from experimental data. Resonance widths are computed to be smaller by about 0.02–0.03 eV. The equilibrium structures obtained for the resonant anions with the two methods show similar trends as CCSD and MP2 results for neutral molecules.

Our results also highlight a shortcoming of the approach: In some cases, the determination of the optimal CAP strength η_{opt} is not straightforward and special care is required to prevent abrupt changes in η_{opt} when changing the molecular structure since this would result in discontinuities in the CPES of the anion. Unfortunately, there are a few cases where such abrupt changes could not be avoided, which affects the accuracy of the results.

Still, despite this deficiency and despite the need to use heavily augmented basis sets so that often only double- ζ quality is affordable for the valence part, our present scheme for the structure optimization of temporary anions has considerable predictive power and is helpful in interpreting ET and EEL spectra. We demonstrated this in two exemplary applications: For the temporary anions of acrylonitrile and methacrylonitrile, our calculations agree well with two-dimensional EEL spectra^{6,7} for AEA values, trends in the resonance widths, and structural differences between the anionic and neutral species.

Our results for the π^* resonances of the unsaturated hydrocarbons ethylene, 1,3-butadiene, and *cis*- and *trans*-1,3,5-hexatriene illustrate that through-space interactions affect their energies and structures considerably and lead to asymmetries in the correlation diagrams. For the ethylene anion and the 1 π^* state of butadiene, our values for the AEAs and the equilibrium structures are in agreement with predictions based on vibrational progression in the ET spectra. We find that the description of the third π^* state of *cis*- and *trans*-hexatriene is not satisfactory with the current approach. However, the experimentally determined gap of 0.55 eV between the 2 π^* states of *cis*- and *trans*-hexatriene is nicely reproduced by both CAP-EOM-EA-CCSD and CAP-EOM-EA-CCSD(2).

■ ASSOCIATED CONTENT

Supporting Information

The Supporting Information is available free of charge on the ACS Publications website at DOI: 10.1021/acs.jctc.8b00128.

CAP strengths, coordinates of optimized structures, electron affinities, and resonance widths (PDF)

AUTHOR INFORMATION

Corresponding Authors

*E-mail: zsuzsanna.benda@cup.uni-muenchen.de.

*E-mail: th.jagau@lmu.de.

ORCID

Thomas-C. Jagau: 0000-0001-5919-424X

Notes

The authors declare no competing financial interest.

ACKNOWLEDGMENTS

We are grateful to Professor Michael Allan for his explanations about the electron-energy loss spectra of acrylonitrile and methacrylonitrile. We thank Professor Anna Krylov for her feedback about the manuscript. This work has been supported by the Fonds der Chemischen Industrie through a PhD fellowship to Z.B. and a Liebig fellowship to T.C.J. and by the Deutsche Forschungsgemeinschaft through grant JA 2794/1-1 (Emmy Noether program).

REFERENCES

- Simons, J. Molecular Anions. *J. Phys. Chem. A* **2008**, *112*, 6401–6511.
- Moiseyev, N. *Non-Hermitian Quantum Mechanics*; Cambridge University Press, 2011.
- Jagau, T.-C.; Bravaya, K. B.; Krylov, A. I. Extending Quantum Chemistry of Bound States to Electronic Resonances. *Annu. Rev. Phys. Chem.* **2017**, *68*, 525–553.
- Moiseyev, N. Forces on Nuclei Moving on Autoionizing Molecular Potential Energy Surfaces. *J. Chem. Phys.* **2017**, *146*, 024101.
- Schulz, G. J. Resonances in Electron Impact on Diatomic Molecules. *Rev. Mod. Phys.* **1973**, *45*, 423–486.
- Regeta, K.; Allan, M. Autodetachment Dynamics of Acrylonitrile Anion Revealed by Two-Dimensional Electron Impact Spectra. *Phys. Rev. Lett.* **2013**, *110*, 203201.
- Regeta, K.; Allan, M. Two-Dimensional Spectra of Electron Collisions with Acrylonitrile and Methacrylonitrile Reveal Nuclear Dynamics. *J. Chem. Phys.* **2015**, *142*, 184307.
- Burrow, P. D.; Michejda, J. A. Electron Transmission Study of the Formaldehyde Electron Affinity. *Chem. Phys. Lett.* **1976**, *42*, 223–226.
- Jordan, K. D.; Burrow, P. D. Temporary Anion States of Polyatomic Hydrocarbons. *Chem. Rev.* **1987**, *87*, 557–588.
- Burrow, P. D.; Howard, A. E.; Johnston, A.; Jordan, K. D. Temporary Anion States of Hydrogen Cyanide, Methyl Cyanide, and Methylene Dicyanide, Selected Cyanoethylenes, Benzonitrile, and Tetracyanoquinodimethane. *J. Phys. Chem.* **1992**, *96*, 7570–7578.
- Jagau, T.-C.; Dao, D. B.; Holtgrewe, N. S.; Krylov, A. I.; Mabbs, R. Same but Different: Dipole-Stabilized Shape Resonances in CuF and AgF. *J. Phys. Chem. Lett.* **2015**, *6*, 2786–2793.
- Benda, Z.; Jagau, T.-C. Communication: Analytic Gradients for the Complex Absorbing Potential Equation-of-Motion Coupled-Cluster Method. *J. Chem. Phys.* **2017**, *146*, 031101.
- Riss, U. V.; Meyer, H.-D. Calculation of Resonance Energies and Widths Using the Complex Absorbing Potential Method. *J. Phys. B: At., Mol. Opt. Phys.* **1993**, *26*, 4503–4536.
- Riss, U. V.; Meyer, H.-D. Reflection-Free Complex Absorbing Potentials. *J. Phys. B: At., Mol. Opt. Phys.* **1995**, *28*, 1475.
- Moiseyev, N. Derivations of Universal Exact Complex Absorption Potentials by the Generalized Complex Coordinate Method. *J. Phys. B: At., Mol. Opt. Phys.* **1998**, *31*, 1431.
- Muga, J. G.; Palao, J. P.; Navarro, B.; Egusquiza, I. L. Complex Absorbing Potentials. *Phys. Rep.* **2004**, *395*, 357–426.
- Sommerfeld, T.; Ehara, M. Complex Absorbing Potentials with Voronoi Isosurfaces Wrapping Perfectly around Molecules. *J. Chem. Theory Comput.* **2015**, *11*, 4627–4633.
- Zuev, D.; Jagau, T.-C.; Bravaya, K. B.; Epifanovsky, E.; Shao, Y.; Sundstrom, E.; Head-Gordon, M.; Krylov, A. I. Complex Absorbing Potentials within EOM-CC Family of Methods: Theory, Implementation, and Benchmarks. *J. Chem. Phys.* **2014**, *141*, 024102.
- Jagau, T.-C.; Zuev, D.; Bravaya, K. B.; Epifanovsky, E.; Krylov, A. I. A Fresh Look at Resonances and Complex Absorbing Potentials: Density Matrix-Based Approach. *J. Phys. Chem. Lett.* **2014**, *5*, 310–315.
- Landau, A.; Moiseyev, N. Molecular Resonances by Removing Complex Absorbing Potentials via Padé; Application to CO⁻ and N₂⁻. *J. Chem. Phys.* **2016**, *145*, 164111.
- Zhou, Y.; Ernzerhof, M. Calculating the Lifetimes of Metastable States with Complex Density Functional Theory. *J. Phys. Chem. Lett.* **2012**, *3*, 1916–1920.
- Santra, R.; Cederbaum, L. S. Complex Absorbing Potentials in the Framework of Electron Propagator Theory. I. General Formalism. *J. Chem. Phys.* **2002**, *117*, 5511–5521.
- Feuerbacher, S.; Sommerfeld, T.; Santra, R.; Cederbaum, L. S. Complex Absorbing Potentials in the Framework of Electron Propagator Theory. II. Application to Temporary Anions. *J. Chem. Phys.* **2003**, *118*, 6188–6199.
- Sommerfeld, T.; Riss, U. V.; Meyer, H.-D.; Cederbaum, L. S.; Engels, B.; Suter, H. U. Temporary Anions - Calculation of Energy and Lifetime by Absorbing Potentials: the N₂⁻ ²Π_g Resonance. *J. Phys. B: At., Mol. Opt. Phys.* **1998**, *31*, 4107.
- Sommerfeld, T.; Santra, R. Efficient Method to Perform CAP/CI Calculations for Temporary Anions. *Int. J. Quantum Chem.* **2001**, *82*, 218–226.
- Kunitsa, A. A.; Granovsky, A. A.; Bravaya, K. B. CAP-XMCDPT2 Method for Molecular Electronic Resonances. *J. Chem. Phys.* **2017**, *146*, 184107.
- Ehara, M.; Sommerfeld, T. CAP/SAC-CI Method for Calculating Resonance States of Metastable Anions. *Chem. Phys. Lett.* **2012**, *537*, 107–112.
- Ghosh, A.; Vaval, N.; Pal, S. Equation-of-Motion Coupled-Cluster Method for the Study of Shape Resonance. *J. Chem. Phys.* **2012**, *136*, 234110.
- Stanton, J. F.; Bartlett, R. J. The Equation of Motion Coupled-Cluster Method. A Systematic Biorthogonal Approach to Molecular Excitation Energies, Transition Probabilities, and Excited State Properties. *J. Chem. Phys.* **1993**, *98*, 7029–7039.
- Nooijen, M.; Bartlett, R. J. Equation of Motion Coupled Cluster Method for Electron Attachment. *J. Chem. Phys.* **1995**, *102*, 3629–3647.
- Stanton, J. F.; Gauss, J. Analytic Energy Derivatives for Ionized States Described by the Equation-of-Motion Coupled Cluster Method. *J. Chem. Phys.* **1994**, *101*, 8938–8944.
- Shao, Y.; Gan, Z.; Epifanovsky, E.; Gilbert, A. T.; Wormit, M.; Kussmann, J.; Lange, A. W.; Behn, A.; Deng, J.; Feng, X.; Ghosh, D.; Goldey, M.; Horn, P. R.; Jacobson, L. D.; Kaliman, I.; Khaliullin, R. Z.; Kúš, T.; Landau, A.; Liu, J.; Proynov, E. I.; Rhee, Y. M.; Richard, R. M.; Rohrdanz, M. A.; Steele, R. P.; Sundstrom, E. J.; Woodcock, H. L., III; Zimmerman, P. M.; Zuev, D.; Albrecht, B.; Alguire, E.; Austin, B.; Beran, G. J. O.; Bernard, Y. A.; Berquist, E.; Brandhorst, K.; Bravaya, K. B.; Brown, S. T.; Casanova, D.; Chang, C.-M.; Chen, Y.; Chien, S. H.; Closser, K. D.; Crittenden, D. L.; Didenhofen, M.; DiStasio, R. A., Jr.; Do, H.; Dutoi, A. D.; Edgar, R. G.; Fatehi, S.; Fusti-Molnar, L.; Ghysels, A.; Golubeva-Zadorozhnaya, A.; Gomes, J.; Hanson-Heine, M. W.; Harbach, P. H.; Hauser, A. W.; Hohenstein, E. G.; Holden, Z. C.; Jagau, T.-C.; Ji, H.; Kaduk, B.; Khistyayev, K.; Kim, J.; Kim, J.; King, R. A.; Klunzinger, P.; Kosenkov, D.; Kowalczyk, T.; Krauter, C. M.; Lao, K. U.; Laurent, A. D.; Lawler, K. V.; Levchenko, S. V.; Lin, C. Y.; Liu, F.; Livshits, E.; Lochan, R. C.; Luenser, A.; Manohar, P.; Manzer, S. F.; Mao, S.-P.; Mardirossian, N.; Marenich, A. V.; Maurer, S. A.; Mayhall, N. J.; Neuscamman, E.; Oana, C. M.; Olivares-Amaya, R.; O'Neill, D. P.; Parkhill, J. A.; Perrine, T. M.; Peverati, R.; Prociuk, A.; Rehn, D. R.; Rosta, E.; Russ, N. J.; Sharada, S. M.; Sharma, S.; Small, D. W.; Sodt, A.; Stein, T.; Stück, D.; Su, Y.-C.; Thom, A. J.; Tsuchimochi, T.; Vanovschi, V.; Vogt, L.; Vydrov,

- O.; Wang, T.; Watson, M. A.; Wenzel, J.; White, A.; Williams, C. F.; Yang, J.; Yeganeh, S.; Yost, S. R.; You, Z.-Q.; Zhang, I. Y.; Zhang, X.; Zhao, Y.; Brooks, B. R.; Chan, G. K.; Chipman, D. M.; Cramer, C. J.; Goddard, W. A., III; Gordon, M. S.; Hehre, W. J.; Klamt, A.; Schaefer, H. F., III; Schmidt, M. W.; Sherrill, C. D.; Truhlar, D. G.; Warshel, A.; Xu, X.; Aspuru-Guzik, A.; Baer, R.; Bell, A. T.; Besley, N. A.; Chai, J.-D.; Dreuw, A.; Dunietz, B. D.; Furlani, T. R.; Gwaltney, S. R.; Hsu, C.-P.; Jung, Y.; Kong, J.; Lambrecht, D. S.; Liang, W.; Ochsenfeld, C.; Rassolov, V. A.; Slipchenko, L. V.; Subotnik, J. E.; Van Voorhis, T.; Herbert, J. M.; Krylov, A. I.; Gill, P. M.; Head-Gordon, M. Advances in molecular quantum chemistry contained in the Q-Chem 4 program package. *Mol. Phys.* **2015**, *113*, 184–215.
- (33) Stanton, J. F.; Gauss, J. Perturbative Treatment of the Similarity Transformed Hamiltonian in Equation-of-Motion Coupled-Cluster Approximations. *J. Chem. Phys.* **1995**, *103*, 1064–1076.
- (34) Kännár, D.; Tajti, A.; Szalay, P. G. Accuracy of Coupled Cluster Excitation Energies in Diffuse Basis Sets. *J. Chem. Theory Comput.* **2017**, *13*, 202–209.
- (35) Tajti, A.; Szalay, P. G. Investigation of the Impact of Different Terms in the Second Order Hamiltonian on Excitation Energies of Valence and Rydberg States. *J. Chem. Theory Comput.* **2016**, *12*, 5477–5482.
- (36) Jagau, T.-C.; Krylov, A. I. Complex Absorbing Potential Equation-of-Motion Coupled-Cluster Method Yields Smooth and Internally Consistent Potential Energy Surfaces and Lifetimes for Molecular Resonances. *J. Phys. Chem. Lett.* **2014**, *5*, 3078–3085.
- (37) Kendall, R. A.; Dunning, T. H., Jr.; Harrison, R. J. Electron Affinities of the First-Row Atoms Revisited. Systematic Basis Sets and Wave Functions. *J. Chem. Phys.* **1992**, *96*, 6796–6806.
- (38) For technical reasons, several calculations on HCOOH and C₂H₄ with the 3p3d augmentation could not be completed.
- (39) Falcetta, M. F.; DiFalco, L. A.; Ackerman, D. S.; Barlow, J. C.; Jordan, K. D. Assessment of Various Electronic Structure Methods for Characterizing Temporary Anion States: Application to the Ground State Anions of N₂, C₂H₂, C₂H₄, and C₆H₆. *J. Phys. Chem. A* **2014**, *118*, 7489–7497.
- (40) Helgaker, T.; Jørgensen, P.; Olsen, J. *Molecular Electronic-Structure Theory*; Wiley and Sons, 2000.
- (41) Jagau, T.-C. Non-Iterative Triple Excitations in Equation-of-Motion Coupled-Cluster Theory for Electron Attachment with Applications to Bound and Temporary Anions. *J. Chem. Phys.* **2018**, *148*, 024104.
- (42) Ghosh, A.; Vaval, N.; Pal, S.; Bartlett, R. J. Complex Absorbing Potential Based Equation-of-Motion Coupled Cluster Method for the Potential Energy Curve of CO₂⁻ Anion. *J. Chem. Phys.* **2014**, *141*, 164113.
- (43) Kunitsa, A. A.; Bravaya, K. B. First-Principles Calculations of the Energy and Width of the ²A_u Shape Resonance in p-Benzoquinone: A Gateway State for Electron Transfer. *J. Phys. Chem. Lett.* **2015**, *6*, 1053–1058.
- (44) Ehara, M.; Kanazawa, Y.; Sommerfeld, T. Low-lying π^* Resonances Associated with Cyano Groups: A CAP/SAC-CI Study. *Chem. Phys.* **2017**, *482*, 169–177.
- (45) Sommerfeld, T.; Meyer, H.-D. Computing the Energy-Dependent Width of Temporary Anions from L² ab initio Methods. *J. Phys. B: At, Mol. Opt. Phys.* **2002**, *35*, 1841–1863.
- (46) Jagau, T.-C.; Krylov, A. I. Characterizing Metastable States Beyond Energies and Lifetimes: Dyson Orbitals and Transition Dipole Moments. *J. Chem. Phys.* **2016**, *144*, 054113.
- (47) Burrow, P. D.; Jordan, K. D. Electron Transmission Spectroscopy of 1,3,5-Hexatriene: Isomeric Differences in π^* Orbital Energies. *J. Am. Chem. Soc.* **1982**, *104*, 5247–5248.
- (48) Burrow, P. D.; Jordan, K. D. On the Electron Affinities of Ethylene and 1,3-Butadiene. *Chem. Phys. Lett.* **1975**, *36*, 594–598.
- (49) Beez, M.; Bieri, G.; Bock, H.; Heilbronner, E. The Ionization Potentials of Butadiene, Hexatriene, and Their Methyl Derivatives: Evidence for Through Space Interaction Between Double Bond π -Orbitals and Non-Bonded Pseudo- π Orbitals of Methyl Groups? *Helv. Chim. Acta* **1973**, *56*, 1028–1046.
- (50) Gavin, R. M., Jr.; Rice, S. A. Spectroscopic Properties of Polyenes. II. The Vacuum Ultraviolet Spectra of cis and trans-1,3,5-Hexatriene. *J. Chem. Phys.* **1974**, *60*, 3231–3237.
- (51) Honda, Y.; Shida, T.; Nakatsuji, H. Excitation Spectra of Cation and Anion Radicals of Several Unsaturated Hydrocarbons: Symmetry Adapted Cluster-Configuration Interaction Theoretical Study. *J. Phys. Chem. A* **2012**, *116*, 11833–11845.
- (52) Walker, I. C.; Stamatovic, A.; Wong, S. F. Vibrational Excitation of Ethylene by Electron Impact: 1–11 eV. *J. Chem. Phys.* **1978**, *69*, 5532–5537.
- (53) Allan, M.; Winstead, C.; McKoy, V. Electron Scattering in Ethene: Excitation of the \tilde{a}^3B_{1u} State, Elastic Scattering, and Vibrational Excitation. *Phys. Rev. A: At, Mol, Opt. Phys.* **2008**, *77*, 042715.
- (54) Khakoo, M. A.; Khakoo, S. M.; Sakaamini, A.; Hlousek, B. A.; Hargreaves, L. R.; Lee, J.; Murase, R. Low-Energy Elastic Electron Scattering from Ethylene: Elastic Scattering and Vibrational Excitation. *Phys. Rev. A: At, Mol, Opt. Phys.* **2016**, *93*, 012710.

3.3 Crossing points between anionic and neutral surfaces

This article shows that the real part of the CAP-EOM-EA-CC analytic gradient for the anionic resonance and the real part of the CAP-CC gradient for its parent neutral state can be utilized to locate crossings between these states when starting from a structure where the anionic state is metastable. For the final optimization of crossing points, or also when starting from a stable anionic structure, regular EOM-CC can be used. The knowledge of the structure and the energy of these crossing points is not only interesting for the nonadiabatic transition from anionic to neutral + free electron states, but also for the stabilization of the resonance against direct autodetachment. The accessibility of the MECP can help in estimating the importance of DEA compared to autodetachment, for example. The MECP is located by minimizing the energy of the degenerate states, which requires analytic gradients of the two states (similar to the MECP of bound states, see Section 2.5.2).

The CAP-EOM-CCSD method usually gives a smooth CPES for the resonance far from the crossing, but near the crossing the determination of the optimal CAP strength parameter might become problematic. This is demonstrated on the π^* anionic resonance of formic acid in this publication. When a parameter value cannot be found according to (2.58), one can use regular EOM-CC, thus approximate the state as stable, which might result in a discontinuity of the real and imaginary surfaces. Alternatively, one can use the correction scheme (2.59) [63], which yields smooth surfaces close to the crossing, but the de-perturbed energy has no analytic gradients available, which makes geometry optimization difficult.

The optimization method was applied to acrylonitrile and methacrylonitrile, whose anionic resonances were already investigated in Publication 2 (Section 3.2). Here, some more features of the electron energy loss spectra [75, 76] could be connected to the properties of the CPESs. In particular, it was shown that the structure of MECPs can help in understanding bright peaks on the threshold line, which correspond to the emission of nearly zero-energy electrons. Presumably, both the direct and the nonadiabatic processes take part in forming the spectra, and further studies are needed to investigate their relative contribution to particular peaks.


Chloro-substituted ethylenes were also investigated in this article. For these compounds, DEA results from the interplay between two types of anionic resonances: a σ^* state that is dissociative along the chlorine-carbon bond, but has a short autoionization lifetime, and a π^* state, that has a longer lifetime and lower vertical attachment energy. The coupling of these states through nuclear motion helps in increasing the probability of dissociation. After determining vertical attachment energies and resonance widths, and locating MECPs between the lowest anionic resonance and the parent neutral state, the possibility of a DEA process for different molecules was discussed. The absence of an easily accessible, dissociative anionic resonance for ethylene explains why DEA is not significant for this molecule. For chloro-substituted ethylenes, the low energy of the MECP is promising, but the structure and resonance position of the minimum-energy $\sigma^*-\pi^*$ crossing are also needed to see if DEA can proceed through a barrierless pathway. These were presented for chloroethylene in Paper 4 (Section 3.4).

In the present article, the difference in measured Cl^- yields for electron attachment to dichloroethylene isomers [130] is connected to the calculated resonance widths. This shows that the characteristics of both the real and the imaginary part of the CPESs are important for understanding the behavior of such systems.

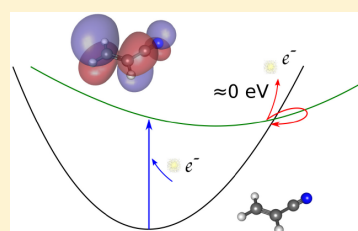
Understanding Processes Following Resonant Electron Attachment: Minimum-Energy Crossing Points between Anionic and Neutral Potential Energy Surfaces

Zsuzsanna Benda* and Thomas-C. Jagau*[✉]

Department of Chemistry, University of Munich (LMU), D-81377 Munich, Germany

 Supporting Information

ABSTRACT: The equation-of-motion coupled-cluster singles and doubles (EOM-CCSD) method with and without a complex absorbing potential (CAP) is applied for the study of the complex potential energy surfaces (CPES) of temporary anions and their parent neutral molecules. Crossings between the anionic state and the neutral state can be connected to the emission of nearly zero-energy electrons, which is demonstrated by the examples of acrylonitrile and methacrylonitrile. We show that the location of the minimum-energy crossing point (MECP) relative to the equilibrium structures of the neutral molecule and the anion can explain experimentally observed peaks on the threshold line of two-dimensional electron-energy loss spectra. The location and energy of the MECP is also crucial in dissociative electron attachment as we illustrate for chloro-substituted ethylenes. It is demonstrated that both the metastable region of the anionic CPES and the crossing with the neutral PES need to be considered to explain trends in the chloride ion formation cross sections of dichloroethylenes.



1. INTRODUCTION

Anions that have higher energy than the neutral ground state are not stable with respect to electron loss.¹ Competing with autodetachment is the nuclear motion, which can lead the system to more stable configurations, and in some cases, it might even lead to stable anions. Such stabilization through nuclear motion drives dissociative electron attachment, where stable fragmented products are formed through the intermediation of an anionic resonance.

The stability of a resonance with respect to autodetachment is defined by its lifetime, which depends on nuclear coordinates. In general, there can be regions in the nuclear coordinate space where the anion is higher in energy than the parent neutral molecule, and its lifetime with respect to electron loss is finite. There can also be regions where the anion has lower energy than the neutral molecule, so that the rate of electron loss is zero and the lifetime with respect to autodetachment is infinite.

In regions where the anion is stable, standard electronic structure methods can be applied. However, where the anion is metastable, it cannot be described as a discrete state in the usual Hermitian formalism. Instead, one can use different non-Hermitian approaches^{2,3} that transform the resonance to a discrete state having complex energy

$$E = E_R - i\Gamma/2 \quad (1)$$

where E_R is the resonance position and Γ is the resonance width.

The rate of autodetachment is given by the resonance width from eq 1 and usually decreases as the energy separation of the anionic state and the neutral state gets smaller (see Figure 1 for

a schematic drawing), but there is no rigorous connection between the two quantities, in general. In the vicinity of the crossing seam, autodetachment through nonadiabatic coupling can become important as well.^{4,5} For a theoretical model of this process, the nonadiabatic coupling between the anionic state and the neutral state plus the outgoing electron needs to be evaluated. This nonadiabatic detachment process is governed by a set of propensity rules;⁵ e.g., for a given energy of the outgoing electron, the rate of electron detachment depends inversely on the energy gap between the two potential energy surfaces (PESs).

Experimentally, electron detachment near the crossing is characterized by the emission of a nearly zero-energy electron (Figure 1) accompanied by a vibronic transition. Therefore, information about the crossing can be inferred, for example, from bright peaks on the threshold line in two-dimensional electron-energy loss (2D EEL) spectra.^{6,7} Alternatively, vibrational autodetachment experiments also provide information about the crossing seam.⁸

It was proposed that in the vicinity of the crossing a low-energy electron can be attached to the neutral molecule efficiently⁵ and that the position of the crossing can be used to estimate the activation energy of dissociative electron transfer processes.^{9,10} This has often been done by calculating the energy of the anionic and neutral states with bound state methods along a particular reaction coordinate neglecting nonadiabatic effects and the metastable nature of the anion.^{9,11–13}

Received: May 7, 2018

Published: July 3, 2018

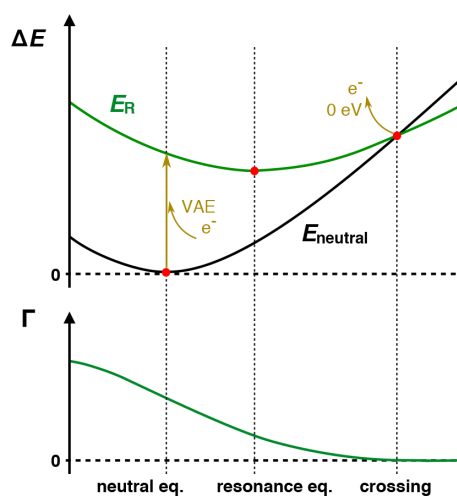


Figure 1. Hypothetical potential curves for an anionic state and its parent neutral state. In the upper panel, the energies relative to the energy of the neutral state at its equilibrium structure are plotted. Left of the crossing the anion is metastable with respect to electron loss having a resonance width that is dependent on the nuclear configuration (bottom panel). In typical experiments, the electron is attached to the neutral state at its equilibrium structure, where the energy difference between the anionic state and the neutral state is the vertical attachment energy (VAE). Emission of a nearly zero-energy electron takes place near the crossing between the two states, but autodetachment can occur at any nuclear configuration where the anionic state has higher energy than its parent neutral state.

Complex PESs (CPESs) of resonances leading to crossings with their parent neutral states have been studied previously only for small systems, mostly diatomics, for which an exploration using only single-point energy calculations is feasible (see, for example, refs 14–18). For larger molecules, such an approach becomes increasingly demanding, and analytic gradients are needed to locate special points such as equilibrium structures and minimum-energy crossing points (MECPs) on multidimensional PESs. While analytic gradients are available for many bound-state methods, corresponding developments for metastable states are limited to the complex absorbing potential equation-of-motion coupled cluster (CAP-EOM-CC) method,^{3,19,20} for which we recently defined a general analytic energy gradient expression.²¹ We implemented analytic gradients for CAP-EOM-CCSD and CAP-EOM-CCSD(2) and utilized them to locate equilibrium structures on the CPES of metastable anionic states.^{21,22} The electron attachment (EA) variant²³ of EOM-CC^{24–26} is especially well suited for the study of anionic resonances as it directly yields the attachment energy for various anionic states in one calculation and hence provides a balanced treatment of neutral and anionic states.

In this work, we combine CAP-EOM-CCSD with regular EOM-CCSD to describe both metastable and stable regions of anionic PESs to gain a better understanding of processes following electron attachment to polyatomic molecules. Within the EOM-CC model, only the description of crossings between noninteracting states is straightforward, whereas the treatment of interacting states requires special care due to the nonsymmetric nature of the EOM-CC Hamiltonian.^{27,28,29} Here, we handle the crossing states within the framework of

regular EOM-EA-CCSD, which provides neutral and anionic states and disregards nonadiabatic effects that would arise from the interaction of the anionic and the neutral plus free electron states. Within this framework of noninteracting states, the crossing seam can be $N-1$ -dimensional, where N is the number of internal nuclear degrees of freedom.

The MECP can be located by minimizing the energy difference along the gradient difference vector while minimizing the energy of one of the states in the orthogonal complement space.³⁰ Starting the MECP search in a region where the anion is metastable, one needs to consider only E_R , the real part of the energy in order to arrive at the anion-neutral crossing. To this end, we modified the regular MECP search algorithm³¹ in the Q-Chem program package³² to handle the real part of the energies and gradients computed with CAP-EOM-CCSD. After getting sufficiently close to the crossing with CAP-EOM-EA-CCSD, we use regular EOM-CCSD for the final optimization of the MECP. This is justified as Γ is expected to be small near the crossing and zero in regions where the anion is stable. It is also possible to locate the MECP using only EOM-EA-CCSD starting from a structure where the anion is bound. However, the energy and structure of the MECP are only meaningful in relation to the neutral and anionic equilibrium structures and the energy of the anion at these points. If the anion is metastable at these structures, like in the cases considered in this article, its description requires CAP-EOM-EA-CCSD.

The remainder of the article is organized as follows: in Section 2, we illustrate the performance of regular and CAP-augmented EOM-CCSD near the crossing seam by the example of formic acid and its anion. Section 3 presents two representative applications to acrylonitrile and methacrylonitrile as well as various chloroethylenes that illustrate how energies and structures of MECPs are connected to the decay or stabilization of temporary anions. Section 4 provides our concluding remarks.

2. POTENTIAL ENERGY SURFACES NEAR A CROSSING POINT

To study the behavior of CAP methods and regular bound state methods near surface crossings, neutral and anionic PESs connecting the resonance equilibrium structure with the MECP were calculated for HCOOH with CCSD and (CAP-)EOM-EA-CCSD using the aug-cc-pVDZ+3p basis set. This basis set was originally described in ref 20 as augmentation scheme “A”, and it was shown²² that for π^* resonances this basis generally gives reliable results. The HCOOH–HCOOH[−] system represents a sensitive test case as the energies and structures of the resonance equilibrium and the MECP are very similar: the largest difference in bond length is for the C–OH bond, which is 0.026 Å longer at the MECP. The distortion from planarity is also only slightly different; the dihedral angle H–O–C–H is smaller by 7° at the MECP (see Supporting Information for internal coordinates).

Regular EOM-EA-CCSD is not able to describe the anion properly in the metastable region, where the anionic state is above the neutral state. Figure 2 shows that the energy of the anion is underestimated, while the corresponding Dyson orbital³³ (shown in Figure S1 of the Supporting Information) illustrates that the farther we go into the metastable region the more the continuum states mix with the π^* resonance. Also, a second anionic state becomes more localized along the path

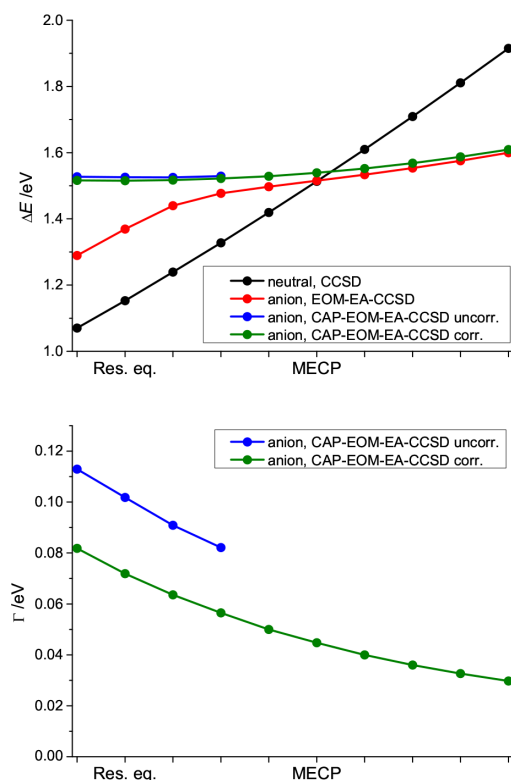


Figure 2. Energy profiles along the pathway connecting the resonance equilibrium structure with the MECP between the π^* resonance and the neutral ground state of formic acid. Structures were generated by linear interpolation and extrapolation using the resonance equilibrium structure and the MECP structure. ΔE is the energy relative to the neutral ground state at its equilibrium structure. Calculations were performed with CCSD for the neutral state; for the anionic state, EOM-EA-CCSD as well as uncorrected and corrected CAP-EOM-EA-CCSD results are plotted. For the anionic state, the resonance widths calculated with CAP-EOM-EA-CCSD are also shown. All calculations were done with the aug-cc-pVDZ+3p basis set.

and has an avoided crossing with the first anionic state (Figure S1). The mixing of the resonance with pseudocontinuum states is a known issue when using regular bound state methods and was, for example, demonstrated in detail in ref 34.

CAP-EOM-EA-CCSD gives reliable results near the resonance equilibrium structure, but close to the crossing, an optimal value of the CAP strength parameter η ^{20,35} can no longer be determined because the minimum in the $|\eta \text{ d}E/\text{d}\eta|$ trajectory, from which the optimal value is identified,³⁵ disappears (Figure S2). If one uses regular EOM-EA-CCSD from the point where CAP-EOM-EA-CCSD can no longer be used, there will be a discontinuity in the CPES: the resonance energy drops by 0.052 eV, while the resonance width drops abruptly from 0.081 eV to zero. In fact, if one uses CAP-EOM-EA-CCSD at the resonance equilibrium structure and EOM-EA-CCSD at the MECP, the energy of the anionic state will be slightly lower (by 0.011 eV) at the MECP than at the resonance equilibrium in this particular example. When using the larger aug-cc-pVTZ+3p basis set, this difference comes down to 0.003 eV.

Alternatively, one can use the deperturbed complex energy $U = E - \eta \text{ d}E/\text{d}\eta$,^{16,35,36} which has been corrected for the perturbation introduced by the CAP in first order. Using U instead of E yields a smooth surface near the crossing in the case of HCOOH^- . However, this surface can have a discontinuity in the bound region if the optimal CAP strength parameter abruptly goes to zero. Also, the resonance width Γ is nonzero in this scheme even after the crossing, where the anion is supposed to be stable. At the MECP, the difference between corrected CAP-EOM-EA-CCSD and EOM-EA-CCSD results amounts to 0.024 eV for ΔE and 0.044 eV for Γ . We note that EOM-EA-CCSD calculations with complex basis functions also lead to a small inconsistency between E_R and Γ near the crossing.¹⁸

3. APPLICATIONS

3.1. Acrylonitrile and Methacrylonitrile. In our previous paper,²² we discussed some features of the 2D EEL spectra of acrylonitrile and methacrylonitrile^{6,7} focusing on the equilibrium structure of the neutral molecules and the lowest π^* anionic resonance. Several bright peaks could be explained by the different structure of the anion and the neutral molecule. Here, we show how the crossing between the anionic and the neutral surface can explain some more features of these spectra.

One of the main observations in the 2D EEL spectra is that high-intensity peaks are arranged for both systems along diagonals that correspond to a specific kinetic energy of the emitted electron.^{6,7} One such diagonal is the threshold line, which corresponds to detachment of a zero-energy electron. A prominent peak near the threshold line of acrylonitrile shows that the anionic resonance, prepared in its vibrational ground state, decays into an excited vibrational state of the neutral molecule. Assignment of this peak is not unambiguous as both the ν_{12} (CH wagging = C2 pyramidalization) and the ν_{13} (CH_2 wagging = C3 pyramidalization) modes of the neutral molecule have frequencies similar to the EEL value of this peak.⁷

In methacrylonitrile, bright peaks near the threshold line were assigned to the ν_8 (CH_2 scissoring) or ν_9 (CH_3 umbrella) modes (EEL value 0.18 eV), the ν_6 ($\text{C}=\text{C}$ stretching) mode (EEL value 0.20 eV), and the ν_{17} (CH_3 asymmetric stretching) or ν_4 (CH_3 symmetric stretching) modes (EEL value 0.36 eV) of the neutral molecule.⁷ The first peak is probably connected to the vibrational ground state of the anion, and the second peak can either be the ground state or an excited state of a low-frequency mode, while the third peak is probably connected to the 6^1 vibrational level of the anion.

According to the Franck–Condon principle, which applies to the direct electronic autodetachment process, decay into vibrationally excited states of the neutral molecule indicates that either the equilibrium structures of the anion and the neutral molecule are shifted along these modes or the anionic PES is very flat, so that there is a high overlap between the vibrational wave functions of the initial and the final state. The rate of this direct process is the resonance width averaged over the probability density of the initial (anionic) vibrational wave function. Thus, the transition probability is expected to be higher if the vibrational state in question samples parts of the CPES where Γ is large. Acrylonitrile has a very small resonance width at the equilibrium structures of both the neutral and the anionic state (0.065 and 0.031 eV at the CAP-EOM-EA-CCSD/aug-cc-pVDZ+3p level),²² which suggests that the nonadiabatic process may also become important for vibrational states with small resonance width.

For the nonadiabatic process, the transition probability is high when the initial and final vibrational states lie close in energy; that is, when the kinetic energy of the emitted electron is small.⁵ For a given energy of the outgoing electron, transition is most likely at those nuclear configurations where the anionic and the neutral PES cross. Furthermore, the derivative overlap of the initial and final vibrational wave functions is also expected to influence the transition probability.⁵ In the case of acrylonitrile, the ν_{12} and ν_{13} modes of the neutral molecule have frequencies (0.121 and 0.118 eV) just slightly lower than the adiabatic attachment energy (0.138 eV),⁷ so the first condition is fulfilled for the $0^0 \rightarrow 12^1$ and $0^0 \rightarrow 13^1$ transitions, and nonadiabatic effects are expected to be significant when the two PESs intersect.

In summary, both processes are expected to contribute to electron detachment, but the relative significance of the direct and the nonadiabatic process is different for the individual vibronic transitions.

By looking at the changes in energy (Table 1) and structure (Table 2) between the neutral equilibrium structure, the

Table 1. Energies of Neutral and π^* Anionic States of Acrylonitrile and Methacrylonitrile Relative to the Neutral State at Its Equilibrium Structure for Various Nuclear Configurations (in eV)^a

	acrylonitrile		methacrylonitrile	
	neutral	anion	neutral	anion
neut. eq	0.000	0.583	0.000	0.707
res. eq	0.194	0.397	0.259	0.506
MECP	0.418	0.412	0.510	0.511

^aIn all calculations, the aug-cc-pVDZ+3p basis set was used. Energies at the neutral and resonance equilibrium structures were presented previously in ref 22.

resonance equilibrium structure, and the MECP, it can be concluded that the anionic surfaces of both systems are very flat; the energy of the anion changes by 0.015 eV (acrylonitrile) and 0.005 eV (methacrylonitrile) between the resonance equilibrium and the MECP, while the energy of the

Table 2. Equilibrium Structures of the π^* Resonance and of the Neutral Ground State and Structure of the MECP for Acrylonitrile and Methacrylonitrile^a

	neutral	anion	MECP
acrylonitrile			
R_{C1-N}	1.172	1.193	1.197
R_{C1-C2}	1.452	1.416	1.409
R_{C2-C3}	1.350	1.424	1.445
$\angle_{C1-C3-H2-C2}$ (C2 pyr.)	0.0	0.0	4.0
$\angle_{C2-H3'-H3-C3}$ (C3 pyr.)	0.0	0.0	16.2
methacrylonitrile			
R_{C1-N}	1.172	1.192	1.196
R_{C1-C2}	1.459	1.418	1.413
R_{C2-C3}	1.351	1.415	1.437
R_{C4-H4}	1.100	1.110	1.109
$R_{C4-H4'}$	1.102	1.103	1.105
$R_{C4-H4''}$	1.102	1.114	1.121
$\angle_{C1-C3-C2-C4}$	180.0	176.1	162.2

^aBond lengths are given in Å and angles in degrees. Computed using the aug-cc-pVDZ+3p basis set.

neutral state changes by 0.224 and 0.251 eV, respectively. One should note that at the resonance equilibrium CAP-EOM-EA-CCSD was used, while the MECP was calculated with regular EOM-EA-CCSD. This may cause a discontinuity in the CPES similar to that observed for HCOOH in Section 2, but it is not expected to change the conclusion that the anionic surface is much flatter than the neutral surface along the modes that lead to the crossing.

The resonance equilibrium structure is planar for acrylonitrile, so in this case, there is no dislocation of the anionic and the neutral PESs along the C2 or C3 pyramidalization modes (ν_{12} and ν_{13}). The direct detachment process might still be important due to the different curvature of the two surfaces, but for the quantification of this process, vibrational states and their resonance widths would need to be calculated.

The MECP has a similar structure as the resonance equilibrium for both molecules, and the largest differences are observed for the C2–C3 bond length and nonplanar distortions (Table 2). The low energy and the structure of the MECP show that crossings are easily accessible already for the vibrational ground state of the anion. This suggests that the bright peaks on the threshold line are at least partly due to nonadiabatic effects.

There are substantial changes between the neutral equilibrium structure and the MECP: The C2–C3 bond is elongated at the MECP for both molecules, and elongation of the C1–N bond is less pronounced, while the C1–C2 bond is compressed somewhat. Pyramidalization at the C3 atom (ν_{13}) is observed for acrylonitrile at the MECP, but pyramidalization at the C2 atom (ν_{12}) is not significant. Since the MECP can be reached along this mode, it seems probable that the ν_{13} mode of the neutral molecule is excited after electron detachment, but we cannot rule out participation of the ν_{12} mode either.

In the case of methacrylonitrile, it seems that both the direct and the nonadiabatic process can produce the 6^1 vibrationally excited state of the neutral molecule because the resonance equilibrium structure already has a significantly elongated C2–C3 bond, which is further increased at the MECP. Significant CH₂ scissoring, CH₃ umbrella, or CH₃ symmetric stretching were not observed between the optimized structures for methacrylonitrile, but CH₃ asymmetric stretching can be noticed in the slightly different C–H bond lengths in the methyl group.

In summary, our results show that several bright peaks at the threshold line in both 2D EEL spectra, in particular, the excitation of ν_{13} for acrylonitrile and that of ν_6 for methacrylonitrile, can be explained by the structure and the energy of the MECP and the resonance equilibrium structure. A more detailed understanding of these spectra, in particular, of the features involving detachment from vibrationally excited anionic states, would require to consider energies and resonance widths of individual vibrational states of the anion, which is beyond the scope of the present work.

3.2. Chloroethylenes. Widely used as chemical intermediates and solvents, chloroethylenes have become one of the most common groundwater contaminants.³⁷ Reductive dehalogenation is a key process in their detoxification that has been studied extensively in various natural and engineered environments^{38–41} and in the gas phase via dissociative electron attachment (DEA),^{42–46} but its mechanism is still not completely understood.

It is believed that in the gas phase electron attachment to the π^* orbital produces an anionic resonance that can convert to a

Table 3. Vertical Attachment Energies and Resonance Widths for the π^* Resonances of Ethylene and Chloro-Substituted Ethylenes and Energy of the MECP between the Lowest-Lying Anionic State and the Neutral Ground State Compared to the Energy of the Neutral State at its Equilibrium Structure^a

	exp. ⁴³		aug-cc-pVDZ+3p			aug-cc-pVTZ+3p		
	VAE	VAE	Γ	$\Delta E(\text{MECP})$	VAE	Γ	$\Delta E(\text{MECP})$	
C ₂ H ₄	1.73	2.229	0.449	2.660	2.155	0.446	2.638	
C ₂ H ₃ Cl	1.28	1.800	0.260	1.059	1.730	0.266	1.146	
cis-C ₂ H ₂ Cl ₂	1.11	1.629	0.071	0.669	1.573	0.056	0.708	
trans-C ₂ H ₂ Cl ₂	0.80	1.401	0.124	0.570	1.335	0.109	0.634	
1,1-C ₂ H ₂ Cl ₂	0.76	1.378	0.240	0.515	1.285	0.245	0.579	
C ₂ HCl ₃	0.59	1.133	0.155	0.358	1.052	0.169	0.395	
C ₂ Cl ₄	0.3	0.982	0.026	0.264	—	—	—	

^aExperimental VAEs determined by Burrow et al.⁴³ using electron transmission spectroscopy are also shown. All values are given in eV.

σ^* state through out-of-plane nuclear motions. The σ^* state dissociates into a chloride ion and a molecular radical; thus, in total, a chlorine is removed from the molecule. The overall driving force of the reaction is the high electron affinity of the chlorine atom; similar reactivity patterns can be observed for other substituents with high electron affinity.

To gain more insight into the DEA process, we located MECPs for the lowest-lying anion-neutral crossings for all chloro-substituted ethylene molecules. At planar structures, for example, at the neutral equilibrium structure, these systems have one π^* and some low-lying C–Cl σ^* resonances depending on the number of chlorine atoms. The C–H σ^* resonances are presumed to have higher energy and thus do not participate in the DEA process. At low electron energies, the electron is captured by the π^* resonance, which has longer lifetime and lower energy than the σ^* resonances.

The experimental vertical attachment energy (VAE) to the π^* state is available from electron transmission spectroscopy (ETS).^{43,45} The calculated VAEs (Table 3) show good correlation with experimental values from ETS, with an average difference of 0.57 eV, which is typical of CAP-EOM-EA-CCSD with the aug-cc-pVDZ+3p basis set.^{21,22} VAE values calculated with the aug-cc-pVTZ+3p basis are closer to experimental values (0.48 eV difference), but tetrachloroethylene could not be investigated with this basis due to high computational cost.

The transition from the π^* state to a σ^* state is enabled through out-of-plane motions. For the description of this process, interstate couplings for metastable states would be necessary. The behavior of the CPESs of resonances near the crossing^{47,48} is quite different from the behavior of the PESs of bound states,^{49–51} and we direct the reader to ref 48, where such an intersection between resonances was studied for chloroethylene with the CAP/ $\Sigma^{(2)}$ method. Here, we concentrate on crossings between anionic and neutral states instead.

Anion–neutral crossings in chloroethylenes have been studied along linear reaction coordinates with bound-state methods, and the positions of the crossings were used to estimate activation barriers.¹³ However, exploring the full geometry space and locating the MECP along the crossing seam can yield more accurate structures and energies and hence more realistic barrier heights.

Our earlier studies showed^{21,22} that the π^* state of ethylene has a nonplanar, C_{2h} equilibrium structure with an elongated C–C bond. The MECP with the neutral state has a nonsymmetric structure with an even longer C–C bond (Figure 3). Structure optimization of the π^* state of

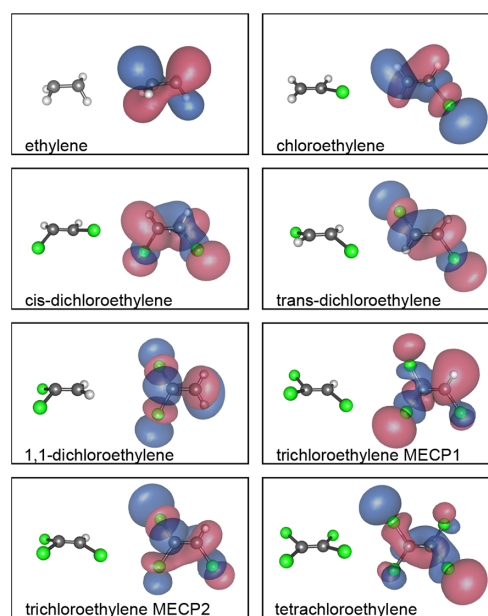


Figure 3. Structures of ethylene and chloro-substituted ethylenes at the MECP between the lowest-energy anionic state and the neutral ground state along with the Dyson orbital of the anionic state at the MECP. In the case of trichloroethylene, two low-energy MECPs were found. Calculations were performed with the aug-cc-pVDZ+3p basis set.

chloroethylenes is problematic due to the interaction with σ^* states and the presence of crossings between these states. The MECP between the lowest anionic state and the neutral state has elongated C–Cl bonds, and the chlorine is bent out of the molecular plane in all cases. At these nonplanar structures, the σ^* , π^* classification is no longer sensible.

In Figure 3, it can be seen that at the MECPs the Dyson orbitals of all chloro-substituted anions have antibonding character between some of the Cl and C atoms driving the dissociation of these bonds. In all three dichloroethylenes, the two Cl atoms are equivalent, and the electron density is symmetric. In the case of trichloroethylene, however, this is not true, and dissociation of different C–Cl bonds leads to different products, namely, cis-, trans-, and 1,1-dichloroethenyl radicals. The four anionic states that might play a role in the DEA process can have mixed $\sigma_{\text{C-Cl}}^*$ and π^* character; thus, it is

possible that different dissociation products can be reached from the same anionic state.

We were able to locate the MECP on the crossing seam of two of these anionic states with the neutral state. The Dyson orbitals in Figure 3 have clear antibonding character along some of the C-Cl bonds, but dissociation routes were also verified by starting structure optimizations from these points. The two MECPs are at substantially different structures but at similar energies. The lower-lying MECP is at 0.358 eV (EOM-CCSD/aug-cc-pVDZ+3p; 0.395 eV with aug-cc-pVTZ+3p), while the other MECP is at 0.386 eV (0.447 eV with aug-cc-pVTZ+3p). Calculations along the reaction coordinates of different dissociation routes with EOM-CCSD are problematic due to the increasing multireference character of the states, but our calculations close to the MECP suggest that barriers along the dissociation routes are much lower in energy than the VAE, so dissociation to all three isomers is possible from both MECP points.

Table 3 shows that for ethylene the MECP has higher energy than the VAE, while for chloro-substituted ethylenes it is at much lower energy, making it easier to reach. The reason for this difference is that chloroethylenes have a low-lying σ^* state that can mix with the π^* state at nonplanar geometries and thus stabilize the anion and lower the energy of the crossing with the neutral state.

Table 3 also illustrates that the aug-cc-pVDZ+3p basis set describes the MECP points quite well: the difference between double- ζ and triple- ζ results is similar to or somewhat smaller than for the VAE values. However, VAE values are lower with the aug-cc-pVTZ+3p basis, while $\Delta E(\text{MECP})$ values are typically higher, with the only exception being C_2H_4 .

Calculations on chloroethylenes were done previously with DFT^{13,52,53} and CCSD(T),^{13,52} but these methods do not account for metastability and hence cannot describe the anion correctly in regions where it has higher energy than the neutral ground state. One important advantage of the CAP method over bound-state methods is that resonance widths can be determined, which gives further insight into the processes following electron attachment. For example, parent anions are observed in mass spectra of tetrachloroethylene^{42,44,46} and in one experiment also for trichloroethylene.⁴⁶ This suggests that the anion can live long enough to reach the detector. According to our calculations (Table 3), the anion of tetrachloroethylene indeed has a very small resonance width.

Resonance widths are also helpful in explaining why some chloroethylene species produce a higher chloride ion yield than others. Cl^- formation cross sections were measured⁴⁶ for several haloethylenes including the three dichloroethylene isomers, and it was found that the cross section grows in the order geminal, trans, cis. This ordering cannot be explained by the energetics of the DEA process alone, as all three isomers have similar VAE and $\Delta E(\text{MECP})$ values (Table 3).

However, if one takes a look at the calculated resonance widths in Table 3, it becomes apparent that the autodetachment process cannot be neglected: the widths are comparable to typical vibrational frequencies of normal modes that are relevant for reaching the MECP point, namely, C-Cl stretching and Cl-C-C-Cl out-of-plane motions that approximately range from a few hundred to a thousand wavenumbers (≈ 0.03 – 0.12 eV).

This means that electron autodetachment is competing with stabilization through nuclear rearrangement, and thus, the probability of reaching a crossing with the neutral state and

subsequent dissociation to Cl^- depends not only on the energy profile along the reaction coordinate but also on the rate of autodetachment.

The resonance width depends on the nuclear coordinates; thus, for a comprehensive characterization, one would need to perform molecular dynamics simulations considering both resonance energies and widths. However, for the three dichloroethylene isomers, a qualitative explanation can already be given considering the resonance widths only at the neutral equilibrium structures. The cis isomer has the smallest resonance width, followed by the trans isomer and the geminal isomer; thus, the anion of the cis isomer has the highest probability to reach the crossing without emitting an electron, become stable, and then dissociate to Cl^- and a molecular radical, while the anions of the trans and geminal isomers have a higher probability to lose an electron on the way. Thus, the ordering of Γ is consistent with the experimentally observed Cl^- yields.

4. CONCLUSIONS

Crossings between anionic resonances and their parent neutral states have been investigated for several polyatomic molecules with CAP-EOM-EA-CCSD and EOM-EA-CCSD. We have shown that CAP-EOM-EA-CCSD gives reliable results in the metastable region but often cannot be used in the vicinity of a crossing. Near the crossing and in regions where the anion is stable, regular EOM-EA-CCSD can be applied, but the shift from CAP-EOM-CCSD to regular EOM-CCSD can lead to discontinuities in the CPES.

The energy and structure of the MECP and the resonance equilibrium compared to the neutral equilibrium energy and structure provide information about vibronic transitions accompanied by the emission of an electron with nearly zero energy. With the examples of acrylonitrile and methacrylonitrile, we demonstrated that differences between these structures can explain some bright peaks on the threshold line of two-dimensional electron-energy loss spectra.

MECPs are also helpful in explaining the production of stable anion fragments in dissociative electron attachment experiments as we illustrated with the example of chloroethylenes. In contrast to vertical attachment, where the electron is attached to a π^* orbital, the Dyson orbitals at the MECPs have antibonding character between the carbon and chlorine atoms. While the MECP is substantially higher in energy than the VAE in ethylene, it has much lower energy in all chloroethylenes, which, combined with the antibonding nature of the Dyson orbital, enables dissociation of a C-Cl bond. However, for a comprehensive characterization of dissociative electron attachment, the finite lifetime of the anion in the metastable region should not be neglected. We have shown that for these systems electron autodetachment competes with dissociation, and the resonance width has a substantial effect on the cross sections of Cl^- formation.

■ ASSOCIATED CONTENT

📄 Supporting Information

The Supporting Information is available free of charge on the ACS Publications website at DOI: 10.1021/acs.jctc.8b00444.

CAP parameters and coordinates of optimized structures. (PDF)

AUTHOR INFORMATION

Corresponding Authors

*E-mail: zsuzsanna.benda@cup.uni-muenchen.de.

*E-mail: th.jagau@lmu.de.

ORCID

Thomas-C. Jagau: 0000-0001-5919-424X

Notes

The authors declare no competing financial interest.

ACKNOWLEDGMENTS

This work has been supported by the Fonds der Chemischen Industrie through a Ph.D. fellowship to Z.B. and a Liebig fellowship to T.-C.J. and by the Deutsche Forschungsgemeinschaft through Grant JA 2794/1-1 (Emmy Noether program).

REFERENCES

- (1) Simons, J. Molecular Anions. *J. Phys. Chem. A* **2008**, *112*, 6401–6511.
- (2) Moiseyev, N. *Non-Hermitian Quantum Mechanics*; Cambridge University Press, 2011.
- (3) Jagau, T.-C.; Bravaya, K. B.; Krylov, A. I. Extending Quantum Chemistry of Bound States to Electronic Resonances. *Annu. Rev. Phys. Chem.* **2017**, *68*, 525–553.
- (4) Berry, R. S. Ionization of Molecules at Low Energies. *J. Chem. Phys.* **1966**, *45*, 1228–1245.
- (5) Simons, J. Propensity rules for vibration-induced electron detachment of anions. *J. Am. Chem. Soc.* **1981**, *103*, 3971–3976.
- (6) Regeta, K.; Allan, M. Autodetachment Dynamics of Acrylonitrile Anion Revealed by Two-Dimensional Electron Impact Spectra. *Phys. Rev. Lett.* **2013**, *110*, 203201.
- (7) Regeta, K.; Allan, M. Two-Dimensional Spectra of Electron Collisions with Acrylonitrile and Methacrylonitrile Reveal Nuclear Dynamics. *J. Chem. Phys.* **2015**, *142*, 184307.
- (8) DeVine, J. A.; Weichman, M. L.; Xie, C.; Babin, M. C.; Johnson, M. A.; Ma, J.; Guo, H.; Neumark, D. M. Autodetachment from Vibrationally Excited Vinylidene Anions. *J. Phys. Chem. Lett.* **2018**, *9*, 1058–1063.
- (9) Savéant, J.-M. A Simple Model for the Kinetics of Dissociative Electron Transfer in Polar Solvents. Application to the Homogeneous and Heterogeneous Reduction of Alkyl Halides. *J. Am. Chem. Soc.* **1987**, *109*, 6788–6795.
- (10) Fabrikant, I. I.; Hotop, H. On the validity of the Arrhenius equation for electron attachment rate coefficients. *J. Chem. Phys.* **2008**, *128*, 124308.
- (11) Bertran, J.; Gallardo, I.; Moreno, M.; Savéant, J.-M. Dissociative Electron Transfer. Ab Initio Study of the Carbon-Halogen Bond Reductive Cleavage in Methyl and Perfluoromethyl Halides. Role of the Solvent. *J. Am. Chem. Soc.* **1992**, *114*, 9576–9583.
- (12) Pause, L.; Robert, M.; Savéant, J.-M. Reductive Cleavage of Carbon Tetrachloride in a Polar Solvent. An Example of a Dissociative Electron Transfer with Significant Attractive Interaction between the Caged Product Fragments. *J. Am. Chem. Soc.* **2000**, *122*, 9829–9835.
- (13) Bylaska, E. J.; Dupuis, M.; Tratnyek, P. G. One-electron-transfer reactions of polychlorinated ethylenes: concerted and stepwise cleavages. *J. Phys. Chem. A* **2008**, *112*, 3712–3721.
- (14) Lauderdale, J. G.; McCurdy, C. W.; Hazi, A. U. Conversion of bound states to resonances with changing internuclear distance in molecular anions. *J. Chem. Phys.* **1983**, *79*, 2200–2205.
- (15) Ghosh, A.; Vaval, N.; Pal, S.; Bartlett, R. J. Complex Absorbing Potential Based Equation-of-Motion Coupled Cluster Method for the Potential Energy Curve of CO₂⁻ Anion. *J. Chem. Phys.* **2014**, *141*, 164113.
- (16) Jagau, T.-C.; Krylov, A. I. Complex Absorbing Potential Equation-of-Motion Coupled-Cluster Method Yields Smooth and Internally Consistent Potential Energy Surfaces and Lifetimes for Molecular Resonances. *J. Phys. Chem. Lett.* **2014**, *5*, 3078–3085.
- (17) White, A. F.; McCurdy, C. W.; Head-Gordon, M. Restricted and unrestricted non-Hermitian Hartree-Fock: Theory, practical considerations, and applications to metastable molecular anions. *J. Chem. Phys.* **2015**, *143*, 074103.
- (18) White, A. F.; Epifanovsky, E.; McCurdy, C. W.; Head-Gordon, M. Second order Møller-Plesset and coupled cluster singles and doubles methods with complex basis functions for resonances in electron-molecule scattering. *J. Chem. Phys.* **2017**, *146*, 234107.
- (19) Ghosh, A.; Vaval, N.; Pal, S. Equation-of-Motion Coupled-Cluster Method for the Study of Shape Resonance. *J. Chem. Phys.* **2012**, *136*, 234110.
- (20) Zuev, D.; Jagau, T.-C.; Bravaya, K. B.; Epifanovsky, E.; Shao, Y.; Sundstrom, E.; Head-Gordon, M.; Krylov, A. I. Complex Absorbing Potentials within EOM-CC Family of Methods: Theory, Implementation, and Benchmarks. *J. Chem. Phys.* **2014**, *141*, 024102.
- (21) Benda, Z.; Jagau, T.-C. Communication: Analytic Gradients for the Complex Absorbing Potential Equation-of-Motion Coupled-Cluster Method. *J. Chem. Phys.* **2017**, *146*, 031101.
- (22) Benda, Z.; Rickmeyer, K.; Jagau, T.-C. Structure Optimization of Temporary Anions. *J. Chem. Theory Comput.* **2018**, *14*, 3468.
- (23) Nooijen, M.; Bartlett, R. J. Equation of Motion Coupled Cluster Method for Electron Attachment. *J. Chem. Phys.* **1995**, *102*, 3629–3647.
- (24) Krylov, A. I. Equation-of-Motion Coupled-Cluster Methods for Open-Shell and Electronically Excited Species: The Hitchhiker's Guide to Fock Space. *Annu. Rev. Phys. Chem.* **2008**, *59*, 433–462.
- (25) Sneskov, K.; Christiansen, O. Excited state coupled cluster methods. *WIREs Comput. Mol. Sci.* **2012**, *2*, 566–584.
- (26) Bartlett, R. J. Coupled-cluster theory and its equation-of-motion extensions. *WIREs Comput. Mol. Sci.* **2012**, *2*, 126–138.
- (27) Kjønstad, E. F.; Myhre, R. H.; Martínez, T. J.; Koch, H. Crossing conditions in coupled cluster theory. *J. Chem. Phys.* **2017**, *147*, 164105.
- (28) Kjønstad, E. F.; Koch, H. Resolving the Notorious Case of Conical Intersections for Coupled Cluster Dynamics. *J. Phys. Chem. Lett.* **2017**, *8*, 4801–4807.
- (29) Kohn, A.; Tajti, A. Can coupled-cluster theory treat conical intersections? *J. Chem. Phys.* **2007**, *127*, 044105.
- (30) Bearpark, M. J.; Robb, M. A.; Schlegel, H. B. A direct method for the location of the lowest energy point on a potential surface crossing. *Chem. Phys. Lett.* **1994**, *223*, 269–274.
- (31) Epifanovsky, E.; Krylov, A. I. Direct location of the minimum point on intersection seams of potential energy surfaces with equation-of-motion coupled-cluster methods. *Mol. Phys.* **2007**, *105*, 2515–2525.
- (32) Shao, Y.; Gan, Z.; Epifanovsky, E.; Gilbert, A. T.; Wormit, M.; Kussmann, J.; Lange, A. W.; Behn, A.; Deng, J.; Feng, X.; Ghosh, D.; Goldey, M.; Horn, P. R.; Jacobson, L. D.; Kaliman, I.; Khaliiullin, R. Z.; Kùs, T.; Landau, A.; Liu, J.; Proynov, E. I.; Rhee, Y. M.; Richard, R. M.; Rohrdanz, M. A.; Steele, R. P.; Sundstrom, E. J.; Woodcock, H. L., III; Zimmerman, P. M.; Zuev, D.; Albrecht, B.; Alguire, E.; Austin, B.; Beran, G. J. O.; Bernard, Y. A.; Berquist, E.; Brandhorst, K.; Bravaya, K. B.; Brown, S. T.; Casanova, D.; Chang, C.-M.; Chen, Y.; Chien, S. H.; Closser, K. D.; Crittenden, D. L.; Diedenhofen, M.; DiStasio, R. A., Jr.; Do, H.; Dutoi, A. D.; Edgar, R. G.; Fatehi, S.; Fusti-Molnar, L.; Ghysels, A.; Golubeva-Zadorozhnyaya, A.; Gomes, J.; Hanson-Heine, M. W.; Harbach, P. H.; Hauser, A. W.; Hohenstein, E. G.; Holden, Z. C.; Jagau, T.-C.; Ji, H.; Kaduk, B.; Khistyayev, K.; Kim, J.; Kim, J.; King, R. A.; Klunzinger, P.; Kosenkov, D.; Kowalczyk, T.; Kruter, C. M.; Lao, K. U.; Laurent, A. D.; Lawler, K. V.; Levchenko, S. V.; Lin, C. Y.; Liu, F.; Livshits, E.; Lochan, R. C.; Luenser, A.; Manohar, P.; Manzer, S. F.; Mao, S.-P.; Mardirossian, N.; Marenich, A. V.; Maurer, S. A.; Mayhall, N. J.; Neuscamman, E.; Oana, C. M.; Olivares-Amaya, R.; O'Neill, D. P.; Parkhill, J. A.; Perrine, T. M.; Peverati, R.; Prociuk, A.; Rehn, D. R.; Rosta, E.; Russ, N. J.; Sharada, S. M.; Sharma, S.; Small, D. W.; Sodt, A.; Stein, T.; Stück, D.; Su, Y.-C.; Thom, A. J.; Tsuchimochi, T.; Vanovschi, V.; Vogt, L.; Vydrov,

- O.; Wang, T.; Watson, M. A.; Wenzel, J.; White, A.; Williams, C. F.; Yang, J.; Yeganeh, S.; Yost, S. R.; You, Z.-Q.; Zhang, I. Y.; Zhang, X.; Zhao, Y.; Brooks, B. R.; Chan, G. K. L.; Chipman, D. M.; Cramer, C. J.; Goddard, W. A., III; Gordon, M. S.; Hehre, W. J.; Klamt, A.; Schaefer, H. F.; Schmidt, M. W.; Sherrill, C. D.; Truhlar, D. G.; Warshel, A.; Xu, X.; Aspuru-Guzik, A.; Baer, R.; Bell, A. T.; Besley, N. A.; Chai, J.-D.; Dreuw, A.; Dunietz, B. D.; Furlani, T. R.; Gwaltney, S. R.; Hsu, C.-P.; Jung, Y.; Kong, J.; Lambrecht, D. S.; Liang, W.; Ochsenfeld, C.; Rassolov, V. A.; Slipchenko, L. V.; Subotnik, J. E.; Van Voorhis, T.; Herbert, J. M.; Krylov, A. I.; Gill, P. M.; Head-Gordon, M. Advances in molecular quantum chemistry contained in the Q-Chem 4 program package. *Mol. Phys.* **2015**, *113*, 184–215.
- (33) Jagau, T.-C.; Krylov, A. I. Characterizing Metastable States Beyond Energies and Lifetimes: Dyson Orbitals and Transition Dipole Moments. *J. Chem. Phys.* **2016**, *144*, 054113.
- (34) Bravaya, K. B.; Zuev, D.; Epifanovsky, E.; Krylov, A. I. Complex-scaled equation-of-motion coupled-cluster method with single and double substitutions for autoionizing excited states: theory, implementation, and examples. *J. Chem. Phys.* **2013**, *138*, 124106.
- (35) Riss, U. V.; Meyer, H.-D. Calculation of Resonance Energies and Widths Using the Complex Absorbing Potential Method. *J. Phys. B: At., Mol. Opt. Phys.* **1993**, *26*, 4503–4536.
- (36) Jagau, T.-C.; Zuev, D.; Bravaya, K. B.; Epifanovsky, E.; Krylov, A. I. A Fresh Look at Resonances and Complex Absorbing Potentials: Density Matrix-Based Approach. *J. Phys. Chem. Lett.* **2014**, *5*, 310–315.
- (37) Carter, J. M.; Lapham, W. W.; Zogorski, J. S. Occurrence of Volatile Organic Compounds in Aquifers of the United States. *J. Am. Water Resour. Assoc.* **2008**, *44*, 399–416.
- (38) He, J.; Ritalahti, K. M.; Yang, K.-L.; Koenigsberg, S. S.; Löffler, F. E. Detoxification of vinyl chloride to ethene coupled to growth of an anaerobic bacterium. *Nature* **2003**, *424*, 62–65.
- (39) Costentin, C.; Robert, M.; Savéant, J.-M. Successive Removal of Chloride Ions from Organic Polychloride Pollutants. Mechanisms of Reductive Electrochemical Elimination in Aliphatic Gem-Polychlorides, α,β -Polychloroalkenes, and α,β -Polychloroalkanes in Mildly Protic Medium. *J. Am. Chem. Soc.* **2003**, *125*, 10729–10739.
- (40) Follett, A.; McNeill, K. Reduction of Trichloroethylene by Outer-Sphere Electron-Transfer Agents. *J. Am. Chem. Soc.* **2005**, *127*, 844–845.
- (41) Heckel, B.; Cretnik, S.; Kliegman, S.; Shouakar-Stash, O.; McNeill, K.; Elsner, M. Reductive Outer-sphere Single Electron Transfer Is an Exception Rather than the Rule in Natural and Engineered Chlorinated Ethene Dehalogenation. *Environ. Sci. Technol.* **2017**, *51*, 9663–9673.
- (42) Johnson, J. P.; Christophorou, L. G.; Carter, J. G. Fragmentation of aliphatic chlorocarbons under low-energy ($\lesssim 10$ eV) electron impact. *J. Chem. Phys.* **1977**, *67*, 2196–2215.
- (43) Burrow, P. D.; Modelli, A.; Chiu, N. S.; Jordan, K. D. Temporary Σ and Π anions of the chloroethylenes and chlorofluoroethylenes. *Chem. Phys. Lett.* **1981**, *82*, 270–276.
- (44) Kaufel, R.; Illenberger, E.; Baumgärtel, H. Formation and Dissociation of the Chloroethylene anions. *Chem. Phys. Lett.* **1984**, *106*, 342–346.
- (45) Olthoff, J. K.; Tossell, J. A.; Moore, J. H. Electron attachment by haloalkenes and halobenzenes. *J. Chem. Phys.* **1985**, *83*, 5627–5634.
- (46) Vasil'ev, Y. V.; Voinov, V. G.; Barofsky, D. F.; Deinzer, M. L. Absolute dissociative electron attachment cross-sections of chloro- and bromo-ethylenes. *Int. J. Mass Spectrom.* **2008**, *277*, 142–150.
- (47) Estrada, H.; Cederbaum, L. S.; Domcke, W. Vibronic coupling of short-lived electronic states. *J. Chem. Phys.* **1986**, *84*, 152–169.
- (48) Feuerbacher, S.; Sommerfeld, T.; Cederbaum, L. S. Intersections of potential energy surfaces of short-lived states: The complex analogue of conical intersections. *J. Chem. Phys.* **2004**, *120*, 3201–3214.
- (49) Köppel, H.; Domcke, W.; Cederbaum, L. S. Multimode Molecular Dynamics Beyond the Born-Oppenheimer Approximation. *Adv. Chem. Phys.* **1984**, *57*, 59–246.
- (50) Yarkony, D. R. Diabatical conical intersections. *Rev. Mod. Phys.* **1996**, *68*, 985–1013.
- (51) Bernardi, F.; Olivucci, M.; Robb, M. A. Potential energy surface crossings in organic photochemistry. *Chem. Soc. Rev.* **1996**, *25*, 321–328.
- (52) Nonnenberg, C.; van der Donk, W. A.; Zipse, H. Reductive Dechlorination of Trichloroethylene: A Computational Study. *J. Phys. Chem. A* **2002**, *106*, 8708–8715.
- (53) Modelli, A. Electron attachment and intramolecular electron transfer in unsaturated chloroderivatives. *Phys. Chem. Chem. Phys.* **2003**, *5*, 2923–2930.

3.4 Locating exceptional points

This article focuses on exceptional points, that is, degeneracies of resonances. EPs are well-known in other fields such as laser physics and optics, but are less known in connection with autoionizing molecular resonances. Similarities and differences between EPs and CIs are discussed: EPs can be regarded as a complex analogue of CIs in the sense that they act as funnels between states, but the topology of surfaces is rather different in the two cases (see also Section 2.5).

An implementation of the imaginary part of the CAP-EOM-CC analytic gradient was presented in this article, and it was shown that the complex-valued gradient can be used for locating EPs and MEEPs. This is done in analogy to the direct optimization of CIs [108] (see also Section 2.5.2), but in this pilot implementation only gradient differences are used. A projection using nonadiabatic coupling vectors as well would probably improve the algorithm, and is a promising future project (see Section 3.5). The algorithm was tested on anionic resonances of hydrogen cyanide and chloroethylene.

In the case of same-symmetry crossings of bound states, it is known [132–134] that truncated EOM-CC methods give a ring of EPs instead of a single CI, which is an artifact due to the non-Hermiticity of the method. It is shown in this article, that such a problem does not exist for EPs, and truncated CAP-EOM-CC methods give crossing seams of the expected dimensionality, and the behavior of the CPESs around EPs is correct. In more detail, $N - 1$ dimensional real and imaginary degeneracy seams branch from the $N - 2$ dimensional EP seam, and form a closed shape in the case of chloroethylene, in agreement with a complex linear vibronic coupling model and previous *ab initio* calculations [79]. Divergence of wave function amplitudes is also observed at EPs, and the phase rigidity [98–101], that can be used to indicate this divergence, is defined for CAP-EOM-CC methods.

With the ability to locate the minimum-energy point on the EP seam, this method can be a strong tool for describing multistate phenomena involving resonances, such as DEA. Similar to the MECP of bound states, the MEEP can determine the rate of a reaction proceeding along that route, so its accessibility is of special interest. In this article, calculations were performed for chloroethylene, whose DEA was already investigated in Publication 3 (Section 3.3). The chloride ion yield is high when the energy of the attached electron corresponds to the vertical attachment energy of the π^* resonance [135–137], which suggests that the dissociation route is easily accessed from this state. In this work, after locating the MEEP between the π^* and σ^* states, a pathway for DEA was constructed using results from Publication 3 (Section 3.3) as well. It was found, that with the energy available from the vertical excitation, the MEEP can be reached easily. The small resonance width along the route ensures that a substantial portion of the molecules can reach the MECP and dissociate instead of losing an electron and falling back to the neutral state.

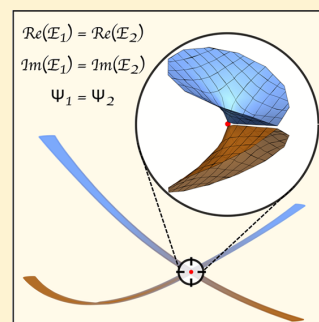
Locating Exceptional Points on Multidimensional Complex-Valued Potential Energy Surfaces

Zsuzsanna Benda*¹ and Thomas-C. Jagau*¹

Department of Chemistry, University of Munich (LMU), D-81377 Munich, Germany

Supporting Information

ABSTRACT: We present a method for locating non-Hermitian degeneracies, called exceptional points (EPs), and minimum-energy EPs between molecular resonances using the complex absorbing potential equation-of-motion coupled-cluster (CAP-EOM-CC) method. EPs are the complex-valued analogue of conical intersections (CIs) and have a similar impact on nonadiabatic processes between resonances as CIs have on nonradiative transitions between bound states. We demonstrate that the CAP-EOM-CC method in the singles and doubles approximation (CAP-EOM-CCSD) yields crossings of the correct dimensionality. The use of analytic gradients enables applications to multidimensional problems. Results are presented for hydrogen cyanide and chloroethylene, for which the location of the crossings of anionic resonances is crucial for understanding the dissociative electron attachment process.



Exceptional points (EPs)¹ are non-Hermitian degeneracies that appear in open quantum systems. They are important in many different fields, such as optics, laser physics, and atomic and molecular physics.^{2,3} In this Letter, we investigate molecules that are unstable with respect to electron loss, that is, subject to autoionization.

In the case of autoionizing resonances, EPs have a similar role in deactivation processes as conical intersections (CIs) have in the decay of bound excited states. It is well-known that the interaction of bound electronic states through nuclear motion is often key for understanding processes such as ultrafast decay, isomerization, and photodissociation that are responsible for the photostability of DNA or vision, for example.⁴ The probability of a nonadiabatic transition is high near a CI and near an EP as well, and interstate couplings are singular at both types of intersections.⁵ EPs are expected to be just as ubiquitous for molecular resonances as CIs are for bound states, but they have been investigated much less.

Linear vibronic coupling (LVC) models were established a long time ago^{5,6} for the description of resonance–resonance interactions. The presence of sharp peaks in the vibrational excitation cross section of $\text{H}_2 + e^-$ was connected to overlapping resonance states.^{7,8} In addition, the interaction of molecular electronic resonances is also important in dissociative electron attachment (DEA), which plays a key role in radiation damage to DNA and in the formation of molecules in interstellar space.⁹ We also mention investigations of nonadiabatic effects in resonant Auger decay¹⁰ and interatomic Coulombic decay.¹¹ However, EPs have been investigated only for a few autoionizing anions: between the 2A_1 and 2B_2 states of the water anion,¹² and between the $^2A'$ (π^* -type) and $^2A'$ ($\sigma_{\text{C-Cl}}^*$ -type) states of the chloroethylene anion.⁶ These investigations were done by scanning the

complex-valued potential energy surfaces (CPESs) along a few modes, which requires a large number of calculations and good chemical intuition. In this Letter, we present a method based on analytic gradients for locating EPs on multidimensional CPESs efficiently.

For the time-independent description of autoionizing resonances, as well as for other dissipative systems, we can use non-Hermitian Hamiltonians. Their complex eigenvalues $E = E_{\text{R}} - i\Gamma/2$ give the energy and the decay rate.¹³ EPs, where the complex eigenvalues of two states become degenerate, are of special interest because of their importance in nonadiabatic decay, but also because they have properties radically different from Hermitian degeneracies (CIs)^{2,14} (see Figure 1). At an EP, not only the eigenvalues but also the eigenvectors coalesce, forming a single self-orthogonal state.¹³ The topology of EPs has been confirmed by experiments.^{15–20} When encircling a CI, the states do not interchange, but the wave function acquires a geometric phase.²¹ In contrast, when encircling an EP, the two states can interchange,^{2,22} and the wave function picks up a geometric phase.²³ Encircling the EP in clockwise or in counterclockwise directions yields different final states, which was demonstrated by calculations^{24–26} and by experiments on microwave transmission through a waveguide¹⁸ and in an optomechanical system.¹⁹

The crossing conditions for same-symmetry intersections can be derived in the two-dimensional subspace of the two strongly interacting states. The energy difference between the eigenvalues of the two-dimensional Hamiltonian matrix

Received: October 23, 2018

Accepted: November 27, 2018

Published: November 27, 2018

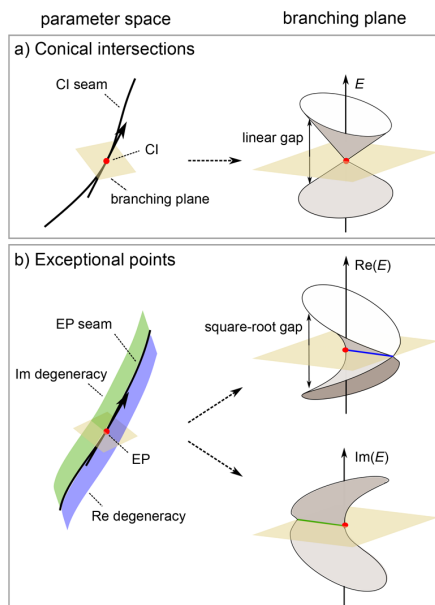


Figure 1. Degeneracy seams in a three-dimensional parameter space and behavior of eigenvalues in the branching plane for (a) Hermitian and (b) non-Hermitian degeneracies.

$$\mathbf{H} = \begin{pmatrix} \epsilon_1 & \omega \\ \omega & \epsilon_2 \end{pmatrix} \quad (1)$$

is $\sqrt{(\epsilon_1 - \epsilon_2)^2 + 4\omega^2}$, where $\epsilon_1 - \epsilon_2$ is the diabatic energy difference and ω is the coupling between the two states. In the case of bound-state crossings, the matrix elements are real, so there are two conditions for degeneracy: $\epsilon_1 - \epsilon_2 = 0$ and $\omega = 0$.^{27,28} The eigenvectors remain orthogonal at the CI.

In the case of resonances, ϵ_1 , ϵ_2 , and ω can be complex; thus, to have an EP between the states, both the real part and the imaginary part of $\sqrt{(\epsilon_1 - \epsilon_2)^2 + 4\omega^2}$ have to be zero.^{6,29} This means that the dimensionality of the EP seam is $N - 2$ (where N is the number of nuclear degrees of freedom), just like the CI seam for bound states, but the behavior of the crossing states differs fundamentally between the two cases. The Hamiltonian becomes defective at the EP, the two wave functions coalesce, which means that the eigenvectors no longer span the entire space. In addition, there is one dimension along which the degeneracy of the real parts or that of the imaginary parts can be kept, while the other parts split (Figure 1). The Re and Im degeneracy seams can even form a closed loop containing two EPs, as was demonstrated by Feuerbacher et al.⁶ using an LVC model including linear resonance widths and complex coupling terms.

Available methods for locating EPs^{30–34} use peculiarities of the EP like the state-exchange phenomenon, the square-root energy gap, or the nonanalytical behavior of energies at the EP. In the method of Cartarius et al.,³¹ calculations are performed along closed adiabatic loops, and the interchange of states is used as a sign that the EP is inside the loop. In the iterative three-point and one-point methods of Uzdin and Lefebvre³³ and in the octagon method of Feldmaier et al.,³⁴ guesses are made for the position of an EP in a two-parameter space utilizing the analytic behavior of the square of the energy

difference. Lefebvre and Moiseyev³² showed that the breakdown of the Padé analytic continuation method can be utilized as well to find EPs.

These methods are most useful for problems with one complex parameter or two real parameters, for example, to describe coalescence in molecular photodissociation, where EPs can arise at specific values of the wavelength and the intensity of the laser.³⁵ It was suggested that population transfer can be achieved between vibronic states of H_2^+ and Na_2 by a chirped laser pulse, which can be utilized for vibrational cooling.^{25,35–38}

In molecules, the number of vibrational degrees of freedom grows quickly with the size of the system ($N = 3N_{\text{atoms}} - 6$ for nonlinear molecules), which makes an EP search according to the above-mentioned methods rather complicated. Also, there is an $(N - 2)$ -dimensional seam of EPs, from which the most relevant point for estimating the importance of a nonadiabatic process is the minimum-energy EP (MEEP). Here, we present a method for locating EPs and MEEPs within the complex absorbing potential equation-of-motion coupled-cluster (CAP-EOM-CC) formalism³⁹ by using analytic gradients. This method opens up the possibility of studying DEA in polyatomic systems without the need to impose geometrical constraints.

We employ the CAP-EOM-CC method with a box-type quadratic CAP added at the Hartree–Fock (HF) level as outlined in refs 39 and 40. CAP-EOM-CC provides the two resonances in one calculation if the same set of parameters (CAP strength parameter η and box size parameters t_{α}^0 , $\alpha = x, y, z$) are used for both states,⁴¹ which ensures the balanced description of the crossing states.⁹

The CAP-EOM-CC right wave function of state λ is defined as

$$|\Psi_{\lambda}\rangle = \hat{R}^{\lambda} e^{\hat{T}} |\Phi_{\text{HF}}\rangle \quad (2)$$

where \hat{T} is the cluster operator and operator \hat{R}^{λ} can be chosen in different forms to create excited, ionized, electron-attached, or spin-flipped states.⁴² The scalar product $\langle \phi_i | \phi_j \rangle$ is replaced by the c -product⁴³ $\langle \phi_i | \phi_j \rangle \equiv \langle \phi_i^* | \phi_j \rangle$, which yields a complete set of eigenvectors if there is no degeneracy.¹³ At EPs, however, the c -norm of the corresponding eigenvector is zero, even though the eigenvector is nonzero (self-orthogonal).^{13,43}

It should be mentioned here that truncated CC and EOM-CC methods do not give the correct shape and dimensionality of same-symmetry crossings of bound states.^{44–46} This is because truncation introduces non-Hermiticity, which changes the crossing conditions. If we look at the problem as a real nonsymmetric perturbation to a real symmetric matrix, a CI is blown up to a circle of EPs because of the perturbation, and complex eigenvalues appear within the circle.⁴⁷

In the case of a truncated CAP-EOM-CC treatment of resonances, the Hamiltonian is complex non-Hermitian. As every complex matrix is similar to a complex symmetric matrix,²⁹ the crossing conditions of a complex symmetric H of eq 1 apply, so truncated CAP-EOM-CC is expected to give the correct dimensionality of the crossing seam. We demonstrate this by calculations on the anions of hydrogen cyanide and chloroethylene. Similar to truncated EOM-CC methods, truncated CAP-EOM-CC can be systematically improved toward the CAP-FCI limit by including higher-order excitations.

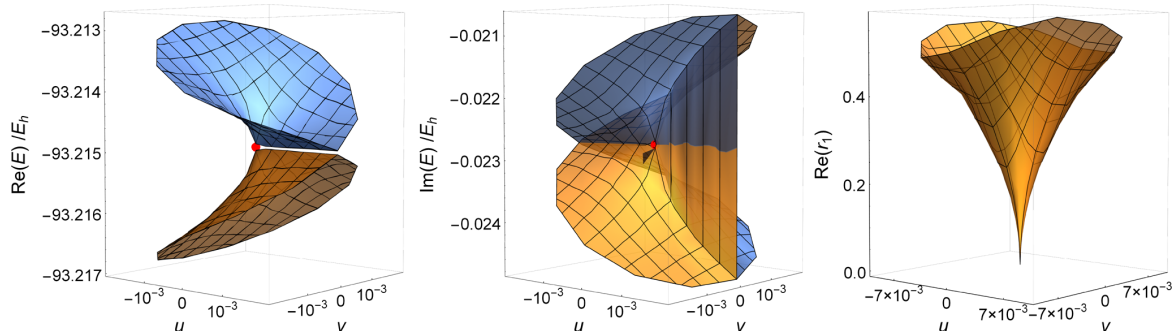


Figure 2. Real and imaginary parts of the CPEs above the branching plane corresponding to the EP at $\angle = 165^\circ$ from Figure 3 (marked by a red dot here). The third panel shows the real part of the phase rigidity for the first state. For the definition of u and v vectors, see the Supporting Information. Calculations were performed with the fixed CAP parameters of the EP (see the Supporting Information).

Because of the coalescence of the wave functions at an EP, the wave function amplitudes diverge.¹³ The phase rigidity (r_λ)^{48–51} is the ratio of the c -norm and the regular norm, and it can be used as an indicator of an EP. Because of the nonsymmetric nature of CAP-EOM-CC we calculate it as

$$r_\lambda = \frac{\langle \tilde{\Psi}_\lambda | \Psi_\lambda \rangle}{\langle \tilde{\Psi}_\lambda | \tilde{\Psi}_\lambda \rangle} = \frac{A}{A^2 + B^2} - i \frac{B}{A^2 + B^2} \quad (3)$$

$$A = 1 + 2 \sum_i \text{Im}(L_i^\lambda) \text{Im}(R_i^\lambda) \quad (4)$$

$$B = 2 \sum_i \text{Re}(L_i^\lambda) \text{Im}(R_i^\lambda) \quad (5)$$

where $\tilde{\Psi}_\lambda$ is the left CAP-EOM-CC wave function; L_i^λ and R_i^λ are the left and the right EOM amplitudes corresponding to single, double, etc. excitations; and we used the fact that left and right eigenvectors are biorthogonalized using the c -product

$$\text{Re}(\tilde{\Psi}_\lambda | \Psi_\lambda) = \sum_i (\text{Re}(L_i^\lambda) \text{Re}(R_i^\lambda) - \text{Im}(L_i^\lambda) \text{Im}(R_i^\lambda)) = 1 \quad (6)$$

$$\text{Im}(\tilde{\Psi}_\lambda | \Psi_\lambda) = \sum_i (\text{Re}(L_i^\lambda) \text{Im}(R_i^\lambda) + \text{Im}(L_i^\lambda) \text{Re}(R_i^\lambda)) = 0 \quad (7)$$

The phase rigidity is complex in our case because of different left and right eigenvectors in truncated CAP-EOM-CC. For well-separated resonances, its value should be close to 1 with a negligible imaginary part, and it should go to 0 as the EP is approached, because the amplitudes and thus the regular scalar product grow. For a full CC expansion, the phase rigidity would have purely real values.

To locate EPs on multidimensional CPEs, we use the fact that both the real and the imaginary energy differences have to go to zero as the EP is approached. The corresponding gradient difference vectors can be used to determine directions in which the energy differences decrease, and a method similar to the direct method by Bearpark et al.⁵² for locating crossing points of bound states can be applied.

We use gradient $\tilde{\mathbf{g}}$ to locate any EP between two states

$$\tilde{\mathbf{g}} = \mathbf{f}_{\text{Re}} + \mathbf{f}_{\text{Im}} \quad (8)$$

$$\mathbf{f}_{\text{Re}} = 2(\text{Re}(E_2) - \text{Re}(E_1)) \frac{\mathbf{x}_{\text{Re}}}{\|\mathbf{x}_{\text{Re}}\|} \quad (9)$$

$$\mathbf{f}_{\text{Im}} = -4(\text{Im}(E_2) - \text{Im}(E_1)) \frac{\mathbf{x}_{\text{Im}}}{\|\mathbf{x}_{\text{Im}}\|} \quad (10)$$

where \mathbf{x}_{Re} and \mathbf{x}_{Im} are the gradient difference vectors

$$\mathbf{x}_{\text{Re}} = \text{Re}(\mathbf{G}_2) - \text{Re}(\mathbf{G}_1) \quad (11)$$

$$\mathbf{x}_{\text{Im}} = -2(\text{Im}(\mathbf{G}_2) - \text{Im}(\mathbf{G}_1)) \quad (12)$$

We presented the implementation of $\text{Re}(\mathbf{G})$ in an earlier paper⁴⁰ and used it for locating resonance equilibrium structures⁵³ and for the initial optimization of minimum-energy crossing points (MECPs) between anionic states and their parent neutral states.⁵⁴ We complement our implementation with $\text{Im}(\mathbf{G})$ in the current work (see the Supporting Information for the gradient formula).

To find the minimum-energy exceptional point (MEEP), one would additionally have to minimize E_{R} of one of the states in the subspace orthogonal to the two-dimensional branching plane, as is done for the MECP of bound states.⁵² While in the latter case the branching plane is spanned by the gradient difference vector and the nonadiabatic force matrix element (\mathbf{h}),^{14,55} in the case of EPs the two-dimensional branching plane is spanned by different combinations of the \mathbf{x}_{Re} , \mathbf{x}_{Im} , \mathbf{h}_{Re} , and \mathbf{h}_{Im} vectors.

In our current implementation, the gradient of the second state is orthogonalized to the plane spanned by \mathbf{x}_{Re} and \mathbf{x}_{Im} using projector \mathcal{P}

$$\mathbf{g} = \mathcal{P} \text{Re}(\mathbf{G}_2) \quad (13)$$

which is expected to cause slower convergence than orthogonalization to the branching plane, but the calculation of \mathbf{h}_{Re} and \mathbf{h}_{Im} is avoided.

The final gradient used for the MEEP optimization is given as

$$\bar{\mathbf{g}} = \mathbf{f}_{\text{Re}} + \mathbf{f}_{\text{Im}} + \mathbf{g} \quad (14)$$

The outlined methods were implemented in Q-Chem,⁵⁶ built upon the MECP search implementation by Epifanovsky and Krylov.⁵⁷

To test the EP optimization and MEEP optimization algorithms and to investigate the topology of EPs within the CAP-EOM-CC singles and doubles (CAP-EOM-CCSD) model, we performed calculations on the HCN⁻ anion,

which can have a one-dimensional EP seam between two resonance states of the same symmetry and multiplicity at bent structures. We looked at crossings between two ${}^2A'$ states that correspond to a ${}^2\Pi$ state and a ${}^2\Sigma^+$ state in linear geometry and presumably play a part in DEA to HCN.

For these calculations we used the CAP-EOM-EA-CCSD method and the standard Dunning basis set aug-cc-pVTZ augmented with three extra p functions on each atom (following the augmentation scheme described in ref 39). The CAP strength parameter was kept fixed at the value 9×10^{-3} a.u.,⁵⁸ but the box size parameters were relaxed during the EP optimization.

First we located EPs at five different constrained bond angles between 155° and 175° using eq 8 for the optimization. To verify the shape of the CPESs around EPs, we investigated the EP corresponding to $\angle = 165^\circ$. Because there are just three degrees of freedom for HCN^- , it is simple to determine the branching plane in this case (see the Supporting Information). In Figures 2 and 3 it can be seen that the dimensionality of the

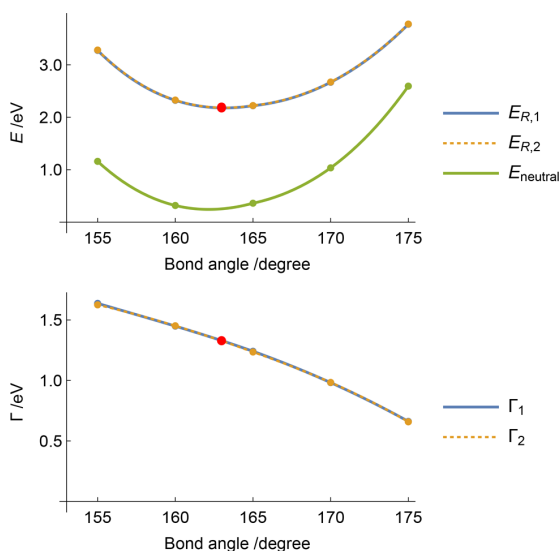


Figure 3. Resonance positions and widths and the energy of the parent neutral state along the EP line of HCN^- . The optimized MEEP is marked by a red dot. Optimized structural parameters and box size parameters are available in the Supporting Information.

EP is correctly described by the CAP-EOM-CCSD method: there is a one-dimensional EP seam, and the degeneracy is lifted in the branching plane, as expected. The real parts of the surfaces remain degenerate in one direction, and the imaginary parts interchange here, while the imaginary parts are degenerate in the opposite direction,⁵⁹ which is also in agreement with analytical models.

The real part of the phase rigidity of state 1 is plotted in Figure 2. It is of the order of 10^{-2} at the approximate EP, but it is below 0.6 already at radius 0.01 (approximately 0.007 Å change in the bond lengths). The imaginary part of the phase rigidity is negligible, with values between -0.008 and 0.007 for all points calculated (see the Supporting Information).

The EPs found at different bond angles cover a large range of E_R and Γ values (Figure 3), and the difference between the two states is typically smaller than 6 meV for both quantities

(see the Supporting Information). The third-order interpolating functions for $E_{R,1}$ and $E_{R,2}$ have a minimum at $\angle = 163.16^\circ$ and 163.18° , respectively. The MEEP (shown as a red dot in Figure 3) was converged with a slightly looser threshold than the previous EP points, so the energy difference of the two states is somewhat larger than before (20 meV for E_R and 2 meV for Γ). The need to use looser thresholds is probably due to the fact that \mathbf{g} is not exactly parallel to the EP line. The MEEP has internal coordinates $R_{\text{CN}} = 1.165$ Å, $R_{\text{CH}} = 1.162$ Å, and $\angle = 162.98^\circ$, the latter in very good agreement with the above approximated values, which indicates that the looser thresholds do not induce a large error in the structure.

To try out our method for a larger system with more degrees of freedom, we investigated chloroethylene, which is a good model for biologically important halogenated compounds. For example, halogenated DNA bases are used as sensitizers in radiation therapy, and it is believed that DEA involving resonance states plays a role in this process by inducing strand breaks in DNA.⁶⁰ Experimental studies of chloro-substituted ethylenes^{61–65} suggest that electron attachment produces a π^* resonance, which, through out-of-plane motions, converts to a σ^* state that is dissociative along a C–Cl bond. This DEA process for removing a chloride ion from the molecule might be important in the detoxification of these substances, which are common pollutants of groundwater.⁶⁶

In an earlier paper we presented vertical attachment energies (VAEs) and MECPs between the lowest-energy anionic state and the parent neutral state for chloro-substituted ethylenes.⁵⁴ Here, we located the MEEP between the π^* and σ^* states of the chloroethylene anion so that we can construct a complete pathway for DEA. These calculations were carried out using CAP-EOM-EA-CCSD and the aug-cc-pVDZ+3p basis set (3 extra p functions on C and Cl atoms). The two states have different symmetry at planar structures (A'' and A'), which means they cannot interact. At the MEEP, the Cl atom is bent slightly out of the molecular plane; this allows for the interaction of the two states. The C–Cl bond and, to a smaller extent, the C–C bond are elongated compared to the equilibrium structure of the neutral molecule (see the Supporting Information). Feuerbacher et al. also located an EP for this system⁶ by changing the C–Cl bond length and the Cl out-of-plane angle in increments and leaving all other coordinates fixed at their value at the neutral equilibrium structure. Our method allows for the efficient optimization of all nuclear coordinates, and in this way it yields the MEEP, which is more relevant for assessing the probability of the DEA process.

To check the shape of the CPESs near the MEEP, we performed calculations in the $\mathbf{x}_{\text{Re}}-\mathbf{x}_{\text{Im}}$ plane. The resulting surfaces (Figure 4) have two EPs in the plane, and the shape formed by the $\text{Re}(E)$ and the $\text{Im}(E)$ degeneracy seams resembles an ellipse. This is in line with LVC results and ab initio calculations of Feuerbacher et al.,⁶ who introduced the term doubly intersecting complex energy surfaces (DICES) for this phenomenon. In Figure 4 the ellipse fitted to the $\text{Im}(E)$ surface crossing can be seen. The optimized MEEP is not exactly on the ellipse; differences in bond lengths between the MEEP and the corresponding approximated point on the ellipse, EP_1 , are smaller than 0.001 Å. The C–Cl bond at the other EP on the ellipse, EP_2 , is shorter by 0.013 Å than at EP_1 , and the H–C–C–Cl dihedral angle is -4.1° at EP_2 compared to 2.3° at EP_1 and MEEP.

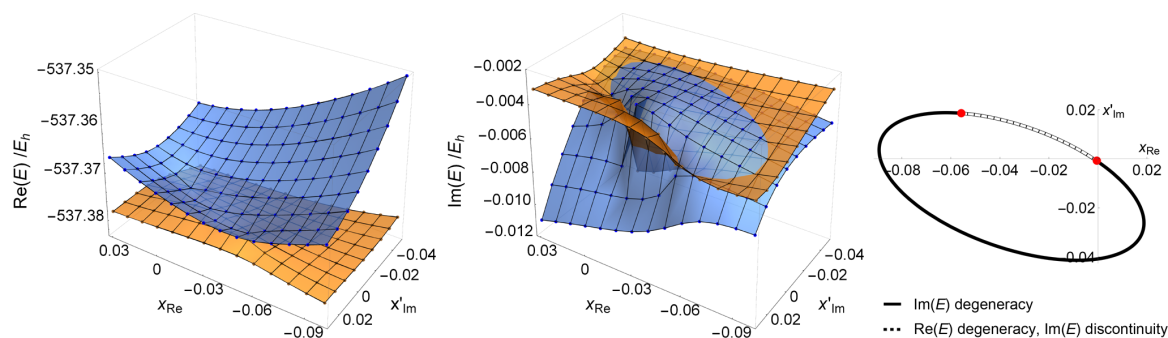


Figure 4. CPEs in the vicinity of the MEEP point (origin) between the π^* and the σ^* states of chloroethylene, plotted above the plane spanned by the real gradient difference vector (\mathbf{x}_{Re}) and the imaginary gradient difference vector orthogonalized to \mathbf{x}_{Re} (\mathbf{x}'_{Im}). Real and imaginary degeneracy seams form an ellipse (see the Supporting Information for details of the fitting), with two EPs (marked with red dots) separating the real and the imaginary seams. Calculations were done with the fixed CAP parameters of the MEEP (see the Supporting Information).

To construct a pathway for DEA, we performed linear interpolation between the neutral equilibrium structure and the MEEP and between the MEEP and the MECP. The π^* state has a much smaller resonance width than the σ^* state in the Franck–Condon region, but the width of the latter state quickly decreases along the DEA pathway (Figure 5). At the

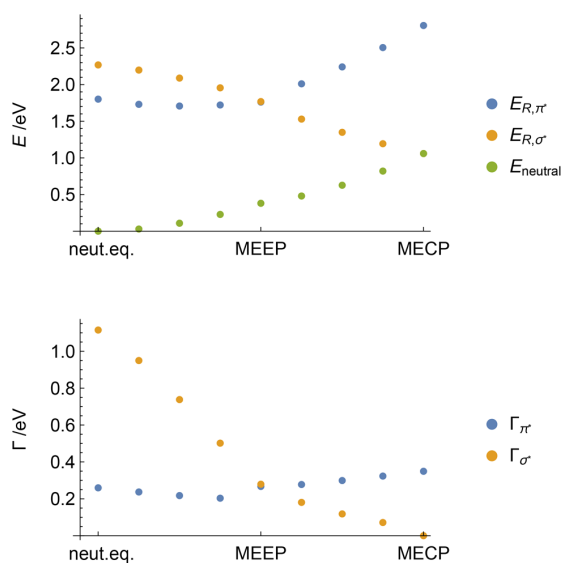


Figure 5. Resonance positions and widths of π^* and σ^* anionic states and energy of the parent neutral state of chloroethylene along the DEA pathway. For π^* and σ^* states, their respective optimal CAP strength parameter⁶⁷ was used at each point where possible (parameter values and additional information are given in the Supporting Information).

MEEP it is similar to the vertical width of the π^* state. Transition from π^* to σ^* occurs near the MEEP where the coupling of the two states is large. From the MEEP both the position and the width of the σ^* resonance decrease monotonically, until the MECP with the neutral state is reached, and the anionic state becomes stable with respect to electron loss. Note that at the MECP regular EOM-CCSD was used for the calculation of the σ^* state; thus, Γ is zero by definition.

The MEEP has slightly lower energy (1.761–1.768 eV) than the VAE of the π^* state (1.801 eV⁵⁴), and the MECP is at a substantially lower energy than the previous two (1.059 eV⁵⁴), which means that DEA can proceed along a completely barrier-free route. The long lifetime of the π^* state relative to the σ^* state and the accessibility of the MEEP makes electron attachment to the π^* orbital very likely to produce chloride ions as suggested also by experiments. However, experiments find the maximum of the DEA cross section at around 1.2–1.3 eV,^{63,64} that is, at considerably lower energy than our VAE. A similar deviation was obtained and analyzed in more detail in ref 6. We also note that the π^* state has a minimum before reaching the MEEP, which is expected to elongate the time the anion is subject to electron loss. To model how the properties of real and imaginary surfaces influence the efficiency of the DEA process, dynamical simulations of nuclear motion would be needed.

In summary, we presented a method for locating EPs and MEEPs on multidimensional CPEs using analytic gradients. The peculiar shape of CPEs around EPs was discussed, and the ability of the CAP-EOM-CCSD method to correctly describe the vicinity of EPs was demonstrated. DEA to chloroethylene was investigated by locating the MEEP between π^* and σ^* anionic states and constructing a pathway from the neutral equilibrium structure to the σ^* -neutral MECP through the MEEP.

■ ASSOCIATED CONTENT

📄 Supporting Information

The Supporting Information is available free of charge on the ACS Publications website at DOI: 10.1021/acs.jpcclett.8b03228.

Complex gradient formula, CAP parameters, structural parameters and energies for optimized points, description of determining the branching plane, and details of fitting (PDF)

■ AUTHOR INFORMATION

Corresponding Authors

*E-mail: zsuzsanna.benda@cup.uni-muenchen.de.

*E-mail: th.jagau@lmu.de.

ORCID

Zsuzsanna Benda: 0000-0002-6714-0337

Thomas-C. Jagau: 0000-0001-5919-424X

Notes

The authors declare no competing financial interest.

ACKNOWLEDGMENTS

We thank Professor Anna Krylov, Professor Lorenz Cederbaum, and Professor Nimrod Moiseyev for helpful comments on the manuscript. This work has been supported by the Deutsche Forschungsgemeinschaft through Grant JA 2794/1-1 (Emmy Noether program).

REFERENCES

- (1) Kato, T. *Perturbation Theory of Linear Operators*; Springer, 1966.
- (2) Berry, M. V. Physics of Nonhermitian Degeneracies. *Czech. J. Phys.* **2004**, *54*, 1039–1047.
- (3) Heiss, W. D. The physics of exceptional points. *J. Phys. A: Math. Theor.* **2012**, *45*, 444016.
- (4) *Conical Intersections: Theory, Computation and Experiment*; Domcke, W., Yarkony, D. R., Köppel, H., Eds.; World Scientific: Singapore, 2011.
- (5) Estrada, H.; Cederbaum, L. S.; Domcke, W. Vibronic coupling of short-lived electronic states. *J. Chem. Phys.* **1986**, *84*, 152–169.
- (6) Feuerbacher, S.; Sommerfeld, T.; Cederbaum, L. S. Intersections of potential energy surfaces of short-lived states: The complex analogue of conical intersections. *J. Chem. Phys.* **2004**, *120*, 3201–3214.
- (7) Narevicius, E.; Moiseyev, N. Fingerprints of Broad Overlapping Resonances in the $e + H_2$ Cross Section. *Phys. Rev. Lett.* **1998**, *81*, 2221–2224.
- (8) Narevicius, E.; Moiseyev, N. Trapping of an Electron due to Molecular Vibrations. *Phys. Rev. Lett.* **2000**, *84*, 1681–1684.
- (9) Jagau, T.-C.; Bravaya, K. B.; Krylov, A. I. Extending Quantum Chemistry of Bound States to Electronic Resonances. *Annu. Rev. Phys. Chem.* **2017**, *68*, 525–553.
- (10) Cederbaum, L. S.; Chiang, Y.-C.; Demekhin, P. V.; Moiseyev, N. Resonant Auger decay of molecules in intense X-ray laser fields: light-induced strong nonadiabatic effects. *Phys. Rev. Lett.* **2011**, *106*, 123001.
- (11) Demekhin, P. V.; Stoychev, S. D.; Kuleff, A. I.; Cederbaum, L. S. Exploring interatomic coulombic decay by free electron lasers. *Phys. Rev. Lett.* **2011**, *107*, 273002.
- (12) Haxton, D. J.; Rescigno, T. N.; McCurdy, C. W. Topology of the adiabatic potential energy surfaces for the resonance states of the water anion. *Phys. Rev. A: At, Mol, Opt. Phys.* **2005**, *72*, 022705.
- (13) Moiseyev, N. *Non-Hermitian Quantum Mechanics*; Cambridge University Press, 2011.
- (14) Yarkony, D. R. Diabolical conical intersections. *Rev. Mod. Phys.* **1996**, *68*, 985–1013.
- (15) Dembowski, C.; Gräf, H.-D.; Harney, H. L.; Heine, A.; Heiss, W. D.; Rehfeld, H.; Richter, A. Experimental Observation of the Topological Structure of Exceptional Points. *Phys. Rev. Lett.* **2001**, *86*, 787–790.
- (16) Lee, S.-B.; Yang, J.; Moon, S.; Lee, S.-Y.; Shim, J.-B.; Kim, S. W.; Lee, J.-H.; An, K. Observation of an Exceptional Point in a Chaotic Optical Microcavity. *Phys. Rev. Lett.* **2009**, *103*, 134101.
- (17) Gao, T.; Estrecho, E.; Bliokh, K. Y.; Liew, T. C. H.; Fraser, M. D.; Brodbeck, S.; Kamp, M.; Schneider, C.; Höfling, S.; Yamamoto, Y.; et al. Observation of non-Hermitian degeneracies in a chaotic exciton-polariton billiard. *Nature* **2015**, *526*, 554.
- (18) Doppler, J.; Mailybaev, A. A.; Böhm, J.; Kuhl, U.; Girschik, A.; Libisch, F.; Milburn, T. J.; Rabl, P.; Moiseyev, N.; Rotter, S. Dynamically encircling an exceptional point for asymmetric mode switching. *Nature* **2016**, *537*, 76–79.
- (19) Xu, H.; Mason, D.; Jiang, L.; Harris, J. G. E. Topological energy transfer in an optomechanical system with exceptional points. *Nature* **2016**, *537*, 80.
- (20) Zhou, H.; Peng, C.; Yoon, Y.; Hsu, C. W.; Nelson, K. A.; Fu, L.; Joannopoulos, J. D.; Soljačić, M.; Zhen, B. Observation of bulk Fermi arc and polarization half charge from paired exceptional points. *Science* **2018**, *359*, 1009–1012.
- (21) Berry, M. V. Quantal phase factors accompanying adiabatic changes. *Proc. R. Soc. London, Ser. A* **1984**, *392*, 45–57.
- (22) Hernández, E.; Jáuregui, A.; Mondragón, A. Non-Hermitian degeneracy of two unbound states. *J. Phys. A: Math. Gen.* **2006**, *39*, 10087–10105.
- (23) Heiss, W. Phases of wave functions and level repulsion. *Eur. Phys. J. D* **1999**, *7*, 1–4.
- (24) Uzdin, R.; Mailybaev, A.; Moiseyev, N. On the observability and asymmetry of adiabatic state flips generated by exceptional points. *J. Phys. A: Math. Theor.* **2011**, *44*, 435302.
- (25) Gilary, I.; Mailybaev, A. A.; Moiseyev, N. Time-asymmetric quantum-state-exchange mechanism. *Phys. Rev. A: At, Mol, Opt. Phys.* **2013**, *88*, No. 010102.
- (26) Milburn, T. J.; Doppler, J.; Holmes, C. A.; Portolan, S.; Rotter, S.; Rabl, P. General description of quasiadiabatic dynamical phenomena near exceptional points. *Phys. Rev. A: At, Mol, Opt. Phys.* **2015**, *92*, 052124.
- (27) von Neumann, J.; Wigner, E. P. Über das Verhalten von Eigenwerten bei adiabatischen Prozessen. *Phys. Z.* **1929**, *30*, 467.
- (28) Teller, E. The Crossing of Potential Surfaces. *J. Phys. Chem.* **1937**, *41*, 109.
- (29) Santra, R.; Cederbaum, L. S. Non-Hermitian electronic theory and applications to clusters. *Phys. Rep.* **2002**, *368*, 1–117.
- (30) Mailybaev, A. A. Computation of multiple eigenvalues and generalized eigenvectors for matrices dependent on parameters. *Numer. Lin. Algebra Appl.* **2006**, *13*, 419–436.
- (31) Cartarius, H.; Main, J.; Wunner, G. Exceptional points in the spectra of atoms in external fields. *Phys. Rev. A: At, Mol, Opt. Phys.* **2009**, *79*, 053408.
- (32) Lefebvre, R.; Moiseyev, N. Localization of exceptional points with Padé approximants. *J. Phys. B: At, Mol. Opt. Phys.* **2010**, *43*, 095401.
- (33) Uzdin, R.; Lefebvre, R. Finding and pinpointing exceptional points of an open quantum system. *J. Phys. B: At, Mol. Opt. Phys.* **2010**, *43*, 235004.
- (34) Feldmaier, M.; Main, J.; Schweiner, F.; Cartarius, H.; Wunner, G. Rydberg systems in parallel electric and magnetic fields: an improved method for finding exceptional points. *J. Phys. B: At, Mol. Opt. Phys.* **2016**, *49*, 144002.
- (35) Lefebvre, R.; Atabek, O.; Šindelka, M.; Moiseyev, N. Resonance Coalescence in Molecular Photodissociation. *Phys. Rev. Lett.* **2009**, *103*, 123003.
- (36) Atabek, O.; Lefebvre, R.; Lepers, M.; Jaouadi, A.; Dulieu, O.; Kokoouline, V. Proposal for a Laser Control of Vibrational Cooling in Na_2 Using Resonance Coalescence. *Phys. Rev. Lett.* **2011**, *106*, 173002.
- (37) Kokoouline, V.; Wearne, A.; Lefebvre, R.; Atabek, O. Laser-controlled rotational cooling of Na_2 based on exceptional points. *Phys. Rev. A: At, Mol, Opt. Phys.* **2013**, *88*, 033408.
- (38) Jaouadi, A.; Desouter-Lecomte, M.; Lefebvre, R.; Atabek, O. Signatures of exceptional points in the laser control of non-adiabatic vibrational transfer. *J. Phys. B: At, Mol. Opt. Phys.* **2013**, *46*, 145402.
- (39) Zuev, D.; Jagau, T.-C.; Bravaya, K. B.; Epifanovsky, E.; Shao, Y.; Sundstrom, E.; Head-Gordon, M.; Krylov, A. I. Complex Absorbing Potentials within EOM-CC Family of Methods: Theory, Implementation, and Benchmarks. *J. Chem. Phys.* **2014**, *141*, 024102.
- (40) Benda, Z.; Jagau, T.-C. Communication: Analytic Gradients for the Complex Absorbing Potential Equation-of-Motion Coupled-Cluster Method. *J. Chem. Phys.* **2017**, *146*, 031101.
- (41) Because the crossing states mix when approaching the EP, the optimal parameters are also expected to become similar for the two states in the vicinity of the EP (at the exact EP, there is only one, self-orthogonal state, but this point is never reached in actual numerical calculations); thus, using the same set of parameters is not expected to cause large errors.
- (42) Krylov, A. I. Equation-of-Motion Coupled-Cluster Methods for Open-Shell and Electronically Excited Species: The Hitchhiker's Guide to Fock Space. *Annu. Rev. Phys. Chem.* **2008**, *59*, 433–462.

- (43) Moiseyev, N.; Certain, P.; Weinhold, F. Resonance properties of complex-rotated hamiltonians. *Mol. Phys.* **1978**, *36*, 1613–1630.
- (44) Hättig, C. In *Response Theory and Molecular Properties (A Tribute to Jan Linderberg and Poul Jørgensen)*; Jensen, H., Ed.; Advances in Quantum Chemistry; Academic Press, 2005; Vol. 50, pp 37–60.
- (45) Köhn, A.; Tajti, A. Can coupled-cluster theory treat conical intersections? *J. Chem. Phys.* **2007**, *127*, 044105.
- (46) Kjøenstad, E. F.; Myhre, R. H.; Martínez, T. J.; Koch, H. Crossing conditions in coupled cluster theory. *J. Chem. Phys.* **2017**, *147*, 164105.
- (47) Kirillov, O. N.; Mailybaev, A. A.; Seyranian, A. P. Unfolding of eigenvalue surfaces near a diabolic point due to a complex perturbation. *J. Phys. A: Math. Gen.* **2005**, *38*, 5531–5546.
- (48) van Langen, S. A.; Brouwer, P. W.; Beenakker, C. W. J. Fluctuating phase rigidity for a quantum chaotic system with partially broken time-reversal symmetry. *Phys. Rev. E: Stat. Phys., Plasmas, Fluids, Relat. Interdiscip. Top.* **1997**, *55*, R1–R4.
- (49) Brouwer, P. W. Wave function statistics in open chaotic billiards. *Phys. Rev. E: Stat. Phys., Plasmas, Fluids, Relat. Interdiscip. Top.* **2003**, *68*, 046205.
- (50) Bulgakov, E. N.; Rotter, I.; Sadreev, A. F. Phase rigidity and avoided level crossings in the complex energy plane. *Phys. Rev. E* **2006**, *74*, 056204.
- (51) Rotter, I. A non-Hermitian Hamilton operator and the physics of open quantum systems. *J. Phys. A: Math. Theor.* **2009**, *42*, 153001.
- (52) Bearpark, M. J.; Robb, M. A.; Schlegel, H. B. A direct method for the location of the lowest energy point on a potential surface crossing. *Chem. Phys. Lett.* **1994**, *223*, 269–274.
- (53) Benda, Z.; Rickmeyer, K.; Jagau, T.-C. Structure Optimization of Temporary Anions. *J. Chem. Theory Comput.* **2018**, *14*, 3468–3478.
- (54) Benda, Z.; Jagau, T.-C. Understanding Processes Following Resonant Electron Attachment: Minimum-Energy Crossing Points between Anionic and Neutral Potential Energy Surfaces. *J. Chem. Theory Comput.* **2018**, *14*, 4216–4223.
- (55) Faraji, S.; Matsika, S.; Krylov, A. I. Calculations of non-adiabatic couplings within equation-of-motion coupled-cluster framework: Theory, implementation, and validation against multi-reference methods. *J. Chem. Phys.* **2018**, *148*, 044103.
- (56) Shao, Y.; Gan, Z.; Epifanovsky, E.; Gilbert, A. T.; Wormit, M.; Kussmann, J.; Lange, A. W.; Behn, A.; Deng, J.; Feng, X.; et al. Advances in molecular quantum chemistry contained in the Q-Chem 4 program package. *Mol. Phys.* **2015**, *113*, 184–215.
- (57) Epifanovsky, E.; Krylov, A. I. Direct location of the minimum point on intersection seams of potential energy surfaces with equation-of-motion coupled-cluster methods. *Mol. Phys.* **2007**, *105*, 2515–2525.
- (58) The vicinity of an exceptional point affects the shape of the η trajectories, and the condition $\eta dE/d\eta = \min$.⁶⁷ no longer gives reliable η_{opt} values. The chosen value (9×10^{-3} a.u.) is slightly larger than η_{opt} of the ${}^2\Pi$ state at the neutral equilibrium structure (8.4×10^{-3} a.u.). Our investigations showed that using different CAP strength parameters affects the position of the EP line in parameter space, but if η is high enough, this change is small compared to the size of the area affected by the vicinity of the EP line. We discuss these properties in another article, and here we focus on the performance of the EP optimization algorithm instead.
- (59) On a larger scale, the real degeneracy seam and imaginary degeneracy seam bend, but we were not able to verify whether they form a closed loop because of the limitations of the CAP-EOM-CCSD method to handle elongated bonds. The area affected by the EP seems to be rather large in parameter space, but this is not always the case as is apparent from the example of chloroethylene. We will present and discuss these interesting properties of HCN^- elsewhere, as they are not directly connected to the question of locating exceptional points.
- (60) Sanche, L. Low energy electron-driven damage in biomolecules. *Eur. Phys. J. D* **2005**, *35*, 367–390.
- (61) Johnson, J. P.; Christophorou, L. G.; Carter, J. G. Fragmentation of aliphatic chlorocarbons under low-energy ($\lesssim 10$ eV) electron impact. *J. Chem. Phys.* **1977**, *67*, 2196–2215.
- (62) Burrow, P. D.; Modelli, A.; Chiu, N. S.; Jordan, K. D. Temporary Σ and Π anions of the chloroethylenes and chlorofluoroethylenes. *Chem. Phys. Lett.* **1981**, *82*, 270–276.
- (63) Kaufel, R.; Illenberger, E.; Baumgärtel, H. Formation and Dissociation of the Chloroethylene anions. *Chem. Phys. Lett.* **1984**, *106*, 342–346.
- (64) Olthoff, J. K.; Tossell, J. A.; Moore, J. H. Electron attachment by haloalkenes and halobenzenes. *J. Chem. Phys.* **1985**, *83*, 5627–5634.
- (65) Vasil'ev, Y. V.; Voinov, V. G.; Barofsky, D. F.; Deinzer, M. L. Absolute dissociative electron attachment cross-sections of chloro- and bromo-ethylenes. *Int. J. Mass Spectrom.* **2008**, *277*, 142–150.
- (66) Carter, J. M.; Lapham, W. W.; Zogorski, J. S. Occurrence of Volatile Organic Compounds in Aquifers of the United States. *J. Am. Water Resour. Assoc.* **2008**, *44*, 399–416.
- (67) Riss, U. V.; Meyer, H.-D. Calculation of Resonance Energies and Widths Using the Complex Absorbing Potential Method. *J. Phys. B: At., Mol. Opt. Phys.* **1993**, *26*, 4503–4536.

3.5 Future plans and further possible applications

As discussed in Section 2.2, the probability of a nonadiabatic transition depends on the magnitude of the derivative coupling of the states in question. The regular EOM-CC derivative coupling vector can be computed from the gradients of the interacting states and of a so-called summed state, as described in Reference [139]. Implementation of this method in the Q-Chem program [140] was presented recently [141], and implementation of CAP-EOM-CC derivative couplings is currently in progress. CAP-EOM-CC derivative couplings will further facilitate the investigation of processes involving multiple resonances, and will probably improve the MEEP optimization algorithm presented in Publication 4 (Section 3.4).

The analytic gradient developed in Publication 1 (Section 3.1) can also be used for simulating photodetachment spectra within the linear vibronic coupling model [21, 22]. This requires vibrational frequencies and normal modes for the initial state, which can be calculated using available analytic second derivatives of regular CC methods, since the initial state is a stable state in this case. Transition dipole moments, that give the intensity of specific transitions, are also available for CAP-EOM-CC methods [74]. For the final states, which are resonances in this case, only the derivatives of the vertical excitation energy in the direction of the normal modes of the initial state are needed to evaluate the so-called intrastate couplings. These derivatives can be calculated easily using CAP-EOM-CC gradients. The interaction of final states can be incorporated in the calculations by evaluating the so-called interstate couplings, which can be done in a similar way as the calculation of nonadiabatic couplings for bound states [19, 139]. The implementation of interstate couplings within the CAP-EOM-CC method is a possible future project.

Second derivatives of the resonance energy will enable the simulation of vibrational spectra within the double harmonic approximation. For CAP-EOM-CC methods this can be done by evaluating first derivatives analytically, then second derivatives numerically.

4 Conclusion

In the present work, new developments in the study of electronic resonances were presented in connection with complex absorbing potential equation-of-motion coupled-cluster (CAP-EOM-CC) methods. With the newly implemented analytic energy gradient and optimization algorithms, it is possible to study the complex-valued potential energy surfaces (CPESs) of polyatomic resonances in an efficient way.

Derivations and implementations of the real and imaginary analytic gradients were presented, and the differences from the calculation of bound-state gradients were highlighted. It was shown, that the real part of the complex-valued gradient can be utilized for locating equilibrium structures of resonances, and it is also helpful in locating intersections between an autoionizing state and its parent state. The performance of CAP-EOM-EA-CCSD and CAP-EOM-EA-CCSD(2) methods with different basis sets was studied. It was suggested, that for π^* -type anionic resonances, the basis set aug-cc-pVDZ+3p or, when affordable, aug-cc-pVTZ+3p should be applied. Methods for locating exceptional points (EPs) and minimum-energy EPs (MEEPs), that require the complex-valued gradients of the interacting states, were also presented, and the correctness of the dimensionalities of degeneration seams was confirmed. Possible applications of the metastable-state analytic gradient to nonadiabatic processes and spectrum simulation were also discussed.

With these newly developed methods, the optimization of metastable systems that were previously out of reach for metastable-state methods became possible. Among the studied systems are acrylonitrile and methacrylonitrile, whose two-dimensional electron energy loss (EEL) spectra provide many opportunities for comparison between theory and experiment. It was shown, that the CAP-EOM-EA-CCSD method can provide accurate adiabatic electron affinities and resonance widths for these systems, and certain peaks in the EEL spectra can be explained by the location of special points on the CPESs. For 1,3,5-hexatriene, it was found that CAP-EOM-EA-CCSD and CAP-EOM-EA-CCSD(2) methods give highly accurate energy differences between the $2\pi^*$ anionic states of *cis* and *trans* isomers with just a 0.03-0.06 eV deviation from the experimental value. Resonance positions and widths at optimized structures were used for assessing the relative importance of dissociation and autoionization for anionic resonances of chloro-substituted ethylenes. The dissociative electron attachment pathway constructed for chloroethylene confirms, that by a nonadiabatic transition, the possibility of autoionization can be kept low, and with the energy available from vertical electron attachment dissociation is possible.

Overall, CAP-EOM-CC analytic gradients provide an efficient way to study processes involving electronic resonances by enabling structure optimizations. Equilibrium structures, MECPs and MEEPs are a key for understanding decay mechanisms and describing the interplay of multiple resonance states.

Bibliography

- [1] G. Gamow. Zur quantentheorie des atomkernes. *Z. Phys.*, 51(3-4):204–212, 1928.
- [2] J. Simons. Roles played by metastable states in chemistry. In *Resonances in Electron–Molecule Scattering, Van der Waals Complexes, and Reactive Chemical Dynamics*, volume 263, pages 3–16. American Chemical Society, Washington, DC, 1984.
- [3] G. B. Armen, H. Aksela, T. Åberg, and S. Aksela. The resonant Auger effect. *J. Phys. B: At. Mol. Opt. Phys.*, 33(2):R49–R92, 2000.
- [4] R. Schinke. *Photodissociation dynamics: Spectroscopy and fragmentation of small polyatomic molecules*. Cambridge University Press, New York, 1995.
- [5] X.-L. Zhou, X.-Y. Zhu, and J. White. Photochemistry at adsorbate/metal interfaces. *Surf. Sci. Rep.*, 13(3):73–220, 1991.
- [6] G. Brivio and T. Grimley. Dynamics of adsorption/desorption at solid surfaces. *Surf. Sci. Rep.*, 17(1):1–84, 1993.
- [7] T. Brabec and F. Krausz. Intense few-cycle laser fields: Frontiers of nonlinear optics. *Rev. Mod. Phys.*, 72(2):545–591, 2000.
- [8] B. Boudaïffa, P. Cloutier, D. Hunting, M. A. Huels, and L. Sanche. Resonant formation of DNA strand breaks by low-energy (3 to 20 eV) electrons. *Science*, 287(5458):1658–1660, 2000.
- [9] F. Martin, P. D. Burrow, Z. Cai, P. Cloutier, D. Hunting, and L. Sanche. DNA strand breaks induced by 0–4 eV electrons: The role of shape resonances. *Phys. Rev. Lett.*, 93(6):068101, 2004.
- [10] L. Sanche. Low energy electron-driven damage in biomolecules. *Eur. Phys. J. D*, 35(2):367–390, 2005.
- [11] J. Simons. How do low-energy (0.1-2 eV) electrons cause DNA-strand breaks? *Acc. Chem. Res.*, 39(10):772–779, 2006.
- [12] R. D. Thomas. When electrons meet molecular ions and what happens next: Dissociative recombination from interstellar molecular clouds to internal combustion engines. *Mass Spectrom. Rev.*, 27(5):485–530, 2008.
- [13] G. J. Schulz. Resonances in electron impact on diatomic molecules. *Rev. Mod. Phys.*, 45:423–486, 1973.
- [14] J. Schiedt and R. Weinkauff. Resonant photodetachment via shape and Feshbach resonances: p-benzoquinone anions as a model system. *J. Chem. Phys.*, 110(1):304–314, 1999.
- [15] S. Klaiman and I. Gilary. On resonance: A first glance into the behavior of unstable states. In C. A. Nicolaidis, E. Brändas, and J. R. Sabin, editors, *Unstable States in the Continuous Spectra, Part II: Interpretation, Theory and Applications*, volume 63 of *Advances in Quantum Chemistry*, pages 1–31. Academic Press, San Diego, 2012.
- [16] N. Moiseyev. *Non-Hermitian Quantum Mechanics*. Cambridge University Press, Cambridge, 2011.
- [17] P. A. M. Dirac. *The Principles of Quantum Mechanics*. Oxford University Press, Oxford, 1930.
- [18] M. Born and R. Oppenheimer. Zur Quantentheorie der Molekeln. *Ann. Phys.*, 389(20):457–484, 1927.
- [19] T. Ichino, J. Gauss, and J. F. Stanton. Quasidiabatic states described by coupled-cluster theory. *J. Chem.*

BIBLIOGRAPHY

- Phys.*, 130(17):174105, 2009.
- [20] L. Cederbaum, H. Köppel, and W. Domcke. Multimode vibronic coupling effects in molecules. *Int. J. Quantum Chem.*, 20(S15):251–267, 1981.
- [21] H. Köppel, W. Domcke, and L. S. Cederbaum. Multimode molecular dynamics beyond the Born-Oppenheimer approximation. *Adv. Chem. Phys.*, 57:59–246, 1984.
- [22] H. Estrada, L. S. Cederbaum, and W. Domcke. Vibronic coupling of short-lived electronic states. *J. Chem. Phys.*, 84(1):152–169, 1986.
- [23] F. Jensen. *Introduction to Computational Chemistry*. John Wiley & Sons, New York, 1998.
- [24] J. A. Pople, J. S. Binkley, and R. Seeger. Theoretical models incorporating electron correlation. *Int. J. Quantum Chem.*, 10:1–19, 1976.
- [25] R. J. Bartlett. Many-body perturbation theory and coupled cluster theory for electron correlation in molecules. *Annu. Rev. Phys. Chem.*, 32(1):359–401, 1981.
- [26] J. Čížek. On the correlation problem in atomic and molecular systems. Calculation of wavefunction components in Ursell-type expansion using quantum-field theoretical methods. *J. Chem. Phys.*, 45(11):4256–4266, 1966.
- [27] P. Jørgensen and J. Simons. *Second Quantization-Based Methods in Quantum Chemistry*. Academic Press, New York, 1981.
- [28] G. D. Purvis III and R. J. Bartlett. A full coupled-cluster singles and doubles model: The inclusion of disconnected triples. *J. Chem. Phys.*, 76(4):1910–1918, 1982.
- [29] J. Noga and R. J. Bartlett. The full CCSDT model for molecular electronic structure. *J. Chem. Phys.*, 86(12):7041–7050, 1987.
- [30] G. E. Scuseria and H. F. Schaefer III. A new implementation of the full CCSDT model for molecular electronic structure. *Chem. Phys. Lett.*, 152(4-5):382–386, 1988.
- [31] I. Shavitt and R. J. Bartlett. *Many-body Methods in Chemistry and Physics: MBPT and Coupled-Cluster Theory*. Cambridge University Press, New York, 2009.
- [32] H. Koch, H. J. Jensen, P. Jørgensen, and T. Helgaker. Excitation energies from the coupled cluster singles and doubles linear response function (CCSDLR). Applications to Be, CH⁺, CO, and H₂O. *J. Chem. Phys.*, 93(5):3345–3350, 1990.
- [33] A. I. Krylov. Equation-of-motion coupled-cluster methods for open-shell and electronically excited species: The hitchhiker’s guide to fock space. *Annu. Rev. Phys. Chem.*, 59(1):433–462, 2008.
- [34] K. Snegov and O. Christiansen. Excited state coupled cluster methods. *WIREs Comput. Mol. Sci.*, 2:566–584, 2012.
- [35] R. J. Bartlett. Coupled-cluster theory and its equation-of-motion extensions. *WIREs Comput. Mol. Sci.*, 2:126–138, 2012.
- [36] J. F. Stanton and R. J. Bartlett. The equation of motion coupled-cluster method. A systematic biorthogonal approach to molecular excitation energies, transition probabilities, and excited state properties. *J. Chem. Phys.*, 98(9):7029–7039, 1993.
- [37] M. Nooijen and R. J. Bartlett. Equation of motion coupled cluster method for electron attachment. *J. Chem. Phys.*, 102(9):3629–3647, 1995.
- [38] J. F. Stanton and J. Gauss. Analytic energy derivatives for ionized states described by the equation-of-motion coupled cluster method. *J. Chem. Phys.*, 101(10):8938–8944, 1994.

BIBLIOGRAPHY

- [39] E. R. Davidson. The iterative calculation of a few of the lowest eigenvalues and corresponding eigenvectors of large real-symmetric matrices. *J. Comput. Phys.*, 17(1):87–94, 1975.
- [40] K. Hirao and H. Nakatsuji. A generalization of the Davidson’s method to large nonsymmetric eigenvalue problems. *J. Comput. Phys.*, 45(2):246–254, 1982.
- [41] C. Møller and M. S. Plesset. Note on an approximation treatment for many-electron systems. *Phys. Rev.*, 46(7):618–622, 1934.
- [42] J. F. Stanton and J. Gauss. Perturbative treatment of the similarity transformed Hamiltonian in equation-of-motion coupled-cluster approximations. *J. Chem. Phys.*, 103(3):1064–1076, 1995.
- [43] J. Aguilar and J. M. Combes. A class of analytic perturbations for one-body Schrödinger Hamiltonians. *Comm. Math. Phys.*, 22(4):269–279, 1971.
- [44] E. Balslev and J. M. Combes. Spectral properties of many-body Schrödinger operators with dilatation-analytic interactions. *Comm. Math. Phys.*, 22(4):280–294, 1971.
- [45] B. Simon. Quadratic form techniques and the Balslev-Combes theorem. *Comm. Math. Phys.*, 27(1):1–9, 1972.
- [46] N. Moiseyev. Quantum theory of resonances: Calculating energies, widths and cross-sections by complex scaling. *Phys. Rep.*, 302(5):211–293, 1998.
- [47] C. McCurdy Jr and T. Rescigno. Extension of the method of complex basis functions to molecular resonances. *Phys. Rev. Lett.*, 41(20):1364–1368, 1978.
- [48] G. Jolicard and E. J. Austin. Optical potential stabilisation method for predicting resonance levels. *Chem. Phys. Lett.*, 121(1-2):106–110, 1985.
- [49] U. V. Riss and H.-D. Meyer. Calculation of resonance energies and widths using the complex absorbing potential method. *J. Phys. B: At. Mol. Opt. Phys.*, 26:4503–4536, 1993.
- [50] N. Moiseyev. Derivations of universal exact complex absorption potentials by the generalized complex coordinate method. *J. Phys. B: At. Mol. Opt. Phys.*, 31(7):1431–1441, 1998.
- [51] R. Santra. Why complex absorbing potentials work: A discrete-variable-representation perspective. *Phys. Rev. A*, 74(3):034701, 2006.
- [52] B. Simon. The definition of molecular resonance curves by the method of exterior complex scaling. *Phys. Lett. A*, 71(2):211–214, 1979.
- [53] P. Balanarayan, Y. Sajeev, and N. Moiseyev. Ab-initio complex molecular potential energy surfaces by the back-rotation transformation method. *Chem. Phys. Lett.*, 524:84–89, 2012.
- [54] C. W. McCurdy and R. C. Mowrey. Complex potential-energy function for the $^2\Sigma_u^+$ shape resonance state of H_2^- at the Self-Consistent-Field level. *Phys. Rev. A*, 25(5):2529–2538, 1982.
- [55] J. G. Lauderdale, C. W. McCurdy, and A. U. Hazi. Conversion of bound states to resonances with changing internuclear distance in molecular anions. *J. Chem. Phys.*, 79(5):2200–2205, 1983.
- [56] A. F. White, C. W. McCurdy, and M. Head-Gordon. Restricted and unrestricted non-Hermitian Hartree-Fock: Theory, practical considerations, and applications to metastable molecular anions. *J. Chem. Phys.*, 143(7):074103, 2015.
- [57] T.-C. Jagau and A. I. Krylov. Complex absorbing potential equation-of-motion coupled-cluster method yields smooth and internally consistent potential energy surfaces and lifetimes for molecular resonances. *J. Phys. Chem. Lett.*, 5(17):3078–3085, 2014.
- [58] A. F. White, E. Epifanovsky, C. W. McCurdy, and M. Head-Gordon. Second order Møller-Plesset and coupled

BIBLIOGRAPHY

- cluster singles and doubles methods with complex basis functions for resonances in electron-molecule scattering. *J. Chem. Phys.*, 146(23):234107, 2017.
- [59] N. Moiseyev, P. Certain, and F. Weinhold. Resonance properties of complex-rotated Hamiltonians. *Mol. Phys.*, 36(6):1613–1630, 1978.
- [60] R. Kosloff and D. Kosloff. Absorbing boundaries for wave propagation problems. *J. Comput. Phys.*, 63(2):363–376, 1986.
- [61] G. Jolicard and E. J. Austin. Optical potential method of calculating resonance energies and widths. *Chem. Phys.*, 103(2-3):295–302, 1986.
- [62] D. Zuev, T.-C. Jagau, K. B. Bravaya, E. Epifanovsky, Y. Shao, E. Sundstrom, M. Head-Gordon, and A. I. Krylov. Complex absorbing potentials within EOM-CC family of methods: Theory, implementation, and benchmarks. *J. Chem. Phys.*, 141(2):024102, 2014.
- [63] T.-C. Jagau, D. Zuev, K. B. Bravaya, E. Epifanovsky, and A. I. Krylov. A fresh look at resonances and complex absorbing potentials: Density matrix-based approach. *J. Phys. Chem. Lett.*, 5(2):310–315, 2014.
- [64] Y. Zhou and M. Ernzerhof. Calculating the lifetimes of metastable states with complex density functional theory. *J. Phys. Chem. Lett.*, 3(14):1916–1920, 2012.
- [65] R. Santra and L. S. Cederbaum. Complex absorbing potentials in the framework of electron propagator theory. I. General formalism. *J. Chem. Phys.*, 117(12):5511–5521, 2002.
- [66] S. Feuerbacher, T. Sommerfeld, R. Santra, and L. S. Cederbaum. Complex absorbing potentials in the framework of electron propagator theory. II. Application to temporary anions. *J. Chem. Phys.*, 118(14):6188–6199, 2003.
- [67] T. Sommerfeld, U. V. Riss, H.-D. Meyer, L. S. Cederbaum, B. Engels, and H. U. Suter. Temporary anions - Calculation of energy and lifetime by absorbing potentials: The N_2^- $^2\Pi_g$ resonance. *J. Phys. B: At. Mol. Opt. Phys.*, 31(18):4107–4122, 1998.
- [68] T. Sommerfeld and R. Santra. Efficient method to perform CAP/CI calculations for temporary anions. *Int. J. Quantum Chem.*, 82(5):218–226, 2001.
- [69] A. A. Kunitsa, A. A. Granovsky, and K. B. Bravaya. CAP-XMCQDPT2 method for molecular electronic resonances. *J. Chem. Phys.*, 146(18):184107, 2017.
- [70] M. Ehara and T. Sommerfeld. CAP/SAC-CI method for calculating resonance states of metastable anions. *Chem. Phys. Lett.*, 537:107–112, 2012.
- [71] A. Ghosh, N. Vaval, and S. Pal. Equation-of-motion coupled-cluster method for the study of shape resonance. *J. Chem. Phys.*, 136(23):234110, 2012.
- [72] T.-C. Jagau. Non-iterative triple excitations in equation-of-motion coupled-cluster theory for electron attachment with applications to bound and temporary anions. *J. Chem. Phys.*, 148:024104, 2018.
- [73] C. M. Oana and A. I. Krylov. Dyson orbitals for ionization from the ground and electronically excited states within equation-of-motion coupled-cluster formalism: theory, implementation, and examples. *J. Chem. Phys.*, 127(23):234106, 2007.
- [74] T.-C. Jagau and A. I. Krylov. Characterizing metastable states beyond energies and lifetimes: Dyson orbitals and transition dipole moments. *J. Chem. Phys.*, 144(5):054113, 2016.
- [75] K. Regeta and M. Allan. Autodetachment dynamics of acrylonitrile anion revealed by two-dimensional electron impact spectra. *Phys. Rev. Lett.*, 110(20):203201, 2013.
- [76] K. Regeta and M. Allan. Two-dimensional spectra of electron collisions with acrylonitrile and methacryloni-

BIBLIOGRAPHY

- trile reveal nuclear dynamics. *J. Chem. Phys.*, 142(18):184307, 2015.
- [77] J. A. DeVine, M. L. Weichman, C. Xie, M. C. Babin, M. A. Johnson, J. Ma, H. Guo, and D. M. Neumark. Autodetachment from vibrationally excited vinylidene anions. *J. Phys. Chem. Lett.*, 9(5):1058–1063, 2018.
- [78] T. Kato. *Perturbation Theory of Linear Operators*. Springer, Berlin, 1966.
- [79] S. Feuerbacher, T. Sommerfeld, and L. S. Cederbaum. Intersections of potential energy surfaces of short-lived states: The complex analogue of conical intersections. *J. Chem. Phys.*, 120(7):3201–3214, 2004.
- [80] J.-M. Savéant. A simple model for the kinetics of dissociative electron transfer in polar solvents. Application to the homogeneous and heterogeneous reduction of alkyl halides. *J. Am. Chem. Soc.*, 109(22):6788–6795, 1987.
- [81] I. I. Fabrikant and H. Hotop. On the validity of the Arrhenius equation for electron attachment rate coefficients. *J. Chem. Phys.*, 128(12):124308, 2008.
- [82] J. Simons. Propensity rules for vibration-induced electron detachment of anions. *J. Am. Chem. Soc.*, 103(14):3971–3976, 1981.
- [83] R. S. Berry. Ionization of molecules at low energies. *J. Chem. Phys.*, 45(4):1228–1245, 1966.
- [84] J. Simons. An analytical model for vibrational non-Born-Oppenheimer induced electron ejection in molecular anions. *J. Chem. Phys.*, 117(20):9124–9132, 2002.
- [85] J. von Neumann and E. P. Wigner. Über das Verhalten von Eigenwerten bei adiabatischen Prozessen. *Phys. Z.*, 30:467, 1929.
- [86] E. Teller. The crossing of potential surfaces. *J. Phys. Chem.*, 41(1):109, 1937.
- [87] W. Domcke, D. Yarkony, and H. Köppel, editors. *Conical Intersections: Electronic Structure, Dynamics & Spectroscopy*. World Scientific, Singapore, 2004.
- [88] E. Epifanovsky and A. I. Krylov. Direct location of the minimum point on intersection seams of potential energy surfaces with equation-of-motion coupled-cluster methods. *Mol. Phys.*, 105(19-22):2515–2525, 2007.
- [89] R. Santra and L. S. Cederbaum. Non-hermitian electronic theory and applications to clusters. *Phys. Rep.*, 368(1):1–117, 2002.
- [90] M. Berry. Physics of nonhermitian degeneracies. *Czech. J. Phys.*, 54(10):1039–1047, 2004.
- [91] E. Hernández, A. Jáuregui, and A. Mondragón. Non-Hermitian degeneracy of two unbound states. *J. Phys. A: Math. Gen.*, 39(32):10087–10105, 2006.
- [92] R. Lefebvre, O. Atabek, M. Šindelka, and N. Moiseyev. Resonance coalescence in molecular photodissociation. *Phys. Rev. Lett.*, 103(12):123003, 2009.
- [93] W. Heiss. Phases of wave functions and level repulsion. *Eur. Phys. J. D*, 7(1):1–4, 1999.
- [94] R. Uzdin, A. Mailybaev, and N. Moiseyev. On the observability and asymmetry of adiabatic state flips generated by exceptional points. *J. Phys. A: Math. Theor.*, 44(43):435302, 2011.
- [95] I. Gilary and N. Moiseyev. Asymmetric effect of slowly varying chirped laser pulses on the adiabatic state exchange of a molecule. *J. Phys. B: At. Mol. Opt. Phys.*, 45(5):051002, 2012.
- [96] I. Gilary, A. A. Mailybaev, and N. Moiseyev. Time-asymmetric quantum-state-exchange mechanism. *Phys. Rev. A*, 88(1):010102, 2013.
- [97] T. J. Milburn, J. Doppler, C. A. Holmes, S. Portolan, S. Rotter, and P. Rabl. General description of quasiadiabatic dynamical phenomena near exceptional points. *Phys. Rev. A*, 92(5):052124, 2015.
- [98] S. A. Langen, P. W. Brouwer, and C. W. J. Beenakker. Fluctuating phase rigidity for a quantum chaotic

BIBLIOGRAPHY

system with partially broken time-reversal symmetry. *Phys. Rev. E*, 55(1):R1–R4, 1997.

- [99] P. W. Brouwer. Wave function statistics in open chaotic billiards. *Phys. Rev. E*, 68(4):046205, 2003.
- [100] E. N. Bulgakov, I. Rotter, and A. F. Sadreev. Phase rigidity and avoided level crossings in the complex energy plane. *Phys. Rev. E*, 74(5):056204, 2006.
- [101] I. Rotter. A non-Hermitian Hamilton operator and the physics of open quantum systems. *J. Phys. A: Math. Theor.*, 42(15):153001, 2009.
- [102] J. Baker. An algorithm for the location of transition states. *J. Comput. Chem.*, 7(4):385–395, 1986.
- [103] A. Banerjee, N. Adams, J. Simons, and R. Shepard. Search for stationary points on surfaces. *J. Phys. Chem.*, 89(1):52–57, 1985.
- [104] C. G. Broyden. The convergence of a class of double-rank minimization algorithms: 2. The new algorithm. *J. Inst. Math. Appl.*, 6(3):222–231, 1970.
- [105] R. Fletcher. A new approach to variable metric algorithms. *Comput. J.*, 13(3):317–322, 1970.
- [106] D. Goldfarb. A family of variable-metric methods derived by variational means. *Math. Comput.*, 24(109):23–26, 1970.
- [107] D. F. Shanno. Conditioning of quasi-Newton methods for function minimization. *Math. Comput.*, 24(111):647–656, 1970.
- [108] M. J. Bearpark, M. A. Robb, and H. B. Schlegel. A direct method for the location of the lowest energy point on a potential surface crossing. *Chem. Phys. Lett.*, 223(3):269–274, 1994.
- [109] T. Helgaker, P. Jørgensen, and J. Olsen. *Molecular Electronic-Structure Theory*. John Wiley & Sons, New York, 2000.
- [110] N. C. Handy and H. F. Schaefer III. On the evaluation of analytic energy derivatives for correlated wave functions. *J. Chem. Phys.*, 81(11):5031–5033, 1984.
- [111] P. Jørgensen and T. Helgaker. Møller-Plesset energy derivatives. *J. Chem. Phys.*, 89(3):1560–1570, 1988.
- [112] T. Helgaker and P. Jørgensen. Configuration-interaction energy derivatives in a fully variational formulation. *Theor. Chim. Acta*, 75(2):111–127, 1989.
- [113] J. Gauss. Molecular properties. In J. Grotendorst, editor, *Modern Methods and Algorithms of Quantum Chemistry*, pages 541–592. John von Neumann Institute for Computing, Jülich, 2000.
- [114] L. Adamowicz, W. Laidig, and R. Bartlett. Analytical gradients for the coupled-cluster method. *Int. J. Quantum Chem.*, 26(S18):245–254, 1984.
- [115] J. Rice and R. Amos. On the efficient evaluation of analytic energy gradients. *Chem. Phys. Lett.*, 122(6):585–590, 1985.
- [116] A. C. Scheiner, G. E. Scuseria, J. E. Rice, T. J. Lee, and H. F. Schaefer III. Analytic evaluation of energy gradients for the single and double excitation coupled cluster (CCSD) wave function: Theory and application. *J. Chem. Phys.*, 87(9):5361–5373, 1987.
- [117] J. Gauss, J. F. Stanton, and R. J. Bartlett. Coupled-cluster open-shell analytic gradients: Implementation of the direct product decomposition approach in energy gradient calculations. *J. Chem. Phys.*, 95(4):2623–2638, 1991.
- [118] J. F. Stanton. Many-body methods for excited state potential energy surfaces. I. General theory of energy gradients for the equation-of-motion coupled-cluster method. *J. Chem. Phys.*, 99(11):8840–8847, 1993.
- [119] J. F. Stanton and J. Gauss. Analytic energy derivatives for the equation-of-motion coupled-cluster method:

BIBLIOGRAPHY

- Algebraic expressions, implementation and application to the S_1 state of HFCO. *Theor. Chim. Acta*, 91:267–289, 1995.
- [120] J. F. Stanton and J. Gauss. Analytic energy gradients for the equation-of-motion coupled-cluster method: Implementation and application to the HCN/HNC system. *J. Chem. Phys.*, 100(6):4695–4698, 1994.
- [121] W. D. Heiss. The physics of exceptional points. *J. Phys. A: Math. Theor.*, 45(44):444016, 2012.
- [122] L. E. Snyder, D. Buhl, B. Zuckerman, and P. Palmer. Microwave detection of interstellar formaldehyde. *Phys. Rev. Lett.*, 22(13):679–681, 1969.
- [123] B. Zuckerman, J. A. Ball, and C. A. Gottlieb. Microwave detection of interstellar formic acid. *Astrophys. J.*, 163:L41–L45, 1971.
- [124] L. E. Snyder and D. Buhl. Observations of radio emission from interstellar hydrogen cyanide. *Astrophys. J.*, 163:L47–L52, 1971.
- [125] F. Gardner and G. Winnewisser. The detection of interstellar vinyl cyanide/acrylonitrile. *Astrophys. J.*, 195:L127–L130, 1975.
- [126] J. M. Carter, W. W. Lapham, and J. S. Zogorski. Occurrence of volatile organic compounds in aquifers of the United States. *J. Am. Water Resour. Assoc.*, 44(2):399–416, 2008.
- [127] J. He, K. M. Ritalahti, K.-L. Yang, S. S. Koenigsberg, and F. E. Löffler. Detoxification of vinyl chloride to ethene coupled to growth of an anaerobic bacterium. *Nature*, 424(6944):62–65, 2003.
- [128] Z. Benda and T.-C. Jagau. Communication: Analytic gradients for the complex absorbing potential equation-of-motion coupled-cluster method. *J. Chem. Phys.*, 146(3):031101, 2017.
- [129] Z. Benda, K. Rickmeyer, and T.-C. Jagau. Structure optimization of temporary anions. *J. Chem. Theory Comput.*, 14(7):3468–3478, 2018.
- [130] Y. V. Vasil'ev, V. G. Voinov, D. F. Barofsky, and M. L. Deinzer. Absolute dissociative electron attachment cross-sections of chloro- and bromo-ethylenes. *Int. J. Mass Spectrom.*, 277(1-3):142–150, 2008.
- [131] Z. Benda and T.-C. Jagau. Understanding processes following resonant electron attachment: Minimum-energy crossing points between anionic and neutral potential energy surfaces. *J. Chem. Theory Comput.*, 14(8):4216–4223, 2018.
- [132] C. Hättig. Structure optimizations for excited states with correlated second-order methods: CC2 and ADC(2). In H. Jensen, editor, *Response Theory and Molecular Properties (A Tribute to Jan Linderberg and Poul Jørgensen)*, volume 50 of *Advances in Quantum Chemistry*, pages 37–60. Academic Press, 2005.
- [133] A. Köhn and A. Tajti. Can coupled-cluster theory treat conical intersections? *J. Chem. Phys.*, 127(4):044105, 2007.
- [134] E. F. Kjørstad, R. H. Myhre, T. J. Martínez, and H. Koch. Crossing conditions in coupled cluster theory. *J. Chem. Phys.*, 147(16):164105, 2017.
- [135] P. D. Burrow, A. Modelli, N. S. Chiu, and K. D. Jordan. Temporary σ and π anions of the chloroethylenes and chlorofluoroethylenes. *Chem. Phys. Lett.*, 82(2):270–276, 1981.
- [136] R. Kaufel, E. Illenberger, and H. Baumgärtel. Formation and dissociation of the chloroethylene anions. *Phys. Lett.*, 106(4):342–346, 1984.
- [137] J. K. Olthoff, J. A. Tossell, and J. H. Moore. Electron attachment by haloalkenes and halobenzenes. *J. Chem. Phys.*, 83(11):5627–5634, 1985.
- [138] Z. Benda and T.-C. Jagau. Locating exceptional points on multidimensional complex-valued potential energy surfaces. *J. Phys. Chem. Lett.*, 9(24):6978–6984, 2018.

BIBLIOGRAPHY

- [139] A. Tajti and P. G. Szalay. Analytic evaluation of the nonadiabatic coupling vector between excited states using equation-of-motion coupled-cluster theory. *J. Chem. Phys.*, 131(12):124104, 2009.
- [140] Y. Shao, Z. Gan, E. Epifanovsky, A. T. Gilbert, M. Wormit, J. Kussmann, A. W. Lange, A. Behn, J. Deng, X. Feng, and *et al.* Advances in molecular quantum chemistry contained in the Q-Chem 4 program package. *Mol. Phys.*, 113(2):184–215, 2015.
- [141] S. Faraji, S. Matsika, and A. I. Krylov. Calculations of non-adiabatic couplings within equation-of-motion coupled-cluster framework: Theory, implementation, and validation against multi-reference methods. *J. Chem. Phys.*, 148(4):044103, 2018.

5 Supporting Information

In this chapter, the supplementary materials corresponding to the published articles of Chapter 3 are given.

**Analytic gradients for the complex absorbing potential
equation-of-motion coupled-cluster method**

Zsuzsanna Benda, Thomas-C. Jagau¹

*Department of Chemistry, University of Munich (LMU), D-81377 Munich,
Germany*

TABLE I. Box size parameters and corresponding optimal CAP strengths. The box size parameters were chosen as the spatial extent of the wave function ($\sqrt{\langle\alpha^2\rangle}$) of the neutral molecule at the equilibrium structure of the neutral molecule (box_0) and at the equilibrium structure of the resonant anion (box_{res}). The corresponding η_{opt} values were determined at the respective structures. The CAP-EOM-EA-CCSD/aug-cc-pVDZ+3s3p(A) method was employed in all calculations. All values are in atomic units.

		r_x^0	r_y^0	r_z^0	η_{opt}
CH_2O^-	box_0	3.900	2.970	6.130	0.0054
	box_{res}	3.900	2.995	6.360	0.0007
HCOOH^-	box_0	9.690	5.320	3.600	0.0070
	box_{res}	9.870	5.485	3.730	0.0012
C_2H_4^-	box_0	7.140	4.670	3.450	0.0070
	$\text{box}_{\text{res}}^{\text{a}}$	7.415	3.520	4.675	0.0065

^a y and z axes are interchanged at the equilibrium structure of the resonance (C_{2h} symmetry) compared to that of the neutral molecule (D_{2h} symmetry).

TABLE II. Comparison of structural parameters for formaldehyde and formic acid. Geometries were optimized with regular CCSD/aug-cc-pVDZ+3s3p(A) for neutral molecules and CAP-EOM-EA-CCSD/aug-cc-pVDZ+3s3p(A) for resonance states. Bond lengths are given in Å, angles in degrees.

	CH_2O	CH_2O^-		HCOOH	HCOOH^-
$R(\text{C}=\text{O})$	1.215	1.286	$R(\text{C}=\text{O})$	1.208	1.276
$R(\text{C}-\text{H})$	1.112	1.114	$R(\text{C}-\text{OH})$	1.354	1.451
$\angle(\text{H}-\text{C}-\text{O})$	121.7	122.3	$\angle(\text{H}-\text{O}-\text{C}-\text{H})$	-180.0	-137.5

Z-matrix coordinatesCH₂O optimized with regular CCSD/aug-cc-pVDZ+3s3p(A)

C

H 1 1.111902

H 1 1.111902 2 116.60068

O 1 1.21549 2 121.699703 3 180 0

CH₂O⁻ optimized with CAP-EOM-EA-CCSD/aug-cc-pVDZ+3s3p(A)

C

H 1 1.114298

H 1 1.114298 2 115.341535

O 1 1.285902 2 122.329232 3 180 0

HCOOH optimized with regular CCSD/aug-cc-pVDZ+3s3p(A)

C

H 1 1.102911

O 1 1.207959 2 125.039614

O 1 1.353773 2 109.950896 3 180 0

H 4 0.971151 1 106.890397 2 180 0

5.1. SI FOR PUBLICATION 1

HCOOH⁻ optimized with CAP-EOM-EA-CCSD/aug-cc-pVDZ+3s3p(A)

```

C
H 1  1.12384
O 1  1.275743  2  121.022739
O 1  1.45142  2  107.906325  3  138.733952  0
H 4  0.97384  1  101.619242  2  -137.489722  0
  
```

C₂H₄ optimized with regular CCSD/aug-cc-pVDZ+3s3p(A)

```

C
H 1  1.093872
H 1  1.093872  2  116.993541
C 1  1.348024  2  121.503229  3  180  0
H 4  1.093872  1  121.503229  2  0  0
H 4  1.093872  1  121.503229  2  180  0
  
```

C₂H₄⁻ optimized with CAP-EOM-EA-CCSD/aug-cc-pVDZ+3s3p(A)

```

C
H 1  1.101802
H 1  1.101802  2  114.732545
C 1  1.438955  2  120.08234  3  154.769797  0
H 4  1.101802  1  120.08234  2  180  0
H 4  1.101802  1  120.08234  2  26.578334  0
  
```

C₂H₄⁻ optimized with regular EOM-EA-CCSD/aug-cc-pVDZ+3s3p(A)

```

C
H 1  1.096882
H 1  1.096882  2  116.349147
C 1  1.404978  2  121.825412  3  179.938380  0
H 4  1.096882  1  121.825412  2  180.000000  0
H 4  1.096882  1  121.825412  2  0.064988  0
  
```

CHAPTER 5. SUPPORTING INFORMATION

C_2H_4 optimized with regular CCSD/aug-cc-pVDZ

C
H 1 1.094088
H 1 1.094088 2 116.983394
C 1 1.348081 2 121.508303 3 -179.994314 0
H 4 1.094088 1 121.508303 2 180.000000 0
H 4 1.094088 1 121.508303 2 -0.005944 0

$C_2H_4^-$ optimized with regular EOM-EA-CCSD/aug-cc-pVDZ

C
H 1 1.097595
H 1 1.097595 2 116.277562
C 1 1.418359 2 121.861218 3 179.983940 0
H 4 1.097595 1 121.861218 2 -180.000000 0
H 4 1.097595 1 121.861218 2 0.016955 0

C_2H_4 optimized with regular CCSD/cc-pVDZ

C
H 1 1.096034
H 1 1.096034 2 116.914952
C 1 1.345179 2 121.542524 3 -179.990817 0
H 4 1.096034 1 121.542524 2 180.000000 0
H 4 1.096034 1 121.542524 2 -0.009608 0

$C_2H_4^-$ optimized with regular EOM-EA-CCSD/cc-pVDZ

C
H 1 1.115273
H 1 1.115273 2 110.170046
C 1 1.456334 2 115.826915 3 133.900596 0
H 4 1.115273 1 115.826915 2 -180.000000 0
H 4 1.115273 1 115.826915 2 48.712720 0

Supporting Information

Structure Optimization of Temporary Anions

Zsuzsanna Benda,* Kerstin Rickmeyer, and Thomas-C. Jagau*

Department of Chemistry, University of Munich (LMU), D-81377 Munich, Germany

E-mail: zsuzsanna.benda@cup.uni-muenchen.de; th.jagau@lmu.de

Table 1: C=O bond lengths (in Å), EA and Γ values (in eV), and η_{opt} parameters (in a.u.) for the neutral and resonance equilibrium structures of the π^* resonance of formaldehyde. Calculated with CCSD/CAP-EOM-EA-CCSD and MP2/CAP-EOM-EA-CCSD(2) methods using aug-cc-pVDZ and aug-cc-pVTZ basis sets augmented by extra diffuse functions.

Basis set	R_0	R_r	VEA	VDE	AEA	Γ_0	Γ_r	$\eta_{\text{opt},0}$	$\eta_{\text{opt},r}$
CH ₂ O CAP-EOM-EA-CCSD									
-DZ	1.21543	1.31719	-1.727	-1.039	-1.390	0.510	0.465	0.03600	0.03500
-DZ+3s	1.21541	1.31720	-1.727	-1.039	-1.390	0.511	0.466	0.03600	0.03500
-DZ+3p	1.21554	1.30125	-1.371	-0.874	-1.133	0.351	0.233	0.00535	0.00500
-DZ+3d	1.21445	1.30766	-1.547	-0.952	-1.255	0.468	0.371	0.02080	0.01900
-DZ+3s3p	1.21549	1.30124	-1.372	-0.873	-1.133	0.353	0.233	0.00540	0.00490
-DZ+6p	1.21552	1.30182	-1.381	-0.877	-1.139	0.360	0.241	0.00590	0.00550
-DZ+3p3d	1.21445	1.29527	-1.308	-0.856	-1.091	0.372	0.224	0.00340	0.00300
-DZ+6p6d	1.21433	1.29633	-1.323	-0.861	-1.101	0.372	0.230	0.00395	0.00360
-TZ+3p	1.20033	1.28228	-1.296	-0.818	-1.068	0.331	0.206	0.00380	0.00350
-TZ+3p3d	1.20047	1.27494	-1.206	-0.799	-1.011	0.387	0.205	0.00180	0.00155
CH ₂ O CAP-EOM-EA-CCSD(2)									
-DZ	1.22290	1.33527	-1.655	-0.897	-1.286	0.496	0.444	0.03500	0.03350
-DZ+3s	1.22287	1.33530	-1.656	-0.898	-1.287	0.497	0.446	0.03500	0.03400
-DZ+3p	1.22307	1.31828	-1.319	-0.763	-1.054	0.333	0.209	0.00540	0.00480
-DZ+3d	1.22189	1.32546	-1.486	-0.826	-1.164	0.454	0.349	0.02100	0.01840
-DZ+3s3p	1.22301	1.31808	-1.319	-0.765	-1.054	0.334	0.211	0.00535	0.00480
-DZ+6p	1.22309	1.31891	-1.328	-0.766	-1.060	0.342	0.218	0.00600	0.00540
-DZ+3p3d	1.22186	1.31207	-1.256	-0.750	-1.015	0.351	0.198	0.00330	0.00295
-DZ+6p6d	1.22186	1.31290	-1.269	-0.752	-1.022	0.351	0.203	0.00390	0.00340
-TZ+3p	1.20883	1.30014	-1.205	-0.673	-0.954	0.299	0.177	0.00375	0.00350
-TZ+3p3d	1.20880	1.28484	-1.122	-0.657	-0.860	0.340	0.175	0.00175	0.00050

Table 2: C=O/C=C bond lengths (in Å), EA and Γ values (in eV), and η_{opt} parameters (in a.u.) for the neutral and resonance equilibrium structures of the π^* resonances of formic acid and ethylene. Calculated with CCSD/CAP-EOM-EA-CCSD and MP2/CAP-EOM-EA-CCSD(2) methods using aug-cc-pVDZ and aug-cc-pVTZ basis sets augmented by extra diffuse functions.

Basis set	R_0	R_r	VEA	VDE	AEA	Γ_0	Γ_r	$\eta_{\text{opt},0}$	$\eta_{\text{opt},r}$
HCOOH CAP-EOM-EA-CCSD									
-DZ+3p	1.20796	1.28195	-2.325	-0.373	-1.526	0.250	0.102	0.00710	0.00560
-DZ+3p3d	1.20684	1.27910	-2.271	-0.411	-1.518	0.337	0.105	0.00430	0.00370
-TZ+3p	1.19329	1.26581	-2.287	-0.417	-1.545	0.271	0.104	0.00475	0.00400
-TZ+3p3d	1.19340	1.26327	-2.354	-0.472	-1.531	0.302	0.057	0.01200	0.00230
HCOOH CAP-EOM-EA-CCSD(2)									
-DZ+3p	1.21477	1.29501	-2.302	-0.174	-1.425	0.243	0.078	0.00710	0.00530
-DZ+3p3d	1.21359		-2.248			0.329		0.00430	
-TZ+3p	1.20094	1.28027	-2.221	-0.175	-1.399	0.251	0.069	0.00470	0.00335
-TZ+3p3d	1.20108	1.27816	-2.283	-0.220	-1.389	0.283	0.066	0.01180	0.00180
C ₂ H ₄ CAP-EOM-EA-CCSD									
-DZ+3p	1.34808	1.43898	-2.229	-1.632	-2.035	0.449	0.302	0.00720	0.00635
-DZ+3p3d	1.34762		-2.132			0.468		0.00465	
-TZ+3p	1.32727	1.41428	-2.155	-1.663	-1.977	0.446	0.291	0.00440	0.00405
-TZ+3p3d	1.32752		-2.028			0.550		0.00230	
C ₂ H ₄ CAP-EOM-EA-CCSD(2)									
-DZ+3p	1.34808	1.45153	-2.109	-1.304	-1.858	0.415	0.244	0.00700	0.00565
-DZ+3p3d	1.34756	1.44431	-2.022	-1.390	-1.817	0.421	0.236	0.00450	0.00370
-TZ+3p	1.32856	1.43012	-2.011	-1.288	-1.777	0.392	0.212	0.00430	0.00360
-TZ+3p3d	1.32880	1.41708	-1.905	-1.439	-1.726	0.455	0.238	0.00220	0.00170

Table 3: Statistics on the CAP-EOM-EA-CCSD(2) - CAP-EOM-EA-CCSD differences in VEA and Γ_0 values using the aug-cc-pVDZ+3p basis set. The investigated resonances are: lowest π^* resonance of formaldehyde, formic acid, acrylonitrile, methacrylonitrile, ethylene, 1,3-butadiene (two states), *cis*- and *trans*-1,3,5-hexatriene (two states).

quantity	mean	std. dev.	min	max
VEA	0.098	0.052	0.023	0.173
Γ_0	-0.020	0.013	-0.007	-0.050

Table 4: Effect of rotation of the molecule with respect to a fixed box on EA and Γ (in eV) values. Calculated for the π^* resonance of HCOOH with the CAP-EOM-EA-CCSD(2)/aug-cc-pVDZ+3p method. The box size parameters are $r_x^0 = 9.726$ a.u., $r_y^0 = 5.321$ a.u., $r_z^0 = 3.603$ a.u. η_{opt} parameters are given in a.u.

rotation	η_{opt}	EA	Γ
0°	0.0072	2.3032	0.2428
15°	0.0072	2.3037	0.2445
30°	0.0072	2.3048	0.2487
45°	0.0073	2.3064	0.2547
60°	0.0072	2.3076	0.2617
75°	0.0071	2.3082	0.2670
90°	0.0071	2.3078	0.2682
105°	0.0073	2.3068	0.2644
120°	0.0074	2.3055	0.2575
135°	0.0074	2.3044	0.2505
150°	0.0074	2.3038	0.2455
165°	0.0072	2.3033	0.2431

Table 5: Effect of rotation of the molecule when the box size is updated on EA and Γ (in eV) values. Calculated for the π^* resonance of HCOOH with the CAP-EOM-EA-CCSD(2)/aug-cc-pVDZ+3p method. Box size parameters and η_{opt} parameters are given in a.u.

rotation	r_x^0	r_y^0	r_z^0	η_{opt}	EA	Γ
0°	9.726	5.321	3.603	0.0072	2.3032	0.2428
15°	9.442	5.810	3.603	0.0076	2.3030	0.2443
30°	8.734	6.828	3.603	0.0080	2.3038	0.2484
45°	7.710	7.967	3.603	0.0081	2.3043	0.2499
60°	6.569	8.931	3.603	0.0080	2.3033	0.2469
75°	5.635	9.548	3.603	0.0074	2.3027	0.2431

5.2. SI FOR PUBLICATION 2

Table 6: Equilibrium structures (in Å) of acrylonitrile and its lowest π^* resonance calculated with the CCSD/CAP-EOM-EA-CCSD methods using the basis set aug-cc-pVDZ+3p.

Neutral equilibrium structure						
C						
N	1	1.1715				
C	1	1.4522	2	179.09		
H	3	1.0926	1	116.08	2	0.00
C	3	1.3497	1	122.17	2	180.00
H	5	1.0921	3	120.36	1	180.00
H	5	1.0927	3	121.59	1	0.00
Resonance equilibrium structure						
C						
N	1	1.1932				
C	1	1.4159	2	179.66		
H	3	1.0951	1	115.62	2	-180.00
C	3	1.4245	1	124.23	2	0.00
H	5	1.0944	3	120.53	1	-180.00
H	5	1.0946	3	121.70	1	0.00

Table 7: Equilibrium structures (in Å) of acrylonitrile and its lowest π^* resonance calculated with the MP2/CAP-EOM-EA-CCSD(2) methods using the basis set aug-cc-pVDZ+3p.

Neutral equilibrium structure						
C						
N	1	1.1880				
C	1	1.4413	2	179.08		
H	3	1.0922	1	116.48	2	0.00
C	3	1.3524	1	122.24	2	-180.00
H	5	1.0906	3	120.18	1	-180.00
H	5	1.0913	3	121.34	1	0.00
Resonance equilibrium structure						
C						
N	1	1.2122				
C	1	1.4085	2	179.62		
H	3	1.0944	1	116.25	2	-180.00
C	3	1.4314	1	123.95	2	0.00
H	5	1.0932	3	120.33	1	-180.00
H	5	1.0933	3	121.40	1	0.00

CHAPTER 5. SUPPORTING INFORMATION

Table 8: Equilibrium structures (in Å) of acrylonitrile and its lowest π^* resonance calculated with the CCSD/CAP-EOM-EA-CCSD methods using the basis set aug-cc-pVTZ+3p.

Neutral equilibrium structure						
C						
N	1	1.15154				
C	1	1.42981	2	178.92		
H	3	1.07671	1	116.16	2	0.00
C	3	1.32858	1	122.42	2	180.00
H	5	1.07685	3	120.48	1	180.00
H	5	1.07729	3	121.39	1	0.00
Resonance equilibrium structure						
C						
N	1	1.17295				
C	1	1.39253	2	179.71		
H	3	1.07840	1	115.64	2	-180.00
C	3	1.40400	1	124.44	2	0.00
H	5	1.07834	3	120.64	1	-180.00
H	5	1.07854	3	121.51	1	0.00

Table 9: Equilibrium structures (in Å) of acrylonitrile and its lowest π^* resonance calculated with the MP2/CAP-EOM-EA-CCSD(2) methods using the basis set aug-cc-pVTZ+3p.

Neutral equilibrium structure						
C						
N	1	1.1681				
C	1	1.4206	2	179.05		
H	3	1.0774	1	116.60	2	0.00
C	3	1.3326	1	122.39	2	-180.00
H	5	1.0765	3	120.34	1	-180.00
H	5	1.0772	3	121.11	1	0.00
Resonance equilibrium structure						
C						
N	1	1.1926				
C	1	1.3857	2	179.63		
H	3	1.0792	1	116.25	2	-180.00
C	3	1.4152	1	124.17	2	0.00
H	5	1.0784	3	120.49	1	180.00
H	5	1.0785	3	121.19	1	0.00

Table 10: Equilibrium structures (in Å) of methacrylonitrile and its lowest π^* resonance calculated with the CCSD/CAP-EOM-EA-CCSD methods using the basis set aug-cc-pVDZ+3p.

Neutral equilibrium structure						
C						
C	1	1.3510				
H	2	1.0921	1	121.54		
H	2	1.0928	1	120.38	3	-180.00
C	1	1.4585	2	119.27	3	0.00
N	5	1.1717	1	177.88	2	-180.00
C	1	1.5147	2	124.64	3	-180.00
H	7	1.1001	1	110.11	2	0.00
H	7	1.1023	1	110.51	2	120.44
H	7	1.1023	1	110.51	2	-120.44
Resonance equilibrium structure						
C						
C	1	1.4150				
H	2	1.0940	1	121.91		
H	2	1.0957	1	120.16	3	-176.90
C	1	1.4181	2	122.13	3	-1.81
N	5	1.1918	1	179.50	2	175.74
C	1	1.5145	2	120.19	3	-177.88
H	7	1.1035	1	111.56	2	-173.99
H	7	1.1104	1	111.22	2	-53.74
H	7	1.1142	1	111.83	2	65.29

Table 11: Equilibrium structures (in Å) of methacrylonitrile and its lowest π^* resonance calculated with the MP2/CAP-EOM-EA-CCSD(2) methods using the basis set aug-cc-pVDZ+3p.

Neutral equilibrium structure					
C					
C	1	1.3549			
H	2	1.0909	1	121.31	
H	2	1.0916	1	120.15	3 -180.00
C	1	1.4469	2	119.37	3 0.00
N	5	1.1886	1	177.73	2 -180.00
C	1	1.5095	2	124.39	3 -180.00
H	7	1.0983	1	110.17	2 0.00
H	7	1.1003	1	110.42	2 120.53
H	7	1.1003	1	110.42	2 -120.53
Resonance equilibrium structure					
C					
C	1	1.4080			
N	2	1.2129	1	179.44	
C	1	1.4276	2	122.13	3 169.51
H	4	1.0931	1	121.60	2 -2.39
H	4	1.0948	1	119.93	2 -178.21
C	1	1.5093	2	118.04	3 -14.24
H	7	1.1020	1	111.58	2 9.91
H	7	1.1092	1	111.31	2 130.09
H	7	1.1121	1	112.13	2 -110.83

Table 12: Optimal CAP strength parameters for neutral (0) and resonance (r) equilibrium structures of acrylonitrile and methacrylonitrile.

	Method	Basis	$\eta_{\text{opt},0}$	$\eta_{\text{opt},r}$
acrylonitrile	-CCSD	-DZ+3p	0.00130	0.00110
	-CCSD(2)	-DZ+3p	0.00120	0.00000
	-CCSD	-TZ+3p	0.00080	0.00055
	-CCSD(2)	-TZ+3p	0.00080	0.00000
methacrylonitrile	-CCSD	-DZ+3p	0.00230	0.00225
	-CCSD(2)	-DZ+3p	0.00225	0.00200

Table 13: Equilibrium structures (in a.u.) for C_4H_6 and $C_4H_6^-$ with CCSD/CAP-EOM-EA-CCSD methods and aug-cc-pVDZ+3p basis set

neutral			
C	1.15824879	-0.77153448	0.00000000
C	-1.15824879	0.77153448	0.00000000
C	3.51572517	0.21593769	0.00000000
C	-3.51572517	-0.21593769	0.00000000
H	0.90796502	-2.82918925	0.00000000
H	-0.90796502	2.82918925	0.00000000
H	3.82136896	2.26200351	0.00000000
H	-3.82136896	-2.26200351	0.00000000
H	5.19135928	-0.99096360	0.00000000
H	-5.19135928	0.99096360	0.00000000
$1\pi^*$			
C	1.14850869	-0.69804120	0.00000000
C	-1.14850869	0.69804120	0.00000000
C	3.63565377	0.25503496	0.00000000
C	-3.63565377	-0.25503496	0.00000000
H	0.94258096	-2.77333918	0.00000000
H	-0.94258096	2.77333918	0.00000000
H	4.01448680	2.29457588	0.00000000
H	-4.01448680	-2.29457588	0.00000000
H	5.27248621	-1.01098074	0.00000000
H	-5.27248621	1.01098074	0.00000000
$2\pi^*$			
C	-1.14332218	0.83628855	-0.04225960
C	1.15535695	-0.87481153	-0.04319739
C	-3.50504564	-0.23288549	0.09140251
C	3.50254222	0.22344763	0.08692577
H	-0.89330313	2.79100779	-0.72847278
H	0.90287608	-2.82617203	-0.74192471
H	-3.72731240	-2.24706632	0.54695201
H	3.67663652	2.23911496	0.55188736
H	-5.23311375	0.90321318	-0.06990385
H	5.25930498	-0.86756682	-0.08194513

Table 14: Equilibrium structures (in a.u.) for C_4H_6 and $C_4H_6^-$ with CCSD/CAP-EOM-EA-CCSD methods and aug-cc-pVTZ+3p basis set

neutral			
C	1.14716647	-0.75661102	0.00000000
C	-1.14716647	0.75661102	0.00000000
C	3.47006818	0.21193579	0.00000000
C	-3.47006818	-0.21193579	0.00000000
H	0.90354454	-2.78580535	0.00000000
H	-0.90354454	2.78580535	0.00000000
H	3.77301689	2.23072223	0.00000000
H	-3.77301689	-2.23072223	0.00000000
H	5.12010090	-0.98230226	0.00000000
H	-5.12010090	0.98230226	0.00000000
$1\pi^*$			
C	1.12297235	-0.70334816	0.00000000
C	-1.12297235	0.70334816	0.00000000
C	3.59181968	0.18797525	0.00000000
C	-3.59181968	-0.18797525	0.00000000
H	0.88646232	-2.74566459	0.00000000
H	-0.88646232	2.74566459	0.00000000
H	4.00221948	2.19222753	0.00000000
H	-4.00221948	-2.19222753	0.00000000
H	5.18135544	-1.09080404	0.00000000
H	-5.18135544	1.09080404	0.00000000

5.2. SI FOR PUBLICATION 2

Table 15: Equilibrium structures (in a.u.) for C_4H_6 and $C_4H_6^-$ with MP2/CAP-EOM-EA-CCSD(2) methods and aug-cc-pVDZ+3p basis set

neutral			
C	1.14793728	-0.77021334	0.00000000
C	-1.14793728	0.77021334	0.00000000
C	3.51105828	0.21742472	0.00000000
C	-3.51105828	-0.21742472	0.00000000
H	0.90192368	-2.82713762	0.00000000
H	-0.90192368	2.82713762	0.00000000
H	3.80737643	2.26207197	0.00000000
H	-3.80737643	-2.26207197	0.00000000
H	5.18130461	-0.99221755	0.00000000
H	-5.18130461	0.99221755	0.00000000
$1\pi^*$			
C	1.13998869	-0.69708393	0.00000000
C	-1.13998869	0.69708393	0.00000000
C	3.64253473	0.25828220	0.00000000
C	-3.64253473	-0.25828220	0.00000000
H	0.94126217	-2.77195943	0.00000000
H	-0.94126217	2.77195943	0.00000000
H	4.01349760	2.29682735	0.00000000
H	-4.01349760	-2.29682735	0.00000000
H	5.27193291	-1.01319449	0.00000000
H	-5.27193291	1.01319449	0.00000000
$2\pi^*$			
C	-1.13850844	-0.87355058	0.03777280
C	1.13210188	0.85373443	0.05328573
C	-3.50842255	0.20989600	-0.08600416
C	3.50238525	-0.22833363	-0.07688891
H	-0.89882402	-2.81197705	0.77977144
H	0.89023986	2.78279689	0.81883977
H	-3.70334046	2.21545387	-0.57232640
H	3.69852758	-2.22735143	-0.58995826
H	-5.23837174	-0.91781401	0.06790966
H	5.23157674	0.89739461	0.09792588

CHAPTER 5. SUPPORTING INFORMATION

Table 16: Equilibrium structures (in a.u.) for C_4H_6 and $C_4H_6^-$ with MP2/CAP-EOM-EA-CCSD(2) methods and aug-cc-pVTZ+3p basis set

neutral			
C	1.13751737	-0.75639288	0.00000000
C	-1.13751737	0.75639288	0.00000000
C	3.46815441	0.21349134	0.00000000
C	-3.46815441	-0.21349134	0.00000000
H	0.89835181	-2.78722821	0.00000000
H	-0.89835181	2.78722821	0.00000000
H	3.76117581	2.23301467	0.00000000
H	-3.76117581	-2.23301467	0.00000000
H	5.11497566	-0.98397297	0.00000000
H	-5.11497566	0.98397297	0.00000000
$1\pi^*$			
C	1.11487154	-0.70356763	0.00000000
C	-1.11487154	0.70356763	0.00000000
C	3.60185330	0.18861391	0.00000000
C	-3.60185330	-0.18861391	0.00000000
H	0.88274112	-2.74761002	0.00000000
H	-0.88274112	2.74761002	0.00000000
H	4.00800401	2.19336193	0.00000000
H	-4.00800401	-2.19336193	0.00000000
H	5.18406482	-1.09909123	0.00000000
H	-5.18406482	1.09909123	0.00000000

Table 17: Equilibrium structure (in a.u.) for *trans*-C₆H₈ and the first *trans*-C₆H₈⁻ resonance with the CCSD/CAP-EOM-EA-CCSD method and aug-cc-pVDZ+3p basis set

neutral			
C	1.14890925	-0.57194635	0.00000000
C	-1.14890925	0.57194635	0.00000000
C	3.55524252	0.80997198	0.00000000
C	-3.55524252	-0.80997198	0.00000000
C	5.84714695	-0.32594812	0.00000000
C	-5.84714695	0.32594812	0.00000000
H	1.25126503	-2.64390473	0.00000000
H	-1.25126503	2.64390473	0.00000000
H	3.44107538	2.87969113	0.00000000
H	-3.44107538	-2.87969113	0.00000000
H	7.59489464	0.77395879	0.00000000
H	-7.59489464	-0.77395879	0.00000000
H	6.02293048	-2.38739919	0.00000000
H	-6.02293048	2.38739919	0.00000000
1π*			
C	1.20158176	-0.57857876	0.00000000
C	-1.20158176	0.57857876	0.00000000
C	3.55513607	0.73085651	0.00000000
C	-3.55513607	-0.73085651	0.00000000
C	5.97926409	-0.29013075	0.00000000
C	-5.97926409	0.29013075	0.00000000
H	1.27062928	-2.65965355	0.00000000
H	-1.27062928	2.65965355	0.00000000
H	3.41714079	2.80950613	0.00000000
H	-3.41714079	-2.80950613	0.00000000
H	7.65366028	0.92303350	0.00000000
H	-7.65366028	-0.92303350	0.00000000
H	6.28897156	-2.33940020	0.00000000
H	-6.28897156	2.33940020	0.00000000

CHAPTER 5. SUPPORTING INFORMATION

Table 18: Equilibrium structures (in a.u.) for *trans*-C₆H₈⁻ resonances with the CAP-EOM-EA-CCSD method and aug-cc-pVDZ+3p basis set

	2π*		
C	1.18248598	-0.50656339	0.00000000
C	-1.18248598	0.50656339	0.00000000
C	3.60303864	0.92023011	0.00000000
C	-3.60303864	-0.92023011	0.00000000
C	5.90547929	-0.33377387	0.00000000
C	-5.90547929	0.33377387	0.00000000
H	1.36806007	-2.57826868	0.00000000
H	-1.36806007	2.57826868	0.00000000
H	3.51596886	2.99144185	0.00000000
H	-3.51596886	-2.99144185	0.00000000
H	7.71114212	0.67878702	0.00000000
H	-7.71114212	-0.67878702	0.00000000
H	5.99555935	-2.40406385	0.00000000
H	-5.99555935	2.40406385	0.00000000
	3π*		
C	1.13778443	-0.62901503	0.00000000
C	-1.13778443	0.62901503	0.00000000
C	3.52748570	0.81794784	0.00000000
C	-3.52748570	-0.81794784	0.00000000
C	5.83325071	-0.31603311	0.00000000
C	-5.83325071	0.31603311	0.00000000
H	1.21715547	-2.70160031	0.00000000
H	-1.21715547	2.70160031	0.00000000
H	3.36170422	2.88559437	0.00000000
H	-3.36170422	-2.88559437	0.00000000
H	7.59021819	0.77700888	0.00000000
H	-7.59021819	-0.77700888	0.00000000
H	5.99168524	-2.38106748	0.00000000
H	-5.99168524	2.38106748	0.00000000

Table 19: Equilibrium structure (in a.u.) for *trans*-C₆H₈ with the MP2 method and aug-cc-pVDZ+3p basis set

	neutral		
C	1.15522611	-0.57300646	0.00000000
C	-1.15522611	0.57300646	0.00000000
C	3.53630344	0.80632650	0.00000000
C	-3.53630344	-0.80632650	0.00000000
C	5.83720385	-0.32836610	0.00000000
C	-5.83720385	0.32836610	0.00000000
H	1.24907461	-2.64498510	0.00000000
H	-1.24907461	2.64498510	0.00000000
H	3.42542272	2.87494027	0.00000000
H	-3.42542272	-2.87494027	0.00000000
H	7.57846682	0.77634495	0.00000000
H	-7.57846682	-0.77634495	0.00000000
H	6.00628350	-2.38740728	0.00000000
H	-6.00628350	2.38740728	0.00000000

CHAPTER 5. SUPPORTING INFORMATION

Table 20: Equilibrium structures (in a.u.) for *trans*-C₆H₈⁻ resonances with the CAP-EOM-EA-CCSD(2) method and aug-cc-pVDZ+3p basis set

	1π*		
C	1.21195118	-0.58013025	0.00000000
C	-1.21195118	0.58013025	0.00000000
C	3.54198287	0.73207454	0.00000000
C	-3.54198287	-0.73207454	0.00000000
C	5.98518561	-0.28206418	0.00000000
C	-5.98518561	0.28206418	0.00000000
H	1.27316459	-2.66110428	0.00000000
H	-1.27316459	2.66110428	0.00000000
H	3.40422004	2.80975905	0.00000000
H	-3.40422004	-2.80975905	0.00000000
H	7.64735799	0.94341347	0.00000000
H	-7.64735799	-0.94341347	0.00000000
H	6.29490773	-2.32882303	0.00000000
H	-6.29490773	2.32882303	0.00000000
	2π*		
C	1.19114934	-0.50232774	0.00000000
C	-1.19114934	0.50232774	0.00000000
C	3.58846164	0.92471910	0.00000000
C	-3.58846164	-0.92471910	0.00000000
C	5.90276364	-0.33765633	0.00000000
C	-5.90276364	0.33765633	0.00000000
H	1.37485704	-2.57395078	0.00000000
H	-1.37485704	2.57395078	0.00000000
H	3.50887236	2.99537622	0.00000000
H	-3.50887236	-2.99537622	0.00000000
H	7.70515870	0.67582992	0.00000000
H	-7.70515870	-0.67582992	0.00000000
H	5.97911355	-2.40628415	0.00000000
H	-5.97911355	2.40628415	0.00000000

Table 21: Equilibrium structure (in a.u.) for *cis*-C₆H₈ with the CCSD method and aug-cc-pVDZ+3p basis set

	neutral		
C	1.28614048	1.46514760	0.00000000
C	-1.28614048	1.46514760	0.00000000
C	2.93311135	-0.77311253	0.00000000
C	-2.93311135	-0.77311253	0.00000000
C	5.48676997	-0.61792344	0.00000000
C	-5.48676997	-0.61792344	0.00000000
H	2.25611649	3.29594339	0.00000000
H	-2.25611649	3.29594339	0.00000000
H	2.04821736	-2.64282058	0.00000000
H	-2.04821736	-2.64282058	0.00000000
H	6.66965158	-2.31057247	0.00000000
H	-6.66965158	-2.31057247	0.00000000
H	6.45068776	1.21277993	0.00000000
H	-6.45068776	1.21277993	0.00000000

CHAPTER 5. SUPPORTING INFORMATION

Table 22: Equilibrium structures (in a.u.) for *cis*-C₆H₈⁻ resonances with the CAP-EOM-EA-CCSD method and aug-cc-pVDZ+3p basis set

	1π*		
C	1.34060280	1.44787996	0.00000000
C	-1.34060280	1.44787996	0.00000000
C	2.99180629	-0.68453295	0.00000000
C	-2.99180629	-0.68453295	0.00000000
C	5.62050253	-0.66842051	0.00000000
C	-5.62050253	-0.66842051	0.00000000
H	2.26244283	3.31159967	0.00000000
H	-2.26244283	3.31159967	0.00000000
H	2.08899496	-2.55755294	0.00000000
H	-2.08899496	-2.55755294	0.00000000
H	6.70339984	-2.42990891	0.00000000
H	-6.70339984	-2.42990891	0.00000000
H	6.69166120	1.10630318	0.00000000
H	-6.69166120	1.10630318	0.00000000
	2π*		
C	1.28548119	1.47528407	0.00000000
C	-1.28548119	1.47528407	0.00000000
C	2.88440530	-0.82089800	0.00000000
C	-2.88440530	-0.82089800	0.00000000
C	5.49183222	-0.59458323	0.00000000
C	-5.49183222	-0.59458323	0.00000000
H	2.29065200	3.29114436	0.00000000
H	-2.29065200	3.29114436	0.00000000
H	1.96959243	-2.67437275	0.00000000
H	-1.96959243	-2.67437275	0.00000000
H	6.74122568	-2.24485004	0.00000000
H	-6.74122568	-2.24485004	0.00000000
H	6.39758342	1.26926134	0.00000000
H	-6.39758342	1.26926134	0.00000000

Table 23: Equilibrium structure (in a.u.) for *cis*-C₆H₈ with the MP2 method and aug-cc-pVDZ+3p basis set

neutral			
C	1.29240559	1.46002076	0.00000000
C	-1.29240559	1.46002076	0.00000000
C	2.91474023	-0.76741988	0.00000000
C	-2.91474023	-0.76741988	0.00000000
C	5.47627787	-0.61818967	0.00000000
C	-5.47627787	-0.61818967	0.00000000
H	2.25790919	3.29272538	0.00000000
H	-2.25790919	3.29272538	0.00000000
H	2.03303769	-2.63727444	0.00000000
H	-2.03303769	-2.63727444	0.00000000
H	6.65058414	-2.31321973	0.00000000
H	-6.65058414	-2.31321973	0.00000000
H	6.43365595	1.21279947	0.00000000
H	-6.43365595	1.21279947	0.00000000

CHAPTER 5. SUPPORTING INFORMATION

Table 24: Equilibrium structures (in a.u.) for *cis*-C₆H₈⁻ resonances with the CAP-EOM-EA-CCSD(2) method and aug-cc-pVDZ+3p basis set

1π*			
C	1.35151012	1.46455408	0.00000000
C	-1.35151012	1.46455408	0.00000000
C	2.98034696	-0.66074508	0.00000000
C	-2.98034696	-0.66074508	0.00000000
C	5.62374930	-0.65924691	0.00000000
C	-5.62374930	-0.65924691	0.00000000
H	2.26556452	3.33167726	0.00000000
H	-2.26556452	3.33167726	0.00000000
H	2.07728581	-2.53247473	0.00000000
H	-2.07728581	-2.53247473	0.00000000
H	6.68964729	-2.42794045	0.00000000
H	-6.68964729	-2.42794045	0.00000000
H	6.69407371	1.11314109	0.00000000
H	-6.69407371	1.11314109	0.00000000
2π*			
C	1.29171663	1.47335809	0.00000000
C	-1.29171663	1.47335809	0.00000000
C	2.86493350	-0.81648694	0.00000000
C	-2.86493350	-0.81648694	0.00000000
C	5.48652921	-0.59579483	0.00000000
C	-5.48652921	-0.59579483	0.00000000
H	2.29329314	3.29060221	0.00000000
H	-2.29329314	3.29060221	0.00000000
H	1.95097122	-2.66918507	0.00000000
H	-1.95097122	-2.66918507	0.00000000
H	6.72682898	-2.25011012	0.00000000
H	-6.72682898	-2.25011012	0.00000000
H	6.38598886	1.26843434	0.00000000
H	-6.38598886	1.26843434	0.00000000

Table 25: EA (in eV), Γ (in eV), and η_{opt} (in a.u.) values for π^* resonances of conjugated hydrocarbons calculated with the CAP-EOM-EA-CCSD and CAP-EOM-EA-CCSD(2) methods using the aug-cc-pVDZ+3p basis set.

Molecule	State	Method	VEA	VDE	AEA	Γ_0	Γ_r	$\eta_{\text{opt},0}$	$\eta_{\text{opt},r}$
C ₂ H ₄	π^*	-CCSD	-2.229	-1.632	-2.035	0.449	0.302	0.00720	0.00635
		-CCSD(2)	-2.109	-1.304	-1.858	0.415	0.244	0.00700	0.00565
C ₄ H ₆	$1\pi^*$	-CCSD	-1.282	-0.800	-1.040	0.136	0.099	0.01500	0.01400
		-CCSD(2)	-1.142	-0.617	-0.878	0.124	0.088	0.01450	0.01300
	$2\pi^*$	-CCSD	-2.874	-2.437	-2.740	0.709	0.568	0.02100	0.02300
		-CCSD(2)	-2.838	-2.327	-2.682	0.683	0.522	0.02100	0.02300
<i>trans</i> -C ₆ H ₈	$1\pi^*$	-CCSD	-0.637	-0.162	-0.401	0.031	0.012	0.00260	0.00200
		-CCSD(2)	-0.497	0.004	-0.244	0.024	0.000	0.00260	0.00000
	$2\pi^*$	-CCSD	-2.647	-2.449	-2.553	0.362	0.272	0.04900	0.04600
		-CCSD(2)	-2.595	-2.362	-2.484	0.337	0.244	0.04800	0.04500
	$3\pi^*$	-CCSD	-2.658	-2.564	-2.613	0.560	0.521	0.05000	0.05000
<i>cis</i> -C ₆ H ₈	$1\pi^*$	-CCSD	-0.680	-0.189	-0.436	0.032	0.012	0.00240	0.00180
		-CCSD(2)	-0.541	-0.025	-0.283	0.025	0.009	0.00240	0.00160
	$2\pi^*$	-CCSD	-2.055	-1.892	-1.974	0.258	0.223	0.04700	0.04200
		-CCSD(2)	-1.983	-1.800	-1.895	0.244	0.206	0.04500	0.04600

Table 26: EA (in eV), Γ (in eV), and η_{opt} (in a.u.) values for π^* resonances of C₄H₆ calculated with the CAP-EOM-EA-CCSD and CAP-EOM-EA-CCSD(2) methods using the aug-cc-pVTZ+3p basis set.

Molecule	State	Method	VEA	VDE	AEA	Γ_0	Γ_r	$\eta_{\text{opt},0}$	$\eta_{\text{opt},r}$
C ₄ H ₆	$1\pi^*$	-CCSD	-1.226	-0.729	-0.978	0.128	0.082	0.00900	0.00900
		-CCSD(2)	-1.053	-0.516	-0.745	0.108	0.069	0.00950	0.00950
	$2\pi^*$	-CCSD	-2.675	—	—	0.831	—	0.01150	—
		-CCSD(2)	-2.632	—	—	0.786	—	0.01150	—

Supporting Information

Understanding processes following resonant electron attachment: Minimum-energy crossing points between anionic and neutral potential energy surfaces

Zsuzsanna Benda* and Thomas-C. Jagau*

Department of Chemistry, University of Munich (LMU), D-81377 Munich, Germany

E-mail: zsuzsanna.benda@cup.uni-muenchen.de; th.jagau@lmu.de

Table 1: HCOOH resonance equilibrium structure and MECP calculated with CAP-EOM-EA-CCSD and EOM-EA-CCSD using the basis set aug-cc-pVDZ+3p. Bond lengths in Å.

Resonance equilibrium						
C						
H	1	1.126984				
O	1	1.281950	2	120.762759		
O	1	1.465019	2	107.189032	3	-135.867439
H	4	0.970919	1	100.733931	2	136.471503
MECP						
C						
H	1	1.132298				
O	1	1.292856	2	118.994072		
O	1	1.490655	2	105.740439	3	-129.986315
H	4	0.970713	1	99.442048	2	129.786837

Table 2: Box size parameters (r_α^0 , $\alpha = x, y, z$) and optimal CAP strength parameters (η_{opt}) used for calculating the uncorrected and corrected CAP-EOM-EA-CCSD/aug-cc-pVDZ+3p potential energy curves of HCOOH⁻ (displayed in Fig. S1). Parameters are given in a.u. From point 'd' an optimal CAP strength cannot be determined in the uncorrected case, due to the vanishing minimum of the $|\eta dE/d\eta|$ trajectory (see Fig. S2).

	r_x^0	r_y^0	r_z^0	η_{opt} uncorr.	η_{opt} corr.
a	9.868	5.500	3.735	0.0056	0.0120
Res. eq.	9.880	5.505	3.744	0.0056	0.0120
b	9.890	5.510	3.754	0.0053	0.0120
c	9.898	5.516	3.763	0.0052	0.0120
d	9.903	5.523	3.773	–	0.0115
MECP	9.907	5.531	3.783	–	0.0115
e	9.908	5.540	3.793	–	0.0115
f	9.907	5.549	3.803	–	0.0110
g	9.903	5.560	3.813	–	0.0110
h	9.898	5.571	3.824	–	0.0110

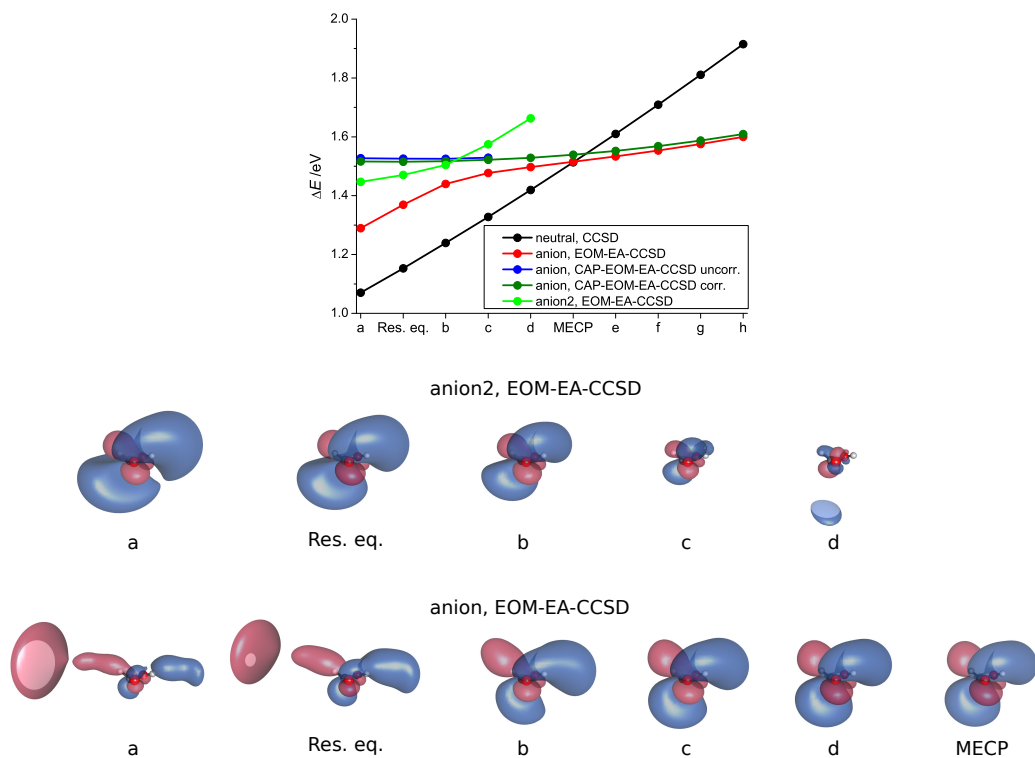


Figure 1: Energy profiles along the pathway connecting the resonance equilibrium structure with the MECP between the π^* resonance and the neutral ground state of formic acid. Structures were generated using linear interpolation and extrapolation using the resonance equilibrium structure and the MECP structure. Calculations were performed with CCSD for the neutral state. For the anionic state EOM-EA-CCSD as well as uncorrected and corrected CAP-EOM-EA-CCSD results are plotted. The Dyson orbitals of the two anionic states present in regular EOM-EA-CCSD calculations in the metastable region are also shown. All calculations were done with the aug-cc-pVDZ+3p basis set.

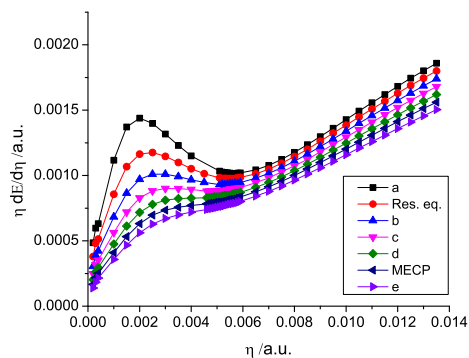


Figure 2: $|\eta dE/d\eta|$ trajectories used for determining the optimal CAP strength parameters for different nuclear configurations of the uncorrected CAP-EOM-EA-CCSD/aug-cc-pVDZ+3p potential energy curve of HCOOH^- plotted in Fig. S1.

Table 3: Acrylonitrile MECP calculated with EOM-EA-CCSD/aug-cc-pVDZ+3p. Bond lengths in Å.

C						
N	1	1.197477				
C	1	1.409300	2	179.556824		
H	3	1.095762	1	115.408426	2	179.813684
C	3	1.445444	1	124.540788	2	6.446210
H	5	1.098069	3	119.869090	1	-15.287186
H	5	1.098246	3	118.826412	1	-168.056804

Table 4: Methacrylonitrile MECP calculated with EOM-EA-CCSD/aug-cc-pVDZ+3p. Bond lengths in Å.

C						
C	1	1.412692				
N	2	1.195576	1	179.278265		
C	1	1.437156	2	121.832567	3	-150.530281
H	4	1.096716	1	120.177435	2	14.558099
H	4	1.099002	1	118.722219	2	168.542772
C	1	1.514251	2	116.858237	3	46.930507
H	7	1.105257	1	111.859686	2	-24.753851
H	7	1.108957	1	111.034133	2	-144.834326
H	7	1.120857	1	112.226242	2	96.566612

CHAPTER 5. SUPPORTING INFORMATION

Table 5: C₂H₄ MECF calculated with EOM-EA-CCSD. Bond lengths in Å.

aug-cc-pVDZ+3p						
C						
H	1	1.123335				
H	1	1.133371	2	105.025105		
C	1	1.525511	2	111.460740	3	-128.285145
H	4	1.123463	1	111.443130	2	164.020645
H	4	1.133613	1	117.497711	2	42.766773
aug-cc-pVTZ+3p						
C						
H	1	1.103128				
H	1	1.112359	2	106.005435		
C	1	1.506563	2	112.015909	3	-129.511494
H	4	1.103133	1	112.013519	2	166.643307
H	4	1.112364	1	117.618097	2	43.472435

Table 6: C₂H₃Cl neutral equilibrium structure calculated with CCSD. Bond lengths in Å.

aug-cc-pVDZ+3p						
Cl						
C	1	1.751506				
H	2	1.091227	1	113.060877		
C	2	1.341480	1	122.835055	3	-180.000000
H	4	1.091911	2	122.089510	1	0.000000
H	4	1.092678	2	119.201497	1	-180.000000
aug-cc-pVTZ+3p						
Cl						
C	1	1.729108				
H	2	1.074196	1	113.343715		
C	2	1.320776	1	123.200792	3	-180.000000
H	4	1.076073	2	121.876806	1	0.000000
H	4	1.077067	2	119.287963	1	-180.000000

Table 7: C₂H₃Cl MECF calculated with EOM-EA-CCSD. Bond lengths in Å.

aug-cc-pVDZ+3p						
Cl						
C	1	2.067891				
H	2	1.098495	1	107.087218		
C	2	1.359662	1	119.827617	3	-147.884380
H	4	1.096160	2	121.353256	1	-32.955248
H	4	1.102907	2	121.795674	1	146.650820
aug-cc-pVTZ+3p						
Cl						
C	1	2.015209				
H	2	1.080192	1	106.114268		
C	2	1.346708	1	120.217167	3	-143.827618
H	4	1.080053	2	121.571808	1	-38.128613
H	4	1.087369	2	121.634884	1	141.538879

Table 8: cis-C₂H₂Cl₂ neutral equilibrium structure calculated with CCSD. Bond lengths in Å.

aug-cc-pVDZ+3p						
Cl						
C	1	1.736045				
H	2	1.090810	1	114.684671		
C	2	1.342729	1	124.753375	3	-180.000000
H	4	1.090804	2	120.579338	1	-180.000000
Cl	4	1.736179	2	124.752544	1	0.000000
aug-cc-pVTZ+3p						
Cl						
C	1	1.713701				
H	2	1.073212	1	115.034160		
C	2	1.322102	1	124.818100	3	-180.000000
H	4	1.073209	2	120.146097	1	-180.000000
Cl	4	1.713708	2	124.818123	1	0.000000

CHAPTER 5. SUPPORTING INFORMATION

Table 9: cis-C₂H₂Cl₂ MECP calculated with EOM-EA-CCSD. Bond lengths in Å.

aug-cc-pVDZ+3p						
Cl						
C	1	1.829700				
H	2	1.092389	1	110.526116		
C	2	1.368134	1	121.865404	3	-149.331747
H	4	1.092378	2	119.937653	1	164.356249
Cl	4	1.829780	2	121.864964	1	-49.100725
aug-cc-pVTZ+3p						
Cl						
C	1	1.800667				
H	2	1.074116	1	110.783265		
C	2	1.350923	1	121.997509	3	-149.256756
H	4	1.074116	2	119.566795	1	163.704951
Cl	4	1.800673	2	121.997420	1	-49.627487

Table 10: trans-C₂H₂Cl₂ neutral equilibrium structure calculated with CCSD. Bond lengths in Å.

aug-cc-pVDZ+3p						
Cl						
C	1	1.745454				
H	2	1.090454	1	114.924338		
C	2	1.340383	1	121.010391	3	-180.000000
H	4	1.090449	2	124.081260	1	0.000000
Cl	4	1.745606	2	121.012672	1	-180.000000
aug-cc-pVTZ+3p						
Cl						
C	1	1.722331				
H	2	1.073289	1	115.178855		
C	2	1.319407	1	121.619426	3	-180.000000
H	4	1.073264	2	123.201764	1	0.000000
Cl	4	1.722332	2	121.619660	1	-180.000000

5.3. SI FOR PUBLICATION 3

Table 11: trans-C₂H₂Cl₂ MECP calculated with EOM-EA-CCSD. Bond lengths in Å.

aug-cc-pVDZ+3p						
Cl						
C	1	1.875033				
H	2	1.090033	1	110.272548		
C	2	1.341581	1	122.106646	3	165.326429
H	4	1.090016	2	125.823343	1	13.259173
Cl	4	1.876219	2	122.059191	1	-149.638398
aug-cc-pVTZ+3p						
Cl						
C	1	1.842139				
H	2	1.072429	1	110.439126		
C	2	1.327301	1	122.361141	3	163.034199
H	4	1.072430	2	124.759473	1	15.938822
Cl	4	1.842192	2	122.360810	1	-144.611145

Table 12: 1,1-C₂H₂Cl₂ neutral equilibrium structure calculated with CCSD. Bond lengths in Å.

aug-cc-pVDZ+3p						
Cl						
C	1	1.744038				
C	2	1.340484	1	122.733746		
H	3	1.090573	2	120.183860	1	0.000000
H	3	1.090577	2	120.182513	1	-180.000000
Cl	2	1.744067	1	114.536061	3	-180.000000
aug-cc-pVTZ+3p						
Cl						
C	1	1.722031				
C	2	1.318772	1	122.739583		
H	3	1.074417	2	120.114621	1	-180.000000
H	3	1.074422	2	120.116060	1	0.000000
Cl	2	1.722143	1	114.533453	3	-180.000000

CHAPTER 5. SUPPORTING INFORMATION

Table 13: 1,1-C₂H₂Cl₂ MECF calculated with EOM-EA-CCSD. Bond lengths in Å.

aug-cc-pVDZ+3p						
Cl						
C	1	1.835702				
C	2	1.372471	1	118.025242		
H	3	1.092488	2	120.100745	1	-163.633820
H	3	1.092501	2	120.106653	1	20.462458
Cl	2	1.835953	1	113.765918	3	-144.664052
aug-cc-pVTZ+3p						
Cl						
C	1	1.807304				
C	2	1.357550	1	117.687463		
H	3	1.076045	2	120.019437	1	-163.695323
H	3	1.076047	2	120.020025	1	22.242334
Cl	2	1.807370	1	113.406236	3	-143.027424

Table 14: C₂HCl₃ neutral equilibrium structure calculated with CCSD. Bond lengths in Å.

aug-cc-pVDZ+3p						
Cl						
C	1	1.730030				
C	2	1.344241	1	124.487400		
H	3	1.089666	2	120.897372	1	-180.000000
Cl	3	1.732813	2	123.690720	1	0.000000
Cl	2	1.743179	1	115.678943	3	-180.000000
aug-cc-pVTZ+3p						
Cl						
C	1	1.708374				
C	2	1.322567	1	124.140967		
H	3	1.071229	2	120.290740	1	-180.000000
Cl	3	1.710191	2	123.970002	1	0.000000
Cl	2	1.720132	1	115.763291	3	-180.000000

Table 15: C_2HCl_3 MECP1 calculated with EOM-EA-CCSD. Bond lengths in Å.

aug-cc-pVDZ+3p						
Cl						
C	1	1.806469				
C	2	1.369628	1	121.864935		
H	3	1.089419	2	121.987553	1	-162.066453
Cl	3	1.754334	2	121.988982	1	31.518549
Cl	2	1.773441	1	114.259607	3	-148.007413
aug-cc-pVTZ+3p						
Cl						
C	1	1.778496				
C	2	1.350729	1	121.764631		
H	3	1.070460	2	121.412750	1	-161.714474
Cl	3	1.733786	2	121.949957	1	33.346973
Cl	2	1.743486	1	114.246038	3	-148.776563

Table 16: C_2HCl_3 MECP2 calculated with EOM-EA-CCSD. Bond lengths in Å.

aug-cc-pVDZ+3p						
Cl						
C	1	1.751683				
C	2	1.358434	1	122.674706		
H	3	1.089113	2	121.238166	1	173.276784
Cl	3	1.770244	2	124.900857	1	-1.588060
Cl	2	1.872080	1	114.525927	3	155.313931
aug-cc-pVTZ+3p						
Cl						
C	1	1.727026				
C	2	1.341318	1	122.311211		
H	3	1.070165	2	120.862173	1	174.778126
Cl	3	1.751820	2	125.008404	1	2.301780
Cl	2	1.837736	1	113.936351	3	154.794601

CHAPTER 5. SUPPORTING INFORMATION

Table 17: C_2Cl_4 neutral equilibrium structure calculated with CCSD. Bond lengths in Å.

aug-cc-pVDZ+3p						
Cl						
C	1	1.732611				
C	2	1.351294	1	122.377288		
Cl	3	1.732675	2	122.374680	1	-180.000000
Cl	3	1.732703	2	122.351106	1	0.000000
Cl	2	1.732865	1	115.265822	3	-180.000000

Table 18: C_2Cl_4 MECP calculated with EOM-EA-CCSD. Bond lengths in Å.

aug-cc-pVDZ+3p						
Cl						
C	1	1.741041				
C	2	1.360979	1	121.305499		
Cl	3	1.741004	2	121.341803	1	178.822011
Cl	3	1.786828	2	123.735319	1	-14.422100
Cl	2	1.789103	1	113.721723	3	-167.290037

Table 19: Box size parameters (r_α^0 , $\alpha = x, y, z$) and optimal CAP strength parameters (η_{opt}) used for calculating the VAE of chloroethylenes. Calculations were done with CAP-EOM-EA-CCSD/aug-cc-pVXZ+3p (X=D,T). Parameters are given in a.u.

	basis	r_x^0	r_y^0	r_z^0	η_{opt}
C ₂ H ₃ Cl	-DZ+3p	13.690	6.460	4.545	0.01600
	-TZ+3p	13.530	6.375	4.500	0.01000
cis-C ₂ H ₂ Cl ₂	-DZ+3p	19.840	10.790	5.425	0.01900
	-TZ+3p	19.585	10.665	5.370	0.01200
trans-C ₂ H ₂ Cl ₂	-DZ+3p	24.745	7.200	5.420	0.02700
	-TZ+3p	24.460	7.105	5.365	0.01700
1,1-C ₂ H ₂ Cl ₂	-DZ+3p	17.185	12.930	5.420	0.05500
	-TZ+3p	16.975	12.760	5.365	0.03200
C ₂ HCl ₃	-DZ+3p	25.010	16.505	6.175	0.00650
	-TZ+3p	24.685	16.285	6.110	0.00425
C ₂ Cl ₄	-DZ+3p	26.260	23.760	6.850	0.01400

Supporting Information: Locating exceptional points on multidimensional complex-valued potential energy surfaces

Zsuzsanna Benda* and Thomas-C. Jagau*

Department of Chemistry, University of Munich (LMU), D-81377 Munich, Germany

E-mail: zsuzsanna.benda@cup.uni-muenchen.de; th.jagau@lmu.de

CAP-EOM-CC complex gradient formula

In Ref. 1 we derived the real part of the general CAP-CC/CAP-EOM-CC analytic gradient, but expressions for the imaginary part or the complex gradient were not given. Following the Lagrangian technique that was also applied in Ref. 1, the elements of the complex CAP-EOM-CC gradient \mathbf{G} can be given as

$$G_{n,\alpha} = \sum_{\mu\nu} D_{\mu\nu} \left[\frac{\partial h_{\mu\nu}}{\partial R_{n,\alpha}} - i\eta \frac{\partial W_{\mu\nu}}{\partial R_{n,\alpha}} - i\eta \left(\frac{Z_n}{\sum_k Z_k} \frac{\partial W_\alpha}{\partial o_\alpha} \right)_{\mu\nu} \right] + \sum_{\mu\nu\sigma\rho} \Gamma_{\mu\nu\sigma\rho} \frac{\partial \langle \mu\sigma || \nu\rho \rangle}{\partial R_{n,\alpha}} + \sum_{\mu\nu} I_{\mu\nu} \frac{\partial S_{\mu\nu}}{\partial R_{n,\alpha}} + \frac{\partial V_{\text{nuc}}}{\partial R_{n,\alpha}}, \quad (1)$$

where $R_{n,\alpha}$ are nuclear coordinates for nucleus n and $\alpha = x, y, z$. The effective one-electron density matrix D , the two-electron density matrix Γ , and the generalized energy-weighted density matrix I are complex-valued, and their forms depend on the specific CC or EOM-CC method used. The one-electron Hamiltonian h , the overlap matrix S and two-electron integrals over atomic orbitals $\langle \mu\sigma || \nu\rho \rangle$ are real, as well as the nuclear repulsion energy V_{nuc} . The dependence of the CAP (W) on nuclear coordinates through basis functions is considered through the term

$$\frac{\partial W_{\mu\nu}}{\partial R_{n,\alpha}} = \frac{\partial (W_x)_{\mu\nu}}{\partial R_{n,\alpha}} + \frac{\partial (W_y)_{\mu\nu}}{\partial R_{n,\alpha}} + \frac{\partial (W_z)_{\mu\nu}}{\partial R_{n,\alpha}}, \quad (2)$$

$$\frac{\partial (W_x)_{\mu\nu}}{\partial R_{n,\alpha}} = \left\langle \frac{\partial \mu}{\partial R_{n,\alpha}} \left| W_x \right| \nu \right\rangle + \left\langle \mu \left| W_x \right| \frac{\partial \nu}{\partial R_{n,\alpha}} \right\rangle. \quad (3)$$

The CAP origin o is defined as the center of nuclear charges Z_k

$$o_\alpha = \frac{\sum_k R_{k,\alpha} Z_k}{\sum_k Z_k}. \quad (4)$$

For a box-type quadratic CAP of the form

$$W = \sum_{\alpha} W_{\alpha}, \quad \alpha = x, y, z, \quad (5)$$

$$W_\alpha = \begin{cases} 0 & \text{if } |r_\alpha - o_\alpha| \leq r_\alpha^0 \\ (|r_\alpha - o_\alpha| - r_\alpha^0)^2 & \text{if } |r_\alpha - o_\alpha| > r_\alpha^0, \end{cases} \quad (6)$$

the derivatives with respect to the CAP origin are given by

$$\frac{\partial W_\alpha}{\partial o_\alpha} = \begin{cases} 0 & \text{if } |r_\alpha - o_\alpha| \leq r_\alpha^0 \\ -2(r_\alpha - o_\alpha - r_\alpha^0) & \text{if } (r_\alpha - o_\alpha) > r_\alpha^0 \\ -2(r_\alpha - o_\alpha + r_\alpha^0) & \text{if } (r_\alpha - o_\alpha) < -r_\alpha^0. \end{cases} \quad (7)$$

The real part of the gradient has already been given in Eq. 8 of Ref. 1. The imaginary part can be written as:

$$\begin{aligned} \text{Im}(G_{n,\alpha}) = & \sum_{\mu\nu} [\text{Im}(D_{\mu\nu}^{\text{HF}}) + \text{Im}(D_{\mu\nu}^{\text{CC}})] \frac{\partial h_{\mu\nu}}{\partial R_{n,\alpha}} \\ & - \eta \sum_{\mu\nu} [\text{Re}(D_{\mu\nu}^{\text{HF}}) + \text{Re}(D_{\mu\nu}^{\text{CC}})] \left[\frac{\partial W_{\mu\nu}}{\partial R_{n,\alpha}} + \frac{Z_n}{\sum_k Z_k} \left(\frac{\partial W_\alpha}{\partial o_\alpha} \right)_{\mu\nu} \right] \\ & + \sum_{\mu\nu\sigma\rho} \left[\frac{1}{2} \text{Re}(D_{\mu\nu}^{\text{HF}}) \text{Im}(D_{\sigma\rho}^{\text{HF}}) + \frac{1}{2} \text{Im}(D_{\mu\nu}^{\text{HF}}) \text{Re}(D_{\sigma\rho}^{\text{HF}}) \right. \\ & \quad \left. + \text{Re}(D_{\mu\nu}^{\text{CC}}) \text{Im}(D_{\sigma\rho}^{\text{HF}}) + \text{Im}(D_{\mu\nu}^{\text{CC}}) \text{Re}(D_{\sigma\rho}^{\text{HF}}) + \text{Im}(\Gamma_{\mu\nu\sigma\rho}^{\text{CC}}) \right] \frac{\partial \langle \mu\sigma || \nu\rho \rangle}{\partial R_{n,\alpha}} \\ & + \sum_{\mu\nu} [\text{Im}(I_{\mu\nu}^{\text{HF}}) + \text{Im}(I_{\mu\nu}^{\text{CC}})] \frac{\partial S_{\mu\nu}}{\partial R_{n,\alpha}} \end{aligned} \quad (8)$$

where CAP-HF and CAP-CC/CAP-EOM-CC contributions (denoted by superscripts 'HF' and 'CC') have been separated.

Hydrogen cyanide

Determining the branching plane

For determining the branching plane for the EP at $\angle=165^\circ$, interpolation was performed in parameter space ($R_{\text{CN}} / \text{\AA}$, $R_{\text{CH}} / \text{\AA}$, \angle / degree) between the EP points found at different bond angles (Table 1), then the tangent of the EP curve was calculated at $\angle=165^\circ$. The branching plane is by definition the plane orthogonal to this tangent vector. The CPES of the two resonances were calculated along loops with different radius around the EP in the branching plane. For Fig. 2 of the manuscript we chose orthonormal vectors \mathbf{u} and \mathbf{v} in the branching plane as $\mathbf{u}=(0.706969, 0.707122, -0.013141)$ and $\mathbf{v}=(0.707083, -0.707083, -0.008230)$ in parameter space.

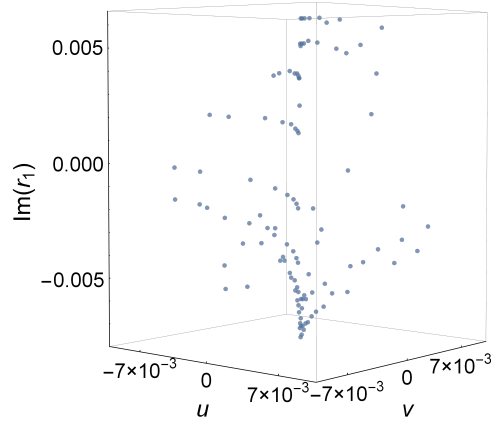


Figure 1: Imaginary part of the phase rigidity of state 1 above the branching plane of the EP at $\angle=165^\circ$.

Table 1: Structural parameters (in degrees and Å) and box size parameters (in a.u.) of HCN^- at EPs with constrained bond angles and at the MEEP. The CAP strength parameter was fixed at $9 \cdot 10^{-3}$ a.u. for all calculations. The aug-cc-pVTZ+3p basis set was used for all atoms.

	\angle	R_{CN}	R_{CH}	r_x^0	r_y^0	r_z^0
	155.00	1.0467	1.1524	5.380	2.980	2.920
	160.00	1.1208	1.1567	5.610	2.995	2.955
EPs	165.00	1.1948	1.1680	5.840	3.015	2.990
	170.00	1.2736	1.1939	6.095	3.035	3.025
	175.00	1.3826	1.2510	6.460	3.075	3.070
MEEP	162.98	1.1647	1.1623	5.745	3.005	2.980

Table 2: Energies of the anionic resonance states and the neutral parent state (in eV) of HCN at EPs, relative to the energy of the neutral state at its equilibrium. Calculations were performed using the aug-cc-pVTZ+3p basis set for all atoms.

	\angle	E_{neutral}	$E_{\text{R},1}$	$E_{\text{R},2}$	Γ_1	Γ_2
	155.00	1.159	3.276	3.283	1.638	1.625
	160.00	0.318	2.323	2.328	1.449	1.452
EPs	165.00	0.361	2.221	2.224	1.241	1.235
	170.00	1.035	2.668	2.673	0.982	0.984
	175.00	2.594	3.774	3.778	0.661	0.658
MEEP	162.98	0.260	2.176	2.197	1.330	1.328

Chloroethylene

Table 3: Structural parameters (in degrees and Å) of the $\pi^*-\sigma^*$ MEEP of chloroethylene. Calculated with the aug-cc-pVDZ+3p basis on C and Cl atoms and aug-cc-pVDZ on H atoms.

Cl						
C	1	1.94152				
H	2	1.09473	1	111.665		
C	2	1.38821	1	119.045	3	177.134
H	4	1.09510	2	120.976	1	2.347
H	4	1.09742	2	121.297	1	-178.849

Table 4: Structural parameters (in degrees and Å) of the neutral equilibrium structure of chloroethylene. Calculated with the aug-cc-pVDZ+3p basis on C and Cl atoms and aug-cc-pVDZ on H atoms. Taken from Ref. 2.

Cl						
C	1	1.75151				
H	2	1.09123	1	113.061		
C	2	1.34148	1	122.835	3	-180.000
H	4	1.09191	2	122.090	1	0.000
H	4	1.09268	2	119.201	1	-180.000

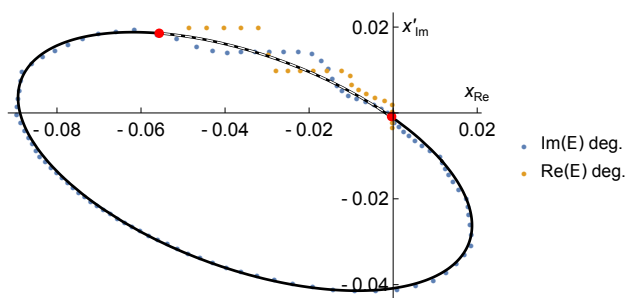


Figure 2: The ellipse was fitted to the crossing points of the interpolated imaginary surfaces presented in Fig. 4 of the manuscript, the points used for the fitting are given in blue. Points where the interpolated real surfaces are closer than 0.002 Hartree are also given, but were not used for the fitting. The optimized MEEP is in the origin, thus does not lie directly on the ellipse, the corresponding point on the ellipse was estimated as EP_1 , which was then mirrored to the minor axis of the ellipse to give the estimated location of EP_2 .

Table 5: Cartesian coordinates (in Å) of EP_1 and EP_2 of chloroethylene.

EP_1			
Cl	1.1447210810	-0.1044185516	-0.0015383398
C	-0.6751812328	0.5746365806	0.0118873160
H	-0.6978638851	1.6689695564	-0.0188074250
C	-1.7303753188	-0.3257904302	-0.0040977793
H	-1.5502490740	-1.4061751557	0.0143686527
H	-2.7728518632	0.0171599389	-0.0160886718
EP_2			
Cl	1.1373988837	-0.1014240913	0.0180901559
C	-0.6746409041	0.5616584823	-0.0336991856
H	-0.6993208418	1.6695581883	-0.0096217898
C	-1.7225010499	-0.3185033114	0.0077707409
H	-1.5496496482	-1.4042887230	0.0030214840
H	-2.7730854325	0.0173805551	0.0001641714

Table 6: Position and width of the π^* and σ^* anionic resonance states and energy of the neutral parent state of chloroethylene along the DEA route (in eV). Energies are given relative to the energy of the neutral state at its equilibrium. Points A1 to A3 were generated using linear interpolation between the neutral equilibrium structure and the π^* - σ^* MEEP, B1 to B3 using linear interpolation between the π^* - σ^* MEEP and the σ^* -neutral MECP. For the resonances CAP-EOM-EA-CCSD was used, the neutral state was calculated with regular CCSD. All calculations were done with aug-cc-pVDZ+3p on C and Cl atoms and aug-cc-pVDZ on H atoms.

	E_{neutral}	E_{R,π^*}	Γ_{π^*}	E_{R,σ^*}	Γ_{σ^*}
neut. eq.	0.000	1.801	0.260	2.268	1.115
A1	0.029	1.731	0.237	2.198	0.950
A2	0.108	1.707	0.218	2.089	0.738
A3	0.228	1.721	0.203	1.956	0.502
MEEP	0.380	1.761	0.267	1.768	0.279
B1	0.480	2.011	0.278	1.529	0.181
B2	0.627	2.241	0.299	1.349	0.118
B3	0.820	2.505	0.323	1.193	0.072
MECP	1.059	2.806	0.349	1.059	0.000

Table 7: Box size parameters and optimal CAP strength parameters (in a.u.) of the π^* and of the σ^* anionic resonance states of chloroethylene along the DEA route. At the MEEP $\eta = 0.01550$ was used, and at the MECP there is no optimal parameter for the σ^* state, thus $\eta = 0$ was applied. All calculations were done with aug-cc-pVDZ+3p on C and Cl atoms and aug-cc-pVDZ on H atoms.

	r_x^0	r_y^0	r_z^0	η_{opt,π^*}	$\eta_{\text{opt},\sigma^*}$
neut. eq.	13.690	6.460	4.545	0.01650	0.04000
A1	13.880	6.510	4.555	0.01600	0.04000
A2	14.070	6.565	4.565	0.01550	0.04000
A3	14.255	6.620	4.575	0.01550	0.04200
MEEP	14.445	6.670	4.585	0.01550 [†]	0.01550 [†]
B1	14.575	6.660	4.600	0.01750	0.01600
B2	14.705	6.640	4.625	0.01800	0.01400
B3	14.830	6.610	4.670	0.01950	0.00900
MECP	14.960	6.570	4.730	0.02200	0.00000 [†]

[†] not optimal values

References

- (1) Benda, Z.; Jagau, T.-C. Communication: Analytic Gradients for the Complex Absorbing Potential Equation-of-Motion Coupled-Cluster Method. *J. Chem. Phys.* **2017**, *146*, 031101.
- (2) Benda, Z.; Jagau, T.-C. Understanding Processes Following Resonant Electron Attachment: Minimum-Energy Crossing Points between Anionic and Neutral Potential Energy Surfaces. *J. Chem. Theory Comput.* **2018**, *14*, 4216–4223.

List of Publications

7. **Benda, Z.** and Jagau, T.-C. "Locating Exceptional Points on Multidimensional Complex-Valued Potential Energy Surfaces" *The Journal of Physical Chemistry Letters* **9** (24), 6978-6984 (2018).
6. **Benda, Z.** and Jagau, T.-C. "Understanding Processes Following Resonant Electron Attachment: Minimum-Energy Crossing Points between Anionic and Neutral Potential Energy Surfaces" *Journal of Chemical Theory and Computation* **14** (8), 4216-4223 (2018).
5. **Benda, Z.**, Rickmeyer, K. and Jagau, T.-C. "Structure Optimization of Temporary Anions" *Journal of Chemical Theory and Computation* **14** (7), 3468-3478 (2018).
4. **Benda, Z.** and Jagau, T.-C. "Communication: Analytic Gradients for the Complex Absorbing Potential Equation-of-Motion Coupled-Cluster Method" *The Journal of Chemical Physics* **146** (3), 031101 (2017).
3. **Benda, Z.** and Szalay, P.G. "Characterization of the Excited States of DNA Building Blocks: a Coupled Cluster Computational Study" *Physical Chemistry Chemical Physics* **18** (34), 23596-23606 (2016).
2. **Benda, Z.** and Szalay, P.G. "Details of the Excited-State Potential Energy Surfaces of Adenine by Coupled Cluster Techniques" *The Journal of Physical Chemistry A* **118** (32), 6197-6207 (2014).
1. Daru, J., **Benda, Z.**, Póti, A., Novák, Z. and Stirling, A. "Mechanistic Study of Silver-Mediated Furan Formation by Oxidative Coupling" *Chemistry – A European Journal* **20** (47), 15395-15400 (2014).